AD-A133 266 ACOUSTIC DIFFRACTION BY AN IMPEDANCE-COVERED EDGE(U) 1/2
PENNSYLVANIA STATE UNIV UNIVERSITY PARK APPLIED
RESEARCH LAB M MARSAN 15 JUN 83 ARL/PSU/TM-83-95
UNCLASSIFIED N00024-79-C-6043 F/G 20/1 NL

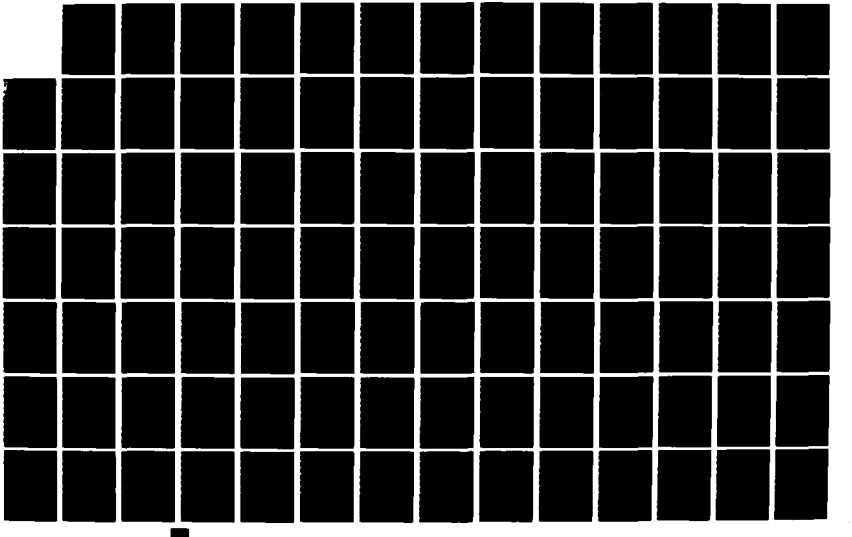

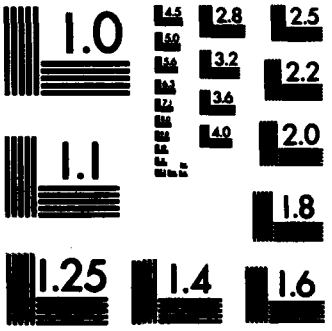

MICROCOPY RESOLUTION TEST CHART
NATIONAL BUREAU OF STANDARDS-1963-A

ACCOUSTIC DIFFRACTION BY AN IMPEDANCE-COVERED EDGE

Mehmet Marsan

Technical Memorandum
File No. TM 83-95
June 15, 1983
Contract No. N00024-79-C-6043

Copy No. 7

The Pennsylvania State University
Intercollege Research Programs and Facilities
APPLIED RESEARCH LABORATORY
Post Office Box 30
State College, PA 16801

APPROVED FOR PUBLIC RELEASE
DISTRIBUTION UNLIMITED

NAVY DEPARTMENT

NAVAL SEA SYSTEMS COMMAND

UNCLASSIFIED

SECURITY CLASSIFICATION OF THIS PAGE (When Data Entered)

REPORT DOCUMENTATION PAGE	READ INSTRUCTIONS BEFORE COMPLETING FORM
1. REPORT NUMBER: 83-95	2. GOVT ACCESSION NO.: AD-A133266	3. RECIPIENT'S CATALOG NUMBER:
4. TITLE (and Subtitle): ACOUSTIC DIFFRACTION BY AN IMPEDANCE-COVERED EDGE	5. TYPE OF REPORT & PERIOD COVERED: Ph.D. Thesis, August 1983
	6. PERFORMING ORG. REPORT NUMBER: 83-95
7. AUTHOR(s): Mehmet Marsan	8. CONTRACT OR GRANT NUMBER(s): N00024-79-C-6043
9. PERFORMING ORGANIZATION NAME AND ADDRESS: The Pennsylvania State University, Applied Research Laboratory, P.O. Box 30, State College, PA 16801	10. PROGRAM ELEMENT, PROJECT, TASK AREA & WORK UNIT NUMBERS:
11. CONTROLLING OFFICE NAME AND ADDRESS: Naval Sea Systems Command, Department of the Navy, Washington, DC 20362	12. REPORT DATE: 15 June, 1983
	13. NUMBER OF PAGES: 141 pages
14. MONITORING AGENCY NAME & ADDRESS(if different from Controlling Office)	15. SECURITY CLASS. (of this report)
	15a. DECLASSIFICATION/DOWNGRADING SCHEDULE

16. DISTRIBUTION STATEMENT (of this Report)

Approved for public release, distribution unlimited, per NSSC (Naval Sea Systems Command), 8 July 1983

17. DISTRIBUTION STATEMENT (of the abstract entered in Block 20, if different from Report)

18. SUPPLEMENTARY NOTES

19. KEY WORDS (Continue on reverse side if necessary and identify by block number)

thesis, acoustic, diffraction

20. ABSTRACT (Continue on reverse side if necessary and identify by block number)

The prediction of the sound scattered by impedance covered wedges is obtained by use of dual integral equations. The impedance of each face of the wedge is modeled as a point reacting complex quantity which is independent of the other face. The solution was constructed as an angular spectrum to satisfy the boundary conditions and Sommerfeld radiation condition. The solution kernel was obtained exactly and is in terms of circular functions. The solution of the scattered pressure was then obtained for far-field and mid-range by use of asymptotic techniques. This solution is much simpler than the one

DD FORM 1 JAN 73 1473 EDITION OF 1 NOV 65 IS OBSOLETE

UNCLASSIFIED

SECURITY CLASSIFICATION OF THIS PAGE (When Data Entered)

developed by Russian scientists (for example, see G.D. Maliuzhinets, "The Radiation of Sound by Vibrating Boundaries of an Arbitrary Wedge," Parts 1 and 2, Soviet Physics Acoustics, pp. 152-174 and 240-248 (1955)) which was obtained by a method similar to Wiener-Hopf technique. Thus, it is easier to use in highway noise applications because of its simplicity.

The solution for the diffracted pressure exhibits clearly the role of the incident and reflected shadow boundaries and shows there is one minimum in the scattered field which depends on the two surface impedances. For backscattered pressure, the solution exhibits two minima. In all cases, the scattered pressure becomes negligible near the wedge surfaces.

ABSTRACT

The prediction of the sound scattered by impedance covered wedges is obtained by use of dual integral equations. The impedance of each face of the wedge is modeled as a point reacting complex quantity which is independent of the other face. The solution was constructed as an angular spectrum to satisfy the boundary conditions and Sommerfeld radiation condition. The solution kernel was obtained exactly and is in terms of circular functions. The solution of the scattered pressure was then obtained for far-field and mid-range by use of asymptotic techniques. This solution is much simpler than the one developed by Russian scientists [for example, see G.D. Maliuzhinets, "The Radiation of Sound by Vibrating Boundaries of an Arbitrary Wedge," Parts 1 and 2, Soviet Physics Acoustics, pp. 152-174 and 240-248 (1955)] which was obtained by a method similar to Wiener-Hopf technique. Thus, it is easier to use in highway noise applications because of its simplicity.

The solution for the diffracted pressure exhibits clearly the role of the incident and reflected shadow boundaries and shows there is one minimum in the scattered field which depends on the two surface impedances. For backscattered pressure, the solution exhibits two minima. In all cases, the scattered pressure becomes negligible near the wedge surfaces.

TABLE OF CONTENTS

Page

ABSTRACT. iii

LIST OF FIGURES vi

LIST OF MAJOR SYMBOLS ix

ACKNOWLEDGEMENTS. xi

Chapter

I. INTRODUCTION. 1
1.1 Background. 1
1.2 Literature Review 1

II. DIFFRACTION OF PLANE WAVE BY AN IMPEDANCE COVERED WEDGE . 6
2.1 Statement of the Problem. 6
2.2 Basic Approach. 7
2.3 Integral Representation 8
2.4 Plane Wave Formulation. 18
2.5 Solution for Plane Wave Incidence 25
2.6 Far-field Solution for a Plane Wave Incidence . . 34
2.7 Geometric Acoustics 39

III. SOLUTIONS VALID FOR MID-RANGE AND AT SHADOW BOUNDARIES . . 44
3.1 Mid-range Solution for a Plane Wave Source. . . . 44
3.2 Mid-range Solution for a Line Source. 50
3.3 Mid-range Solution for a Point Source 56

IV. NUMERICAL RESULTS. 64
4.1 Dependence on Surface Impedances. 65
4.2 Dependence on the Wedge Angle 67
4.3 Dependence on kr_o 67
4.4 Excess Attenuation. 80
4.5 Backscattering from a Wedge 80
4.6 Comparison with the Maliuzhinets Solution 87

V. DISCUSSION OF NUMERICAL RESULTS AND CONCLUSIONS. 96
5.1 Introduction. 96
5.2 Physical Interpretation of $P(\cos\alpha)$. 96
5.3 Discussion of Numerical Results 98
5.3.1 Transition Regions 98
5.3.2 Influence of Impedance Coverage. . . . 100
5.3.3 Influence of the Wedge Angle 100
5.3.4 Influence of the Sphericity of the Point Source Field 101

TABLE OF CONTENTS (Continued)

Page

5.3.5 Backscattered Field 102
5.4 Conclusions. 102
5.5 Suggestions for Further Research 103

REFERENCES. 104

APPENDIX A: CONDITION OF ZERO VALUE OF THE LOOP INTEGRAL . . . 107

APPENDIX B: COMPUTER PROGRAM LISTINGS. 108

LIST OF FIGURES

Figure		Page
2.1	Geometry of the impedance covered wedge	9
2.2	Possible integration paths γ and regions of convergence (shaded areas)	13
2.3a	Regions of convergence for $y > 0$	15
2.3b	Regions of convergence for $y < 0$	16
2.4	γ-paths chosen for boundary condition at $\phi = \beta$	21
2.5	Γ-path and covergence regions..	22
2.6	γ-paths chosen for boundary condition at $\phi = -\beta$	24
2.7	The γ-paths for continuity of velocity.	26
2.8	Closure of path for boundary conditions	28
2.9	Closure of path for satisfying continuity of velocity . .	35
2.10	Path of steepest descent.	38
2.11	Path of integration for the far-field with $2\beta-\phi_o-\pi<\phi<\beta$.	40
2.12	Path of integration for the far-field with $0>\phi>2\beta-\phi_o-\pi$.	41
2.13	Regions of validity of the solution (Eq. 2.64).	43
3.1	Regions of convergence of the γ'-path	45
3.2	Regions of convergence and branch cuts for a point source	59
4.1	Diffraction of plane wave with impedance cover on the insonified surface with $kr = 20$, $\theta^- = 0°$, $\phi_o = 60°$ and $\beta = 135°$	66
4.2	Diffraction of plane wave with impedance cover on the uninsonified surface with $kr = 20$, $\theta^- = 0°$, $\phi_o = -60°$ and $\beta = 135°$.	68
4.3	Diffraction of plane wave with total absorption on the insonified surface with $kr = 20$, $\theta^+ = 90-i5$, $\theta^- = 0°$ $\phi_o = 105$ and $\beta = 135°$	69
4.4	Diffraction of plane wave with total absorption on the uninsonified surface with $kr = 20$, $\theta^+ = 90°-i5$, $\theta^- = 0°$, $\phi_o = -105°$ and $\beta = 135°$.	70

LIST OF FIGURES (Continued)

Figure		Page
4.5	Diffraction of plane wave with impedance cover on both surfaces with kr = 20, $\theta^+ = 60°$, $\theta^- = 30°$, $\phi_o = 105°$ and $\beta = 135°$	71
4.6	Diffraction of plane wave from a 120° wedge with $\phi_o = 110°$, $\theta^+ = 30°$, $\theta^- = 0°$ and kr = 20	72
4.7	Diffraction of plane wave from a 135° wedge with $\phi_o = 110°$, $\theta^+ = 30°$, $\theta^- = 0$ and kr = 20.	73
4.8	Diffraction of plane wave from a 165° wedge with $\phi_o = 110°$, $\theta^+ = 30°$, $\theta^- = 0°$ and kr = 20	74
4.9	Diffraction of plane wave from a 180° wedge with $\phi_o = 110°$, $\theta^+ = 30°$, $\theta^- = 0°$ and kr = 20	75
4.10	Diffraction of plane wave from a 120° wedge with $\phi_o = 30°$, $\theta^+ = 30°$, $\theta^- = 0°$ and kr = 20.	76
4.11	Diffraction of plane wave from a 135° wedge with $\phi_o = 30°$, $\theta^+ = 30°$, $\theta^- = 0°$ and $\beta = 135°$	77
4.12	Diffraction of plane wave from a 165° wedge with $\phi_o = 30°$, $\theta^+ = 30°$, $\theta^- = 0°$ and kr = 20.	78
4.13	Diffraction of plane wave from a 180° wedge with $\phi_o = 30°$, $\theta^+ = 30°$, $\theta^- = 0°$ and kr = 20.	79
4.14	Diffraction of point source radiation with $kr_o = 5$, $\theta^+ = 60°$, $\theta^- = 30°$, $\phi_o = 60°$ and $\beta = 135°$.	81
4.15	Diffraction of point source radiation with $kr_o = 10$, $\theta^+ = 60°$, $\theta^- = 30°$, $\phi_o = 60°$ and $\beta = 135°$.	82
4.16	Diffraction of point source radiation with $kr_o = 20$, $\theta^+ = 60°$, $\theta^- = 30°$, $\phi_o = 60°$ and $\beta = 135°$.	83
4.17	Diffraction of point source radiation with $kr_o = 200$, $\theta^+ = 60°$, $\theta^- = 30°$, $\phi_o = 60°$ and $\beta = 135°$.	84
4.18	Diffraction of point source radiation with $kr_o = 2000$, $\theta^+ = 60°$, $\theta^- = 30°$, $\phi_o = 60°$ and $\beta = 135°$.	85
4.19	Excess attenuation as a function of kr (Eq. 4.1).	86
4.20	Backscattering of plane wave from a 120° wedge with $\theta^+ = 60°$, $\theta^- = 30°$, kr = 20 and $\phi_o = 110°$	88

LIST OF FIGURES (Continued)

Figure		Page
4.21	Backscattering of plane wave from a 135° wedge with $\theta^+ = 60°$, $\theta^- = 30°$, kr = 20 and $\phi_o = 110°$	89
4.22	Backscattering of plane wave from a 165° wedge with $\theta^+ = 60°$, $\theta^- = 30°$, kr = 20 and $\phi_o = 110°$	90
4.23	Backscattering of plane wave from a 180° wedge with $\theta^+ = 60°$, $\theta^- = 30°$, kr = 20 and $\phi_o = 110°$	91
4.24	Backscattering of plane wave from a 135° wedge with $\theta^+ = 30°$, $\theta^- = 30°$, kr = 20 and $\phi_o = 110°$	92
4.25	Backscattering of plane wave from a 135° wedge with $\theta^+ = 30°$, $\theta^- = 30°$, kr = 200 and $\phi_o = 110°$.	93
4.26	Comparison of far-field diffracted pressure predicted by this study with Maliuzhinets	94
4.27	Comparison of far-field diffracted pressure predicted by this study with Maliuzhinets'.	95

LIST OF MAJOR SYMBOLS

R	line source: $R = \sqrt{r^2+r_o^2-2rr_o\cos(\phi-\phi_o)}$
	point source: $R = \sqrt{r^2+r_o^2-2rr_o\cos(\phi-\phi_o) + (z-z_o)^2}$
S	line source: $S = \sqrt{r^2+r_o^2-2rr_o\cos(\phi+\phi_o)}$
	point source: $S = \sqrt{r^2+r_o^2-2rr_o\cos(\phi+\phi_o) + (z-z_o)^2}$
R_1	line source: $R_1 = r + r_o$
	point source: $R_1 = \sqrt{(r+r_o)^2 + (z-z_o)^2}$
$\psi_{1,2}(\alpha)$	diffraction factor
$M_{1,2}(\alpha)$	angle factor
$F_{\pm}^1$	transition function for plane wave diffraction
$F_{\pm}^2$	transition function for line source diffraction
$F_{\pm}^3$	transition function for point source diffraction
$a^{\pm}(x)$	argument of transition functions
C_r	coefficient of reflection
$p(r,\phi)$	scattered pressure
$p_d(r,\phi)$	diffracted pressure
k	acoustic wave number
$P(\cos\alpha)$	specular distribution of plane waves
α	variable of integration
$\gamma,\bar{\gamma}$	path of integration
$Z^{\pm}$	surface impedances of the wedge
$\theta^{\pm}$	Brewster angle

ρ	density of the acoustic medium
ϕ_o	angle of incidence
β	wedge angle
(r,ϕ,z)	location of the observer in cylindrical coordinates
(r_o,ϕ_o,z_o)	location of point source
(r_o,ϕ_o)	location of the line source
$S^*_{\pm}$	line source: $S^*_{\pm}(x) = \sqrt{(r+r_o)^2 - 2rr_o\, a^{\mp}(x)}$

ACKNOWLEDGEMENTS

The author wishes to express his deepest gratitude to Professor Sabih I. Hayek, thesis advisor, for his continuing guidance and support throughout this study. He also wishes to thank Professor Eugen J. Skudrzyk, committee member, for his instruction and active participation during the course of this study. Appreciation is also expressed to Professors William Thompson, Jr., Ling-Wen Hu and Vernon H. Neubert for their participation in the doctoral committee.

This work was supported under the Exploratory and Foundational Research program directed by Dr. M. T. Pigott of the Applied Research Laboratory under contract with the U. S. Naval Sea Systems Command.

CHAPTER I

INTRODUCTION

1.1 Background

In recent years, noise reduction by barriers has become a common measure for environmental protection. Ideally such design should be based on easily applicable equations which characterize the diffraction around the barrier. However, the complexity of the available solutions has necessitated the introduction of variety of approximations and idealizations, such as ideal boundaries and limited geometric shapes.

This study deals with the diffraction of sound by wedges whose surfaces are characterized by locally reacting finite acoustic impedances and have general wedge angles. The solutions obtained are much simpler than the ones being used presently. Thus they are easier to use in noise attenuation applications.

1.2 Literature Review

The problem of diffraction by sharp-edged objects has been studied extensively in acoustics, electromagnetics, optics and water-wave theory. The following literature review is mainly concentrated on diffraction by wedges.

The first investigator who succeeded in deriving the first exact solution of diffraction of a plane wave by a wedge was Sommerfeld [1]. His solution is only applicable to a particular case of two-dimensional problem of diffraction, namely two types of ideal boundary conditions where both surfaces are either perfectly soft (pressure release) sur-

faces or perfectly hard (rigid) surfaces. The Sommerfeld theory has been considered to be very difficult to understand because the solution is derived by a heuristic image method. Sommerfeld arrived at his results by seeking an appropriate solution to the wave equation of period 4π and by combining it with its "image." The solution that resulted is valid in the far-field, but it becomes unbounded at the incident and reflected shadow boundaries. MacDonald [2] approached the wedge diffraction problem using the classical separation of variables technique and expressed the solution as an infinite series of appropriate eigenfunctions for point and line sources.

The first solution of diffraction by an imperfectly conducting obstacle was obtained by Senior [3]. The general problem of diffraction of a plane wave by a non-ideal surface wedge of arbitrary angle was considered. In order to obtain the solution, Senior made some assumptions without physical reasoning which hold only for a pressure release wedge. Williams [4] obtained a solution for diffraction by impedance covered arbitrary wedge. He reduced the original problem to the solution of an ordinary difference equation. This equation was then solved in terms of the double Gamma function defined by Barnes [5]. The resulting solution is an infinite product form and can only be solved in closed form if the wedge angle is $\pi p/q$ where p and q are relative prime integers, with p odd.

Russian physicist Maliuzhinets [6] demonstrated that the kernel of the problem obtained in the Fourier transform approach is the solution of a difference equation. He gave conditions and proved theorems about this fact. However, his method for obtaining the

solution of this difference equation was not published in the open literature. The solution is quite similar to the Weiner-Hopf technique of factoring a function into the product of two functions each valid in one half space. Skudrzyk [7] and VanLennep [8] made two independent attempts and derived the so called Maliuzhinets functions. Maliuzhinets functions consist of the product of four complicated functions with four different arguments. These functions are typical of those found in Weiner-Hopf solution, i.e., they are exponential functions each of whose argument is a proper integral of another function. Several applications of these functions to propagation problems were published by Maliuzhinets [9-11] and other Russian scientists [12-15]. The closed form solution obtained by using these functions is limited by the same conditions applied to the solution of Williams. For a general wedge angle the solution was approximated by Skudrzyk [7].

In more recent studies Pierce [16] and Kouyoumjian [17] extended the available solutions of Williams and Sommerfeld for applications in electromagnetic waves and acoustic absorbing barriers, respectively. Pierce was interested in the application to more complicated barrier structures which involve more than one wedge -- thick absorbing barrier or trapezoid absorbing barrier -- by using the diffraction coefficient for the absorbing wedge in conjunction with Keller's Geometric Theory of Diffraction (GTD). In Kouyoumjian's original paper only diffraction by a perfectly conducting wedge whose edge is a curved line was studied. The diffraction coefficient obtained by incorporating asymptotic results by Pauli [18] and Oberhettinger [19] is continuous across the incident and reflection shadow bound-

aries. The expressions for the acoustic wedge diffraction coefficients contain Fresnel integrals, which ensure that the total field is continuous at the incident and reflection shadow boundaries. These diffraction coefficients were modified for non-ideal boundary conditions by using Maliuzhinets functions. A complete summary of these solutions were published by Hayek, et al. [20]. Rawlins [21] proposed a superposition method for perfectly absorbing wedges by combining the known solutions for hard and soft wedges and derived a simple closed form solution for an absorbing wedge.

The most widely studied special wedge is the half-plane. Carslaw [22] extended Sommerfeld's plane wave solution for a half-plane with ideal (either rigid or soft) boundary conditions for line and point sources. MacDonald [23] showed that his wedge solution reduces to Carslaw's half-plane solution. He also derived asymptotic solutions in terms of Fresnel integrals which are widely used in modern diffraction analysis. Rawlins [24] obtained a closed form solution for diffraction by a semi-infinite plane with rigid-soft surfaces by using a modified Wiener-Hopf method (which is a standard method for half-plane problems).

The first exact solution of diffraction by a semi-infinite metallic sheet with finite conductivity was obtained by Senior [25]. He considered this particular case of wedge by means of the Wiener-Hopf technique. The result is in integral form and cannot be easily computed. Clemmow [26] introduced a "dual integral" method for ideal boundaries. In a more recent study Kendig and Hayek [27] employed an extension of a dual integral method for a hard-soft

barrier. Kendig [28] also utilized the same method to solve for the diffraction by an impedance covered half-plane. Kendig and Hayek obtained by Fourier transforms two integral equations, each holding for a different side of the half-plane. These dual integral equations were solved and continuous solutions at the incident and reflection shadow boundaries for the plane wave, line and point sources were derived.

Extensive reviews of diffraction from wedges are given by Bowman, Senior, Usleghi [29], Pierce [16], Christiansen [30], Skudrzyk [7] and Hayek, et al. [20].

CHAPTER II

DIFFRACTION OF PLANE WAVE BY AN IMPEDANCE COVERED WEDGE

2.1 Statement of the Problem

When an acoustic wave is incident upon a discontinuous body, having acoustic characteristics different from those of the surrounding medium, the resulting acoustic field is modified from the incident wave. The modified wave field is caused by scattering from the continuous and discontinuous parts of the body. Therefore, in addition to the initial field, there is scattered field which is propagated outward away from the discontinuity and interfering with the incident field.

In this study, solution is sought for the diffraction of an incident plane, line or point source by a wedge with an arbitrary wedge angle and covered by surfaces possessing locally reacting impedances. It should be pointed out that even diffraction from a half-plane, which is one limiting case of a wedge, is approached by ideal boundary conditions. These ideal surface conditions are characterized as either the pressure release or the rigid cases. In this study more realistic and mathematically more complicated surface conditions are to be considered. The acoustic impedances of the wedge surfaces are finite, locally reacting and complex. The real and imaginary parts of the complex impedance are the acoustic resistance and reactance, respectively. The acoustic resistance of the surface impedance represents the acoustic energy that is absorbed by the surface of the wedge. The acoustic reactance of the surface impedance represents the inertia and the compliance of the surface coverage.

One can conceive a surface possessing locally reacting point impedance Z on which $p=Zv_n$, with v_n being the normal velocity and p is the surface pressure holds at each and every point. This impedance is independent of the angle of incidence of the acoustic wave. The locally reacting point impedance model works well for materials such as grass covered ground, porous media, fiberous material such as fiberglass wool, etc. However, this model ignores the wave effects on the surface or the effects of refraction in the material of the wedge. A locally reacting surface can be best visualized as a surface which consists of isolated simple oscillators. In other words, there is no coupling with the neighboring points of the surface, which excludes elastic waves propagating on the surface.

2.2 Basic Approach

The solution of the problem is partially based on the works of Clemmow [26], Kendig [28], and Kendig and Hayek [27]. It begins with writing separately, the equations representing the acoustic field generated by a plane wave source valid in the two half spaces symmetric about an infinite wedge. By employing Fourier transform techniques and taking advantage of the symmetry of the wedge, two integral equations are obtained. The solution was constructed as an angular spectrum function which satisfies these two integral equations and the Sommerfeld radiation condition. Since the acoustic field can be produced by various kinds of sources, the scattered field due to line and point sources is also investigated. The scattered pressure was then obtained for far-field and mid-range by use of asymptotic techniques.

2.3 Integral Representation

The wedge is defined in terms of cylindrical coordinates (r,ϕ,z) by the equations $\phi=\beta$ (upper surface) and $\phi=-\beta$ (lower surface) and its edge is coincident with the z-axis as shown in Fig. 2.1.

A scattering problem consists of finding the scattering pressure p when an incident plane wave p_i impinges on the obstacle. The total field pressure must satisfy three requirements, the differential equation, the boundary conditions and a continuity condition. The standard Fourier method is not applicable to a space with a discontinuity. Fourier integrals converge only in half-space. To assure the continuity at the intersection of two half spaces, the continuity of the pressure and the normal velocity are imposed.

Consider the homogeneous wave equation for pressure

$$\nabla^2\bar{p} = \frac{1}{c^2}\frac{\partial^2\bar{p}}{\partial t^2} \tag{2.1}$$

where c is the sound speed of the acoustic medium

Assuming the pressure to be periodic in time as $\bar{p}(x,t) = p(x)\, e^{i\omega t}$, then Eq. (2.1) reduces to the Helmholtz equation:

$$\nabla^2 p + k^2 p = 0 \tag{2.2}$$

where $k = \omega/c$

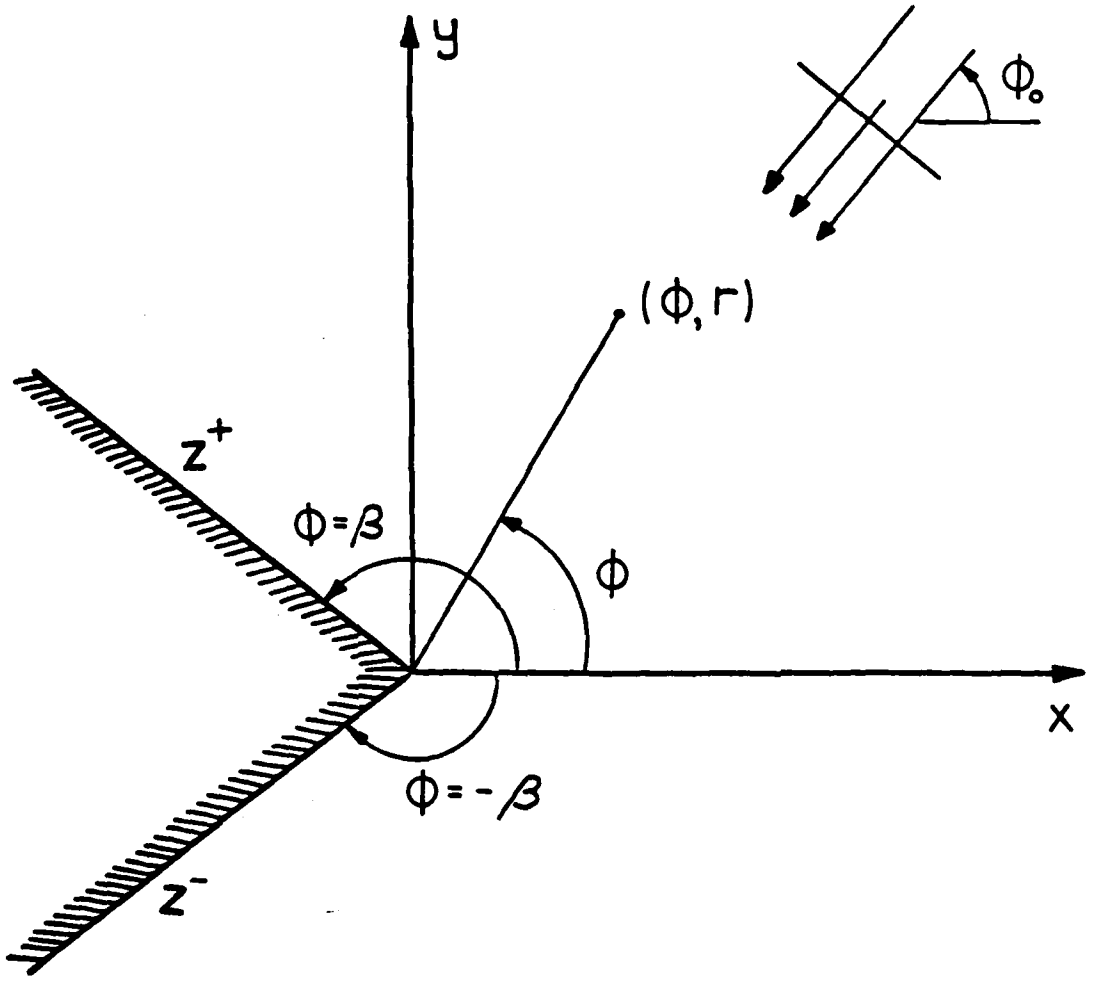

Fig. 2.1 Geometry of the impedance covered wedge.

Define the Fourier Transform pair

$$f(x) = \frac{1}{2\pi} \int_{-\infty}^{\infty} F(\gamma)\ e^{-i\gamma x} d\gamma \tag{2.3}$$

$$F(\gamma) = \int_{-\infty}^{\infty} f(x)\ e^{i\gamma x} dx \tag{2.4}$$

Applying the above transform on x in Eq. (2.2), one obtains:

$$\frac{\partial^2 p}{\partial y^2} + (k^2 - \gamma^2)\ p = 0 \tag{2.5}$$

or

$$\frac{\partial^2 p}{\partial y^2} + \eta^2 p = 0 \tag{2.6}$$

where $$\eta = k\sqrt{1 - \left(\frac{\gamma}{k}\right)^2}$$

Then the solution of the Helmholtz equation, Eq. (2.2) is

$$p = A(\gamma)\ e^{\pm i\eta y} \tag{2.7}$$

Since the wave equation is of the second order, it has two independent solutions. One solution has to be discarded because it represents energy sources at infinity. The diffracted pressure is directed away from the wedge boundaries, so the solution must describe outgoing waves. Using plus sign (+) for $y < 0$, and the minus (-) sign for $y > 0$, the requirement of waves propagating

and decaying away from the wedge is satisfied.

Using the inverse transform, Eq. (2.3), solution of the wave equation is obtained as

$$p(x,y) = \frac{k}{2\pi} \int_{-\infty}^{\infty} A(\gamma)\ e^{\pm iky\sqrt{1-\lambda^2}}\ e^{-ik\lambda x} d\lambda \tag{2.8}$$

where $\lambda = \gamma/k$, and $A(\lambda)$ is the spectral amplitude function. The above integral represents the solution of the wave equation when integrated in the proper convergent space.

Although the convergence properties of the integrand are not affected by a coordinate transformation, at this point it is advantageous to introduce polar coordinates.

Let

$$\begin{aligned} x &= r\cos\phi \\ y &= r\sin\phi \end{aligned} \tag{2.9}$$

and

$$\lambda = \cos\alpha$$

The exponent in the integrand thus becomes

$$\begin{aligned} &-ikr(\cos\phi\ \cos\alpha \pm \sin\phi\ \sin\alpha) \\ &= -ikr\cos(\phi \mp \alpha) \end{aligned} \tag{2.10}$$

The limits on λ ($-\infty$ to $+\infty$) are given by

$$\begin{aligned} \lambda = \cos\alpha &= \cos(\alpha_r + i\alpha_i) \\ &= \cos\alpha_r\ \cosh\alpha_i - i\sin\alpha_r\ \sinh\alpha_i \end{aligned} \tag{2.11}$$

where subscripts r and i designate real and imaginary parts. Due to periodicity of $\cos\alpha$, the entire λ-space is mapped into a strip of π width which repeats with periodicity π. Certain values for α_r and α_i must be chosen in order to determine the mapping of the λ-path in the α-space.

$$\alpha_r = 0 \quad \alpha_i = \pm\infty \quad \text{for} \quad \lambda = \infty \tag{2.12}$$

$$\alpha_r = \pi \quad \alpha_i = \pm\infty \quad \text{for} \quad \lambda = -\infty \tag{2.13}$$

The multiplicity of all possible α-paths is shown in Fig. 2.2.

After the change of variables and the coordinate transformation, Eq. (2.8) becomes:

$$p(r,\phi) = \int_\gamma P(\cos\alpha) e^{-ikr\cos(\phi \mp \alpha)} d\alpha, \qquad \begin{matrix} + \text{ for } y > 0 \\ - \text{ for } y < 0 \end{matrix} \tag{2.14}$$

where $P(\cos\alpha) = \frac{k}{2\pi} A(\cos\alpha)$.

At this point it should be pointed out that beyond the interval $0 \leq \mathrm{Re}\,\alpha \leq \pi$ the notation $P(\cos\alpha)$ must not be taken to imply that the function is necessarily either even or having a period 2π.

It does not make much difference which sign is selected for the exponential; convergence can be obtained for each sign by selecting the new limits of integration properly. To assure convergence, the real part of the exponential must be negative. This means one must have for $y > 0$:

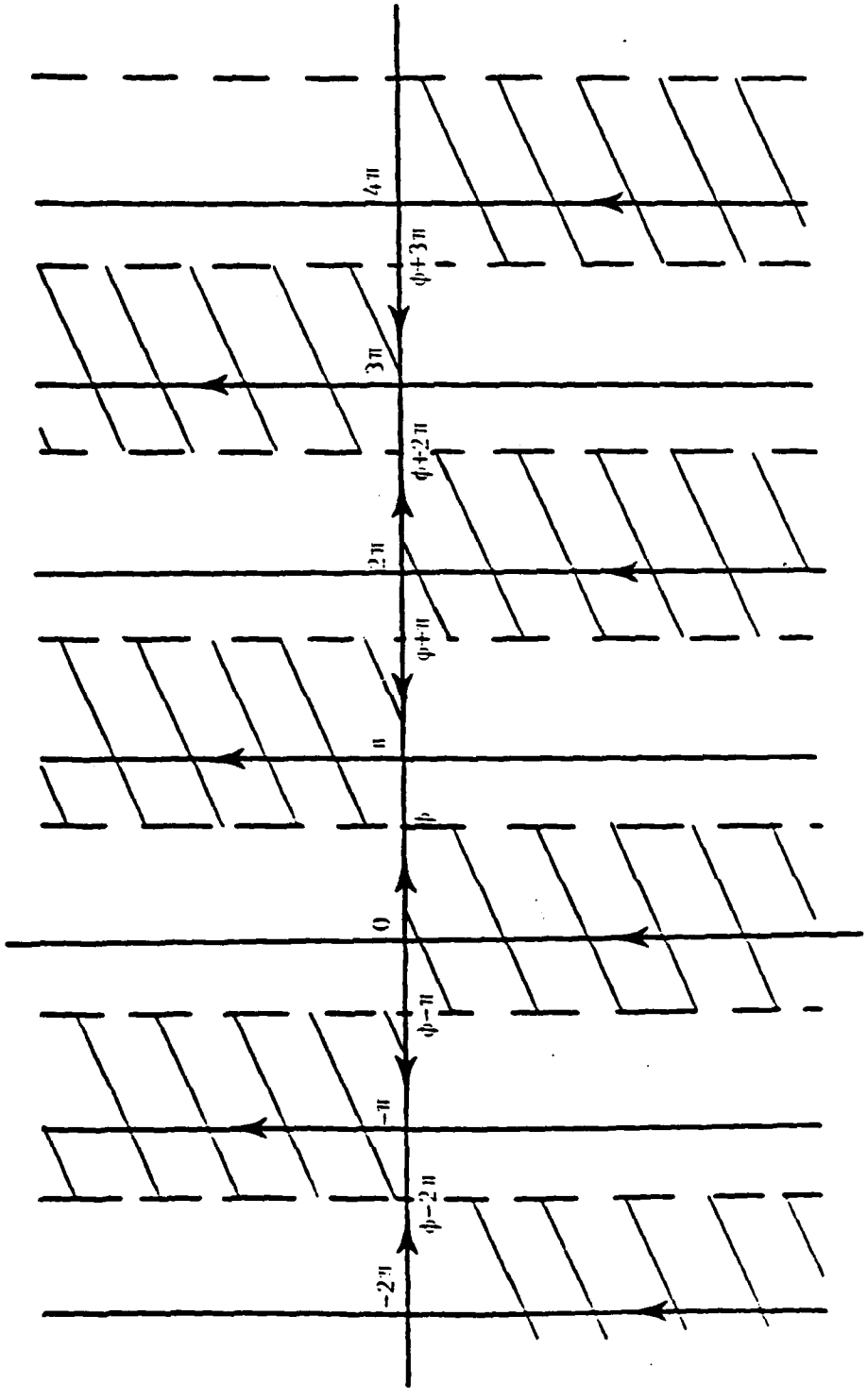

Fig. 2.2 Possible integration paths γ and regions of convergence (shaded areas).

$$\mathrm{Re}[-ikr\{\cos(\phi-\alpha_r)\cosh\alpha_i + i\sinh\alpha_i \sin(\phi-\alpha_r)\}] \tag{2.15}$$

$$= kr\sinh\alpha_i \sin(\phi-\alpha_r) < 0$$

If $\alpha_i < 0$, then

$$\phi + (2n-1)\pi \leq \alpha_r \leq 2n\pi + \phi \tag{2.16}$$

If $\alpha_i > 0$, then

$$\phi + 2n\pi \leq \alpha_r \leq \phi + (2n+1)\pi \tag{2.17}$$

Similarly for $y < 0$:

If $\alpha_i < 0$, then

$$-\phi + (2n-1)\pi \leq \alpha_r \leq -\phi + 2n\pi \tag{2.18}$$

If $\alpha_i > 0$, then

$$-\phi + 2n\pi \leq \alpha_r \leq -\phi + (2n-1)\pi \tag{2.19}$$

It is therefore necessary for the convergence of the integral that the extremes of any path of integration must lie in the shaded regions of Figs. 2.3a and 2.3b.

The part of the path along the real axis represents homogeneous plane waves fanning out to free space, whereas the vertical parts represent inhomogeneous waves decaying away from the wedge. The

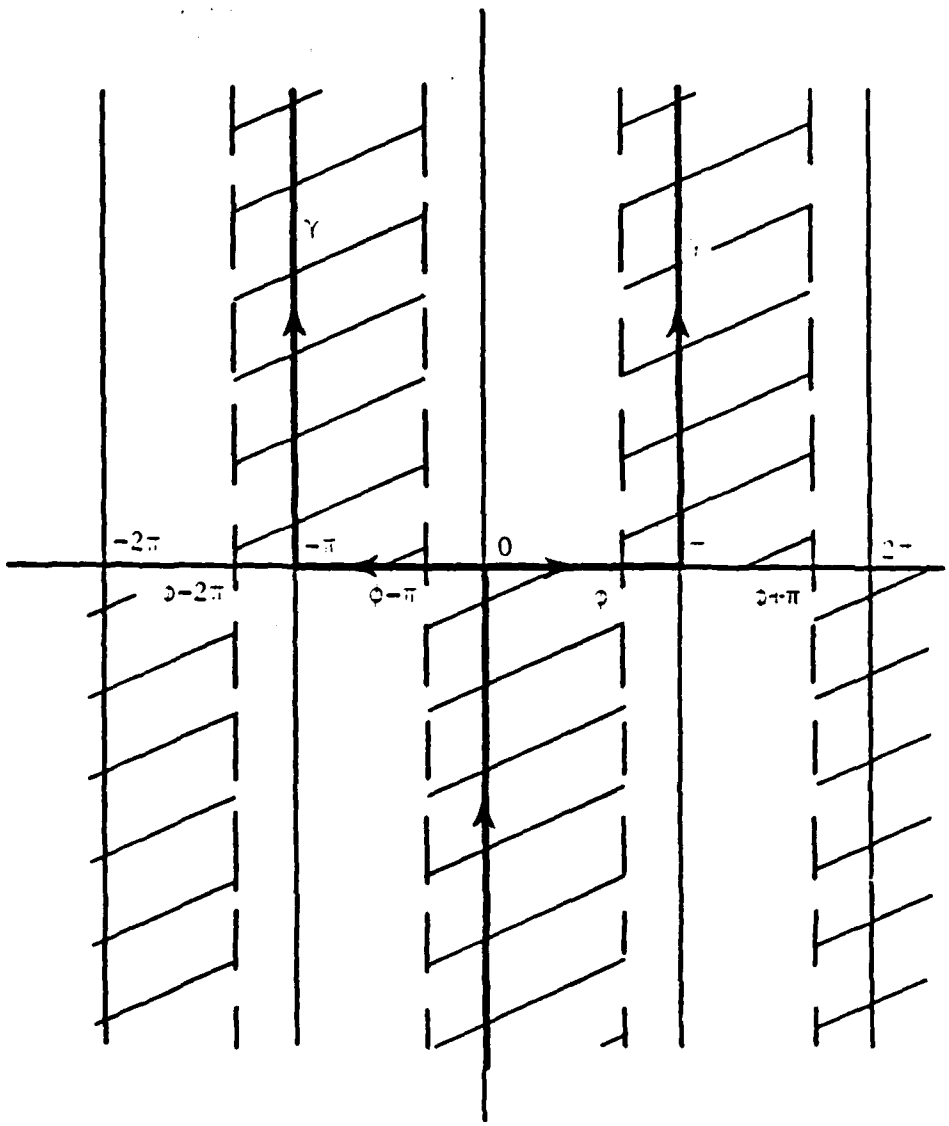

Fig. 2.3a Regions of convergence for $\gamma > 0$.

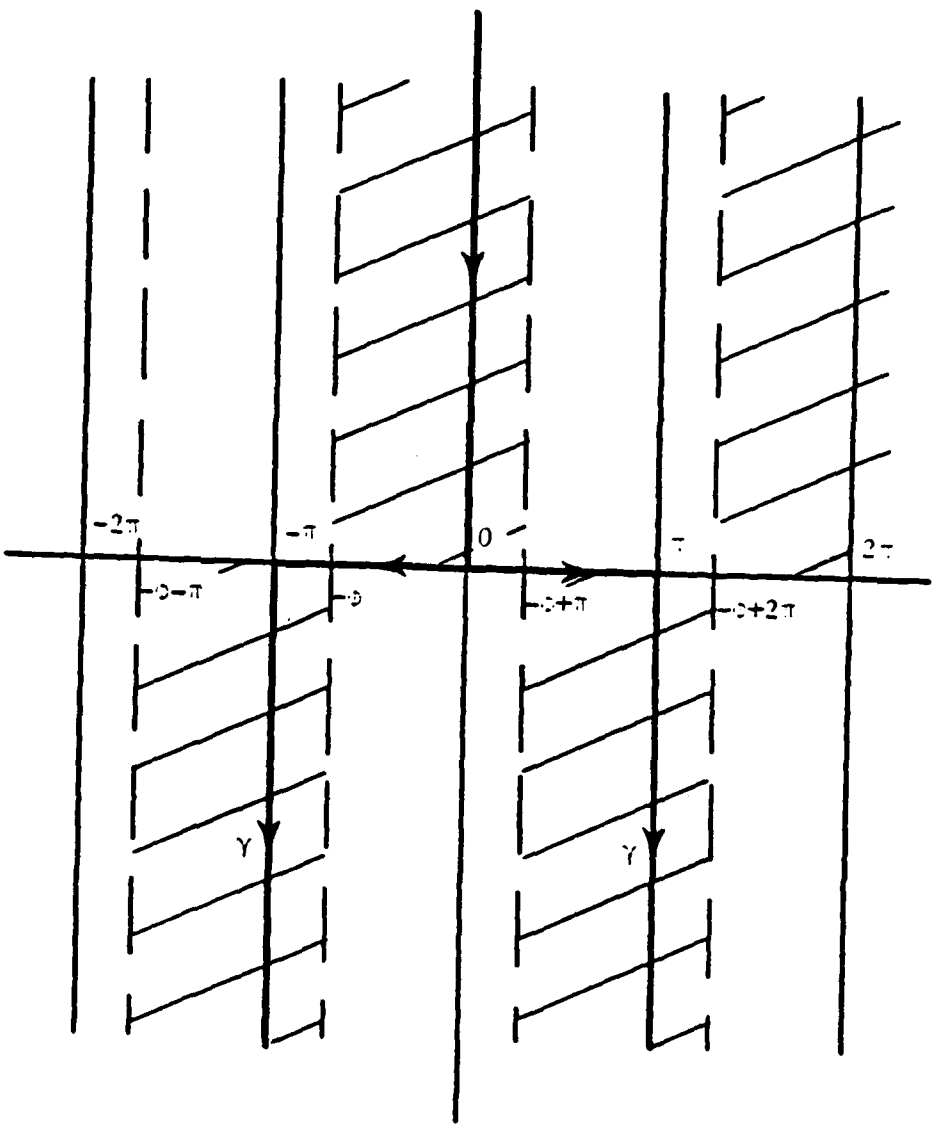

Fig. 2.3b Regions of convergence for y < 0.

spectrum function $P(\cos\alpha)$ specifies in terms of amplitude and phase the weight attached to each plane wave of the spectrum. By this physical reasoning the above integral could have been written down heuristically as superposition of plane waves propagating in all directions multiplied by a weighting function which contains the amplitude and the phase of each plane wave.

To characterize the scattered wave caused by the wedge, it must be required that the scattered field does not have a source at infinity. This condition is described by the "Sommerfeld radiation condition."

$$\lim_{r \to \infty} \{\sqrt{r} \left[\frac{\partial p}{\partial r} + ikp\right]\} \to 0 \tag{2.20}$$

Substituting the expression for scattered pressure into the above expression yields

$$\lim_{r \to \infty} \{\sqrt{r} \left[\int_\gamma P(\cos\alpha)(1-\cos(\phi \mp \alpha))\, e^{-ikr\cos(\phi \mp \alpha)} d\alpha\right]\} \to 0 \tag{2.21}$$

This limit is satisfied if the path of integration is in the convergence regions of the α-plane, which are shown as the shaded regions in Figs. 2.3a and 2.3b. So the right choice of γ-paths that fall in the convergence regions will automatically satisfy the Sommerfeld radiation condition.

2.4 Plane Wave Formulation

An incident plane wave in free space can be represented as follows:

$$p_i = p_o e^{ikr\cos(\phi-\phi_o)} \tag{2.22}$$

where p_o is the amplitude of the incoming wave and ϕ_o is the angle the wave normal makes with the positive x-axis, see Fig. 2.1.

The surface impedance is the ratio of the total pressure to the normal component of the velocity. Then the boundary conditions that have to be satisfied are

$$\left.\frac{p_t}{v_{tn}}\right|_{\phi=\pm\beta} = \left.\frac{p_i+p}{v_{in}+v_n}\right|_{\phi=\pm\beta} = Z^{\pm} \tag{2.23}$$

where p_t is the total pressure and v_{tn} is the normal component of the total field particle velocity.

The reflection coefficient for a plane wave incident at a plane surface with impedance Z is given by

$$R = \frac{\cos u - c/Z}{\cos u + c/Z} \tag{2.24}$$

where u is the angle of incidence with the normal to the surface. There will be no reflection if the numerator is zero, that is the angle of incidence is equal to the grazing acoustic Brewster angle given by

$$\sin\theta^{+} = \frac{\rho c}{z^{+}} \tag{2.25}$$

and

$$\sin\theta^{-} = \frac{\rho c}{z^{-}} \tag{2.26}$$

Then the boundary conditions, Eq. (2.23), can be written as

$$ikp_{total}\sin\theta^{+} = \frac{1}{r}\left(\frac{\partial p_{total}}{\partial\phi}\right)_{\phi=\beta} \tag{2.27}$$

and

$$ikp_{total}\sin\theta^{-} = -\frac{1}{r}\left(\frac{\partial p_{total}}{\partial\phi}\right)_{\phi=-\beta} \tag{2.28}$$

or in more familiar form

$$\pm\frac{\partial p_{total}}{\partial\phi} + ikr\sin\theta^{\pm}p_{total} = 0 \qquad \phi = \pm\beta \tag{2.29}$$

Using the expressions found in Eqs. (2.22) and (2.14) for the incident and the scattered pressure the boundary conditions Eqs. (2.29) for $\phi = \beta$ and $\phi = -\beta$, respectively, become

$$\int_{\gamma} P(\cos\alpha)[\sin\theta^{+} + \sin(\beta-\alpha)]e^{-ikr\cos(\beta-\alpha)}d\alpha$$

$$= -p_o(\sin\theta^{+} - \sin(\beta-\phi_o))e^{ikr\cos(\beta-\phi_o)} \tag{2.30}$$

$$\int_\gamma P(\cos\alpha)[\sin\theta^- + \sin(\beta+\alpha)]e^{-ikrcos(\beta+\alpha)}d\alpha$$

$$= -p_o(\sin\theta^- - \sin(\beta+\phi_o))e^{ikrcos(\beta+\phi_o)} \qquad (2.31)$$

For reasons which will be explained in the next section it is beneficial to modify the boundary conditions into a different form. First consider the left hand side of the boundary condition for $\phi = \beta$, Eq. (2.30), on two different γ-paths, γ_1 and γ_2, shown on Fig. 2.4.

$$\int_{-i\infty}^{\pi+i\infty} P(\cos\alpha)[\sin\theta^+ + \sin(\beta-\alpha)]e^{-ikrcos(\beta-\alpha)}d\alpha$$

$$= \int_{-2\pi+\beta-i\infty}^{-\pi+\beta+i\infty} P(\beta-\alpha-\pi)[\sin\theta^+ - \sin\alpha]e^{ikrcos\alpha}d\alpha \qquad (2.32)$$

and

$$\int_{-\pi+i\infty}^{-2\pi-i\infty} P(\cos\alpha)[\sin\theta^+ + \sin(\beta-\alpha)]e^{-ikrcos(\beta-\alpha)}d\alpha$$

$$\int_{-\pi+\beta+i\infty}^{\beta-i\infty} P(\beta-\alpha-\pi)[\sin\theta^+ - \sin\alpha]e^{ikrcos\alpha}d\alpha \qquad (2.33)$$

where a new variable $\alpha' = \beta - \alpha - \pi$ is introduced in both of the above integrals, α' is replaced by α and the limits of integration are changed correspondingly. Adding the expressions in Eqs. (2.32) and (2.33), a new path $\bar{\gamma}$ is established as shown in Fig. 2.5, so that Eq. (2.30) reduces to

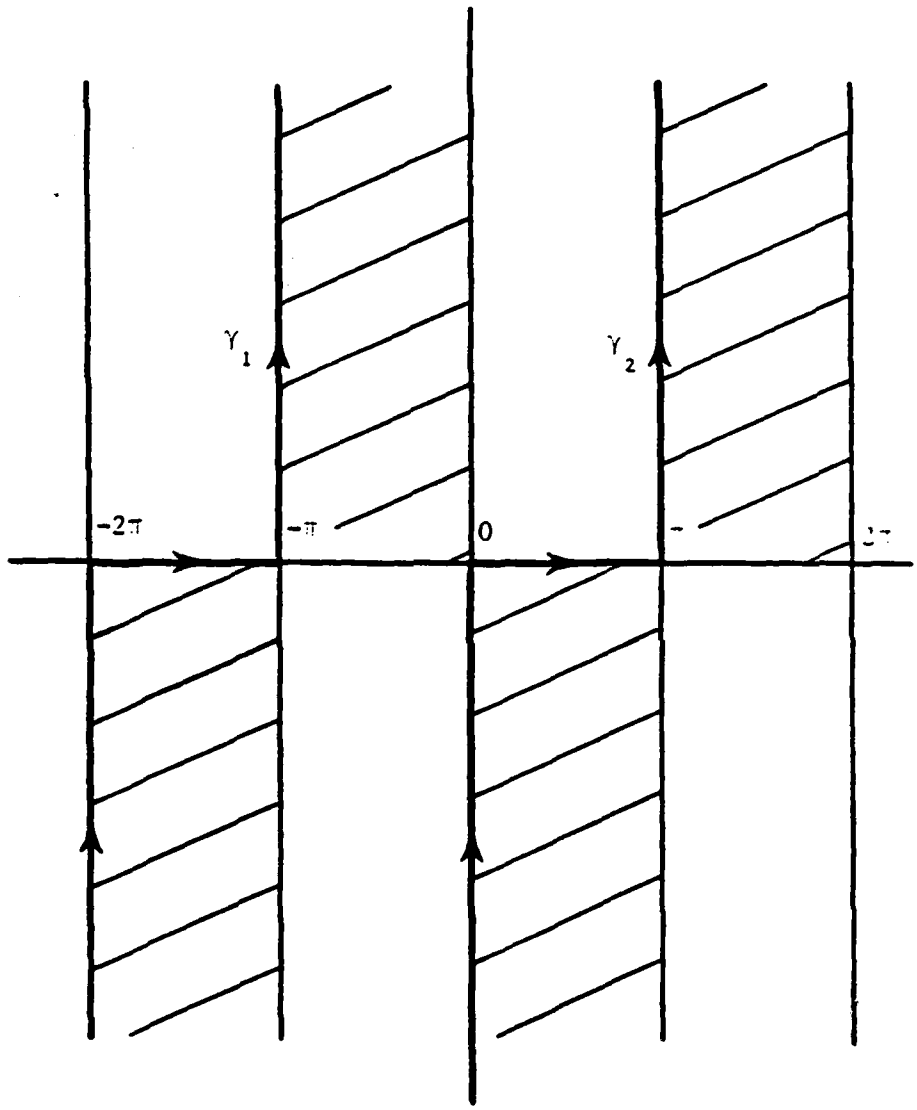

Fig. 2.4 γ-paths chosen for boundary condition at $\zeta = \xi$.

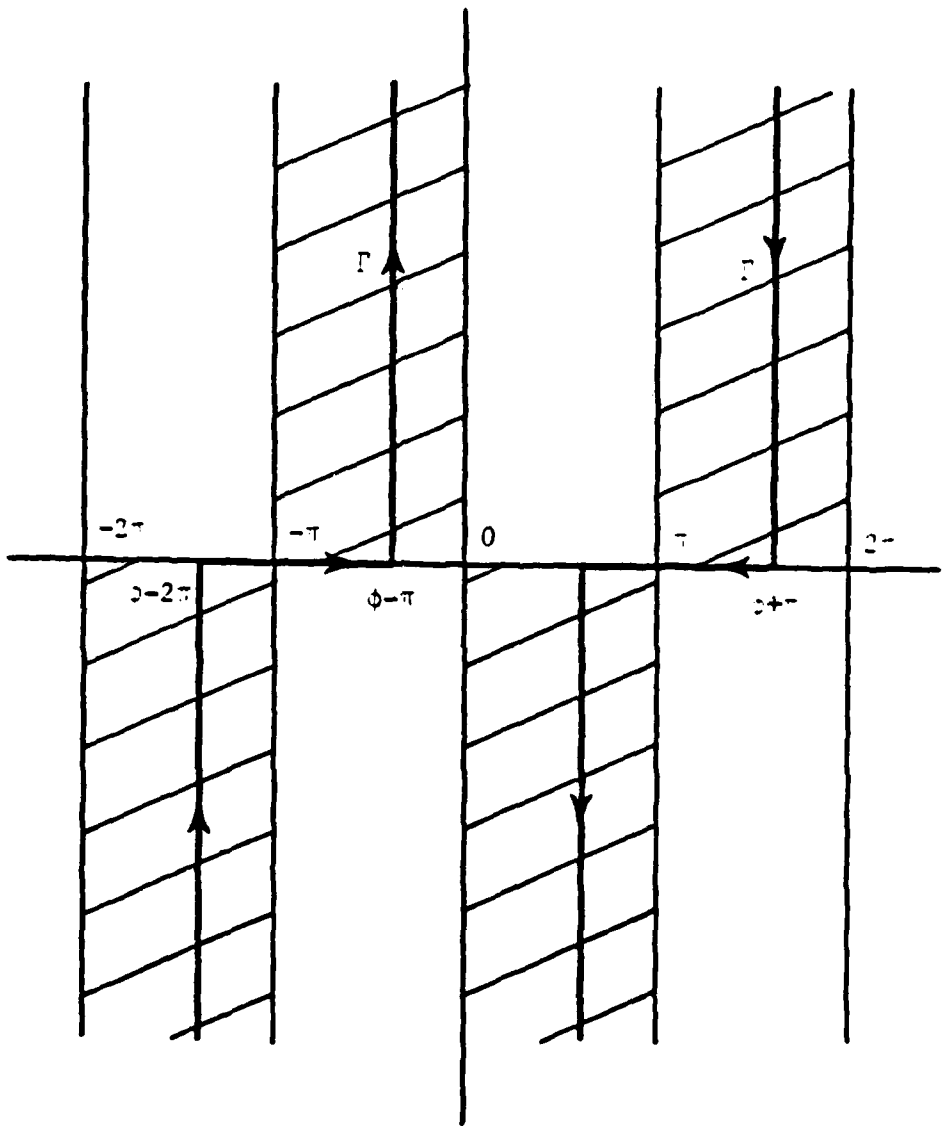

Fig. 2.5 Γ-path and convergence regions.

$$\int_{\Gamma} P(\beta-\alpha-\pi)[\sin\theta^{+} - \sin\alpha]e^{ikr\cos\alpha}d\alpha$$

$$= -2p_o(\sin\theta^{+} - \sin(\beta-\phi_o))e^{ikr\cos(\beta-\phi_o)} \quad . \tag{2.34}$$

The new path Γ is thus the addition of two γ paths.

Similarly, if the above procedure is performed on the second boundary condition, Eq. (2.31), integrated on the path shown in Fig. 2.6, with a change of variable $\alpha' = \beta+\alpha-\pi$, the resulting equation is

$$\int_{\Gamma} P(-\beta+\alpha+\pi)[\sin\theta^{-} - \sin\alpha]e^{ikr\cos\alpha}d\alpha$$

$$= -2p_o(\sin\theta^{-} - \sin(\beta+\phi_o))e^{ikr\cos(\beta+\phi_o)} \quad . \tag{2.35}$$

In addition to the above integral equations there are two more conditions that are to be satisfied, namely continuity of pressure and velocity at $y = 0$ between the two regions $y \lesseqgtr 0$. The two regions are joined together at $\phi = 0°$. Then the continuity of pressure at $\phi = 0°$, using Eqs. (2.14) and (2.22) is as follows:

$$\int_{\gamma_1} P(\cos\alpha)e^{-ikr\cos\alpha}d\alpha + p_o e^{ikr\cos\phi_o}$$

$$= \int_{\gamma_2} P(\cos\alpha)e^{-ikr\cos\alpha}d\alpha + p_o e^{ikr\cos\phi_o} \quad , \tag{2.36}$$

where the paths γ_1 and γ_2 may be taken as one of the many possible γ-paths.

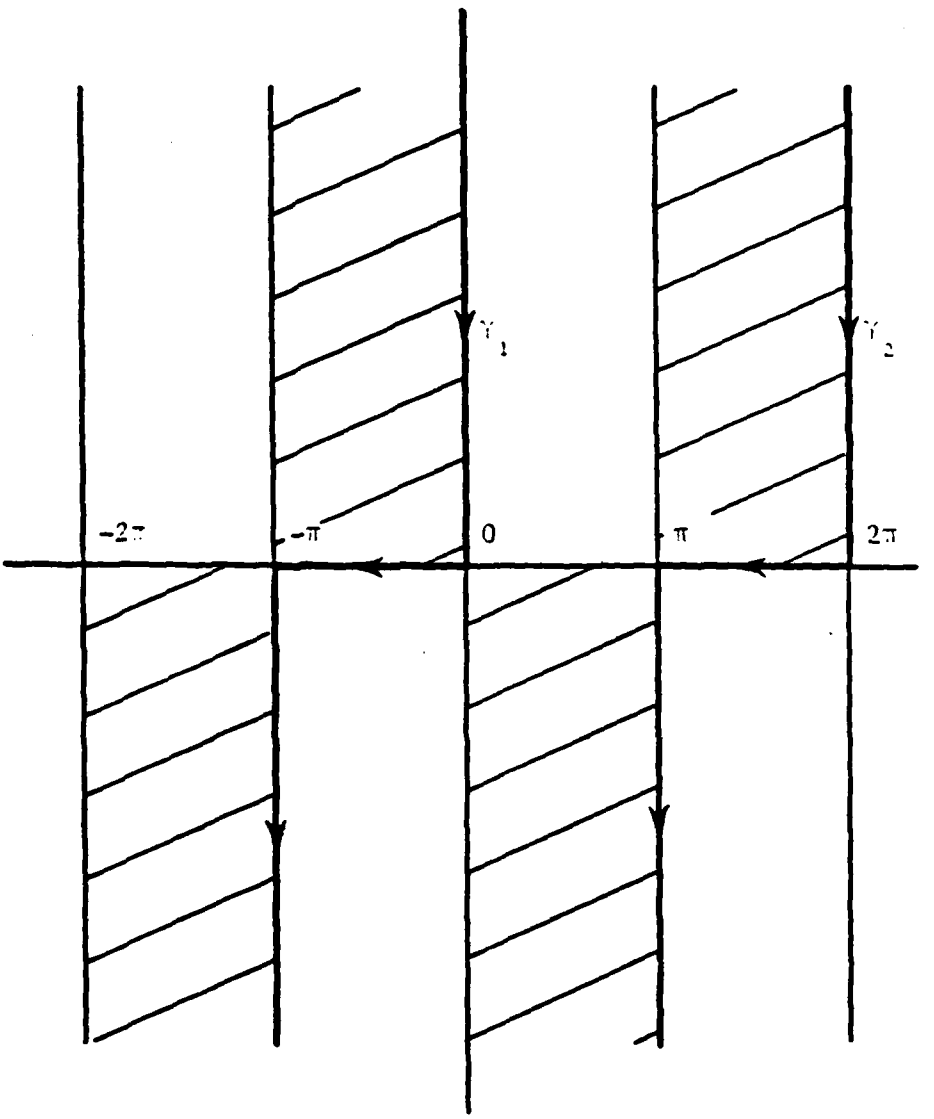

Fig. 2.6 γ-paths chosen for boundary condition at $\zeta = -\beta$.

The transverse component of the velocity for the incident wave is given by

$$v_{i\phi} = \frac{i}{k\rho cr}\frac{\partial}{\partial\phi}p_i = p_o\frac{\sin(\phi-\phi_o)}{\rho c}e^{ikr\cos(\phi-\phi_o)} \tag{2.37}$$

and the velocity for the diffracted pressure is given by

$$v = \frac{i}{k\rho cr}\frac{\partial}{\partial\phi}p(r,\phi) = -\frac{1}{\rho c}\int_\gamma P(\cos\alpha)\sin(\phi\mp\alpha)e^{-ikr\cos(\phi\mp\alpha)}d\alpha \tag{2.38}$$

Then the condition for the continuity of velocity at $\phi=0°$ becomes

$$\int_{\gamma_1} P(\cos\alpha)\sin\alpha e^{-ikr\cos\alpha}d\alpha = -\int_{\gamma_2} P(\cos\alpha)\sin\alpha e^{-ikr\cos\alpha}d\alpha \tag{2.39}$$

The paths of integration for Eqs. (2.36) and (2.39) are given in Fig. 2.7.

2.5 Solution for Plane Wave Incidence

To solve the problem one must attempt to construct a spectrum function $P(\cos\alpha)$, that will satisfy the boundary conditions and the continuity requirements.

The construction of the function can be made by closing the Γ-path in Eqs. (2.35) and (2.36) within a region of convergence and invoking the Cauchy integral formula. If one succeeds in closing the path Γ, then the encircled poles would have residues that satisfy the right hand side of the boundary conditions.

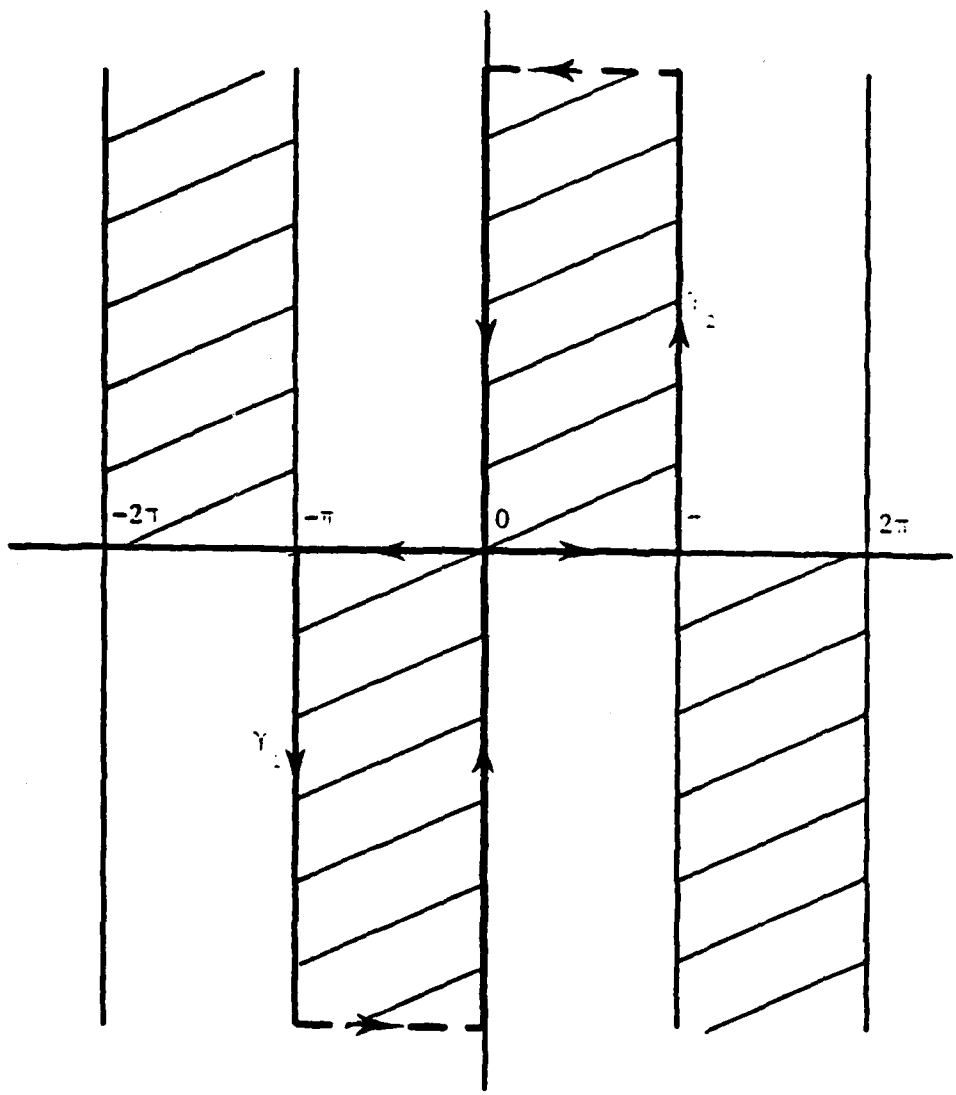

Fig. 2.7 The γ-paths for continuity of velocity.

Fig. 2.8 shows how a Γ-path may be closed. The integrals, Eqs. (2.35) and (2.36), around a closed Γ-path must have the sum of their residues equal to the right-hand side of these equations. For example, consider the first boundary condition Eq. (2.35)

$$[\int_{\Gamma}+\int_{U_1}+\int_{U_2}]P(\beta-\alpha-\pi)(\sin\theta^{+}-\sin\alpha)e^{-ikr\cos\alpha}d\alpha$$

$$= -2p_o(\sin\theta^{+} - \sin(\beta-\phi_o))e^{ikr\cos(\beta-\phi_o)} \qquad (2.40)$$

The paths U_1 plus U_2 are called loop integral in Maliuzhinets' theorem I (Appendix A). A loop integral is zero

$$\int_{U_1+U_2} S(z)e^{ikr\cos z}dz = 0 \qquad (2.41)$$

if the function S(z) is even, i.e., if S(z) = S(-z). Thus one has to impose a condition of evenness on the function $P(\beta-\alpha-\pi)$ on path Γ, to make the loop integral contribution zero. This condition is imposed on the integrand to guarantee that the two integrals on U_1 and U_2 cancel out, so that the main contributions to the integral come from the poles which are encircled by the closed path.

The exponential parts of the integrand suggest that there are simple poles located at $\pm(\beta-\phi_o) \pm 2n\pi$ and the residues of these simple poles account for the right-hand side of the Eq. (2.35) which is

$$-2p_o(\sin\theta^{+} - \sin(\beta-\phi_o))e^{ikr\cos(\beta-\phi_o)}.$$

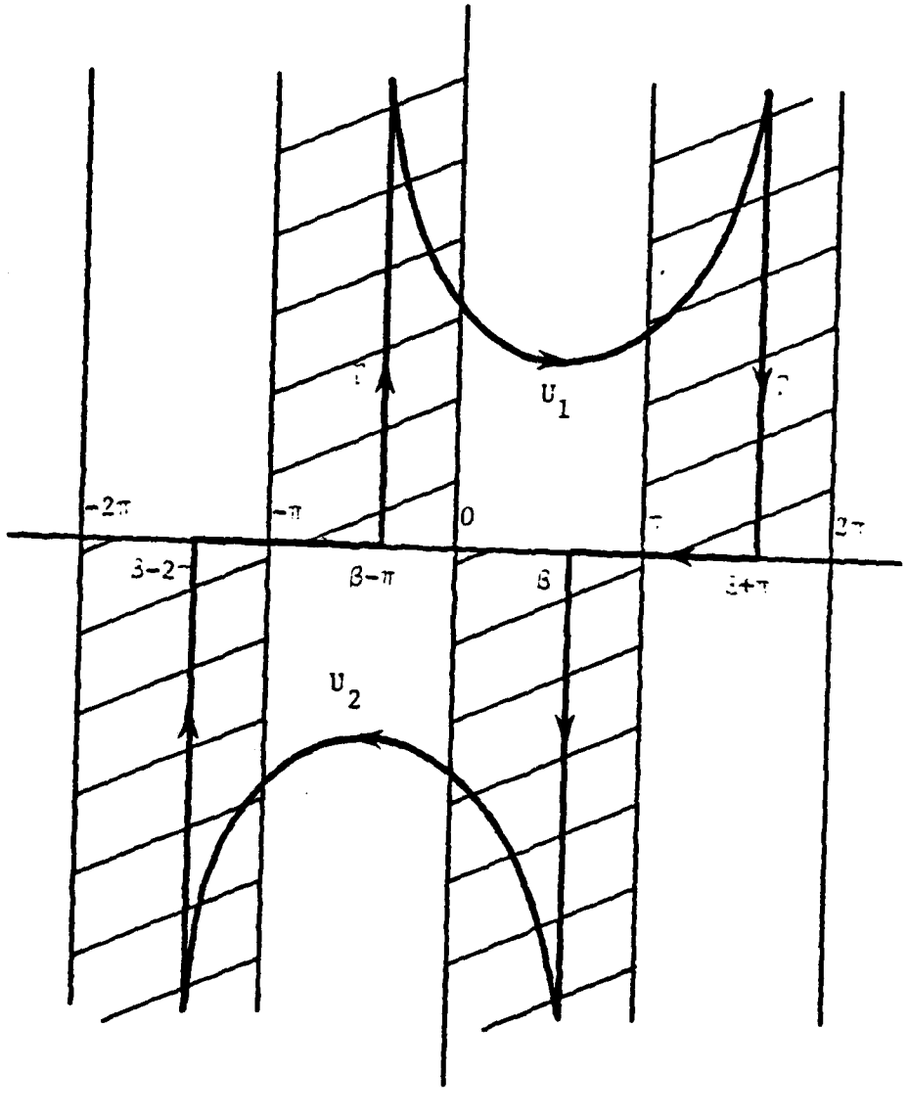

Fig. 2.8 Closure of path for boundary conditions.

The major characteristics for a function that will satisfy Eq. (2.35) are:

1) $P(\beta-\alpha-\pi)(\sin\theta^{+} - \sin\alpha)$ is even in α,

2) $P(\beta-\alpha-\pi)(\sin\theta^{+} - \sin\alpha)$ has simple poles at $\pm(\beta-\phi_o)\pm 2n\pi$ with corresponding residues

$$-\frac{P_o}{2\pi i}(\sin\theta^{+} - \sin(\beta-\phi_o))e^{ikr\cos(\beta-\phi_o)}$$

Likewise, the integral Eq. (2.36)

$$[\int_{\Gamma}+\int_{U_1}+\int_{U_2}]P(-\beta+\alpha+\pi)[\sin\theta^{-} - \sin\alpha]e^{ikr\cos\alpha}d\alpha$$

$$= -2p_o(\sin\theta^{-} - \sin(\beta+\phi_o))e^{ikr\cos(\beta+\phi_o)} \qquad (2.42)$$

suggests the following requirements.

1) $P(-\beta+\alpha+\pi)(\sin\theta^{-} - \sin\alpha)$ is even in α,

2) $P(-\beta+\alpha+\pi)(\sin\theta^{-} - \sin\alpha)$ has simple poles at $\pm(\beta+\phi_o)\pm 2n\pi$ and corresponding residues

$$-\frac{P_o}{2\pi i}(\sin\theta^{-} - \sin(\beta+\phi_o))e^{ikr\cos(\beta+\phi_o)}$$

To accommodate all of the above requirements the spectrum function is considered as the sum of two parts. One part has poles whose residues satisfy the first boundary condition, the other part has poles whose residues satisfy the second boundary condition. Two such functions that have the proper singularities and provide the proper residues are chosen as

$$-\frac{p_o}{4\beta i}\frac{\cos\frac{\pi}{2\beta}\phi_o/2\beta}{\sin\frac{\pi}{2\beta}(\alpha+\pi)-\sin\frac{\pi}{2\beta}\phi_o}\quad\frac{\sin\theta^+ - \sin(\beta-\alpha)}{\sin\theta^+ + 2\sin(\frac{\beta-\alpha}{2})\sin(\frac{\beta-\phi_o}{2})} \tag{2.43}$$

and

$$\frac{p_o}{4\beta i}\frac{\cos\frac{\pi}{2\beta}\phi_o/2\beta}{\sin\frac{\pi}{2\beta}(\alpha-\pi)-\sin\frac{\pi}{2\beta}\phi_o}\quad\frac{\sin\theta^- - \sin(\beta+\alpha)}{\sin\theta^- + 2\sin(\frac{\beta+\alpha}{2})\sin(\frac{\beta+\phi_o}{2})} \tag{2.44}$$

If one takes the first of the above functions and encloses the simple pole at $\alpha=\beta-\phi_o$, the resulting residue is

$$\frac{p_o}{2\pi i}(\sin\theta^+ - \sin(\beta-\phi_o))e^{ikr\cos(\beta-\phi_o)}$$

Similarly, the residues at $\alpha=\beta+\phi_o$ is given by

$$-\frac{p_o}{2\pi i}(\sin\theta^- - \sin(\beta+\phi_o))e^{ikr\cos(\beta+\phi_o)}$$

The two functions happen to be what is required to satisfy the boundary conditions. The condition of evenness can be easily verified by substituting $\beta-\alpha-\pi$ and $-\beta+\alpha+\pi$ in Eqs. (2.40) and (2.42) respectively.

One further heuristic requirement is that for an absorbent wedge, solution of the far-field pressure must cancel out identically at both boundaries due to the absorption of the energy by the wedge surfaces. By introducing two new functions that multiply Eqs. (2.43)

and (2.44), the final form of $P(\cos\alpha)$ is obtained.

$$P(\cos\alpha) = M_1(\alpha)\psi_1(\alpha) - M_2(\alpha)\psi_2(\alpha) \tag{2.45}$$

where $M_1(\alpha)$ and $M_2(\alpha)$ are the Maliuzhinets angle factors.

$$M_1(\alpha) = \frac{\cos\pi\phi_o/2\beta}{\sin\frac{\pi}{2\beta}(\alpha+\pi)-\sin\frac{\pi}{2\beta}\phi_o} \tag{2.46}$$

$$M_2(\ ) = \frac{\cos\pi\phi_o/2\beta}{\sin\frac{\pi}{2\beta}(\alpha-\pi)-\sin\frac{\pi}{2\beta}\phi_o} \tag{2.47}$$

and $\psi_1(\alpha)$ and $\psi_2(\alpha)$ are defined by

$$\psi_1(\alpha) = \frac{p_o}{4\beta i}\frac{[\sin\vartheta^+ - \sin(\beta-\alpha)]}{[\sin\vartheta^+ + 2\sin(\frac{\beta-\alpha}{2})\sin(\frac{\beta-\phi_o}{2})]}$$

$$\{\sin\vartheta^- + 4\tan(\frac{2\beta-\alpha-\phi_o-\pi}{4})\tan(\frac{\alpha-\phi_o+\pi}{4})$$

$$[\sin(\frac{\beta-\alpha}{2})\tan(\frac{2\beta-\alpha-\phi_o-\pi}{4})\tan(\frac{\alpha-\phi_o+\pi}{4}) + \sin(\frac{\beta-\alpha}{4})\cos(\frac{3\beta-\alpha}{4})\cos\beta]\} /$$

$$\{\sin\vartheta^- + 4\tan(\frac{2\beta-\alpha-\phi_o-\pi}{4})\tan(\frac{\alpha-\phi_o+\pi}{4})$$

$$[\sin(\frac{\beta-\alpha}{2})\tan(\frac{2\beta-\alpha-\phi_o-\pi}{4})\tan(\frac{\alpha-\phi_o+\pi}{4}) - \sin(\frac{\beta-\alpha}{4})\cos(\frac{3\beta-\alpha}{4})\sin(\frac{\beta+\phi_o}{4})]\} \tag{2.48}$$

$$\psi_2(\alpha) = \frac{P_o}{4\beta i} \frac{[\sin\theta^- - \sin(\beta-\alpha)]}{[\sin\theta^- + 2\sin(\frac{\beta+\alpha}{2})\sin(\frac{\beta+\phi_o}{2})]}$$

$$\{\sin\theta^+ + 4\tan(\frac{2\beta+\alpha+\phi_o-\pi}{4})\tan(\frac{-\alpha+\phi_o+\pi}{4})$$

$$[\sin(\frac{\beta+\alpha}{2})\tan(\frac{2\beta+\alpha+\phi_o-\pi}{4})\tan(\frac{-\alpha+\phi_o-\pi}{4}) + \sin(\frac{\beta+\alpha}{4})\cos(\frac{3\beta+\alpha}{4})\cos\beta]\}/$$

$$\{\sin\theta^+ + 4\tan(\frac{2\beta+\alpha+\phi_o-\pi}{4})\tan(\frac{-\alpha+\phi_o+\pi}{4})$$

$$[\sin(\frac{\beta+\alpha}{4})\tan(\frac{2\beta+\alpha+\phi_o-\pi}{4})\tan(\frac{-\alpha+\phi_o+\pi}{4}) - \sin(\frac{\beta+\alpha}{2})\cos(\frac{3\beta+\alpha}{4})\sin(\frac{\beta-\phi_o}{4})]\} \quad (2.49)$$

When one of the surfaces is rigid, a special form of $P(\cos\alpha)$ is needed since there is no absorption at that boundary. For these special cases, the functions $\psi_1(\alpha)$ and $\psi_2(\alpha)$ can be modified as follows when $\theta^- = 0°$

$$\psi_1(\alpha) = \frac{P_o}{4\beta i} \frac{[\sin\theta^+ - \sin(\beta-\alpha)]}{[\sin\theta^+ + 2\sin(\frac{\beta-\alpha}{2})\sin(\frac{\beta-\phi_o}{2})]}$$

$$\{\sin(\frac{\beta-\alpha}{2}) + 2\tan(\frac{2\beta-\alpha-\phi_o-\pi}{4})\tan(\frac{\alpha-\phi_o+\pi}{4})\cos\beta\}/$$

$$\{\sin(\frac{\beta-\alpha}{2}) - 4\tan(\frac{2\beta-\alpha-\phi_o-\pi}{4})\tan(\frac{\alpha-\phi_o+\pi}{4})\sin(\frac{2\beta-\alpha-\phi_o}{4})\cos(\frac{\alpha+\phi_o}{4})\} \quad (2.50a)$$

$$\psi_2(\alpha) = \frac{p_o}{4\beta i} \frac{-\cos(\frac{\beta+\alpha}{2})}{\sin(\frac{\beta+\phi_o}{2})}$$

$$\{\sin\theta^+ + 4\tan(\frac{2\beta+\alpha+\phi_o-\pi}{4})\tan(\frac{-\alpha+\phi_o+\pi}{4})$$

$$[\sin(\frac{\beta+\alpha}{2})\tan(\frac{2\beta+\alpha+\phi_o-\pi}{4})\tan(\frac{-\alpha+\phi_o+\pi}{4}) + \sin(\frac{\beta+\alpha}{4})\cos(\frac{3\beta+\alpha}{4})\cos\beta]\}/$$

$$\{\sin\theta^+ + 4\tan(\frac{2\beta+\alpha+\phi_o-\pi}{4})\tan(\frac{-\alpha+\phi_o+\pi}{4})$$

$$[\sin(\frac{\beta+\alpha}{2})\tan(\frac{2\beta+\alpha+\phi_o-\pi}{4})\tan(\frac{-\alpha+\phi_o+\pi}{4}) - \sin(\frac{\beta+\alpha}{4})\cos(\frac{3\beta+\alpha}{4})\sin(\frac{\beta-\phi_o}{4})]\} \quad (2.51a)$$

and when $\theta^+ = 0°$

$$\psi_1(\alpha) = \frac{p_o}{4\beta i} \frac{-\cos(\frac{\beta-\alpha}{2})}{\sin(\frac{\beta-\phi_o}{2})}$$

$$\{\sin\theta^- + 4\tan(\frac{2\beta-\alpha-\phi_o-\pi}{4})\tan(\frac{\alpha-\phi_o+\pi}{4})$$

$$[\sin(\frac{\beta-\alpha}{2})\tan(\frac{2\beta-\alpha-\phi_o-\pi}{4})\tan(\frac{\alpha-\phi_o+\pi}{4}) + \sin(\frac{\beta-\alpha}{4})\cos(\frac{3\beta-\alpha}{4})\cos\beta]\}/$$

$$\{\sin\theta^- + 4\tan(\frac{2\beta-\alpha-\phi_o-\pi}{4})\tan(\frac{\alpha-\phi_o+\pi}{4})$$

$$[\sin(\frac{\beta-\alpha}{2})\tan(\frac{2\beta-\alpha-\phi_o-\pi}{4})\tan(\frac{\alpha-\phi_o+\pi}{4}) - \sin(\frac{\beta-\alpha}{4})\cos(\frac{3\beta-\alpha}{4})\sin(\frac{\beta+\phi_o}{4})] \quad (2.50b)$$

$$\psi_2(\alpha) = \frac{P_o}{4\beta i} \frac{[\sin\theta^- - \sin(\beta+\alpha)]}{[\sin\theta^- + 2\sin(\frac{\beta+\alpha}{2})\sin(\frac{\beta+\phi_o}{2})]}$$

$$\{\sin(\frac{\beta+\alpha}{2}) + 2\tan(\frac{2\beta+\alpha+\phi_o-\pi}{4})\tan(\frac{-\alpha+\phi_o+\pi}{4})\cos\beta\}\Big/$$

$$\{\sin(\frac{\beta+\alpha}{2}) - 4\tan(\frac{2\beta+\alpha+\phi_o-\pi}{4})\tan(\frac{-\alpha+\phi_o+\pi}{4})\sin(\frac{2\beta+\alpha+\phi_o}{4})\cos(\frac{\alpha+\phi_o}{4}) \qquad (2.51b)$$

It is necessary to show that the function $P(\cos\alpha)$, when substituted in Eqs. (2.36) and (2.39), represents continuous pressure and velocity fields. Eq. (2.36) clearly implies that the pressure is continuous at $\phi = 0°$. Continuity of velocity requires further attention. Consider two paths of integration in the domain $-\pi \leq \alpha \leq \pi$, where there are two possible poles: $2\beta - \phi_o - \pi$ and $-\pi + \phi_o$. A small absorption should be added to avoid wave generation at infinity, so that the simple poles become $2\beta - \phi_o - \pi - i\eta$ and $-\pi + \phi_o + i\eta$ (Fig. 2.9). Then there are no poles left in the convergent regions and hence the residues are zero. Therefore, the continuity of the velocity is identically satisfied.

2.6 Far-field Solution for a Plane Wave Incident

Frequently in wave propagation problems the field pressure at large distances from the source is desired. Consider the integral in Eq. (2.14) with the upper sign for the case when $0 \leq \phi \leq \beta$.

$$p = \int_\gamma P(\cos\alpha)\, e^{-ikr\cos(\theta-\alpha)}\, d\alpha \qquad (2.52)$$

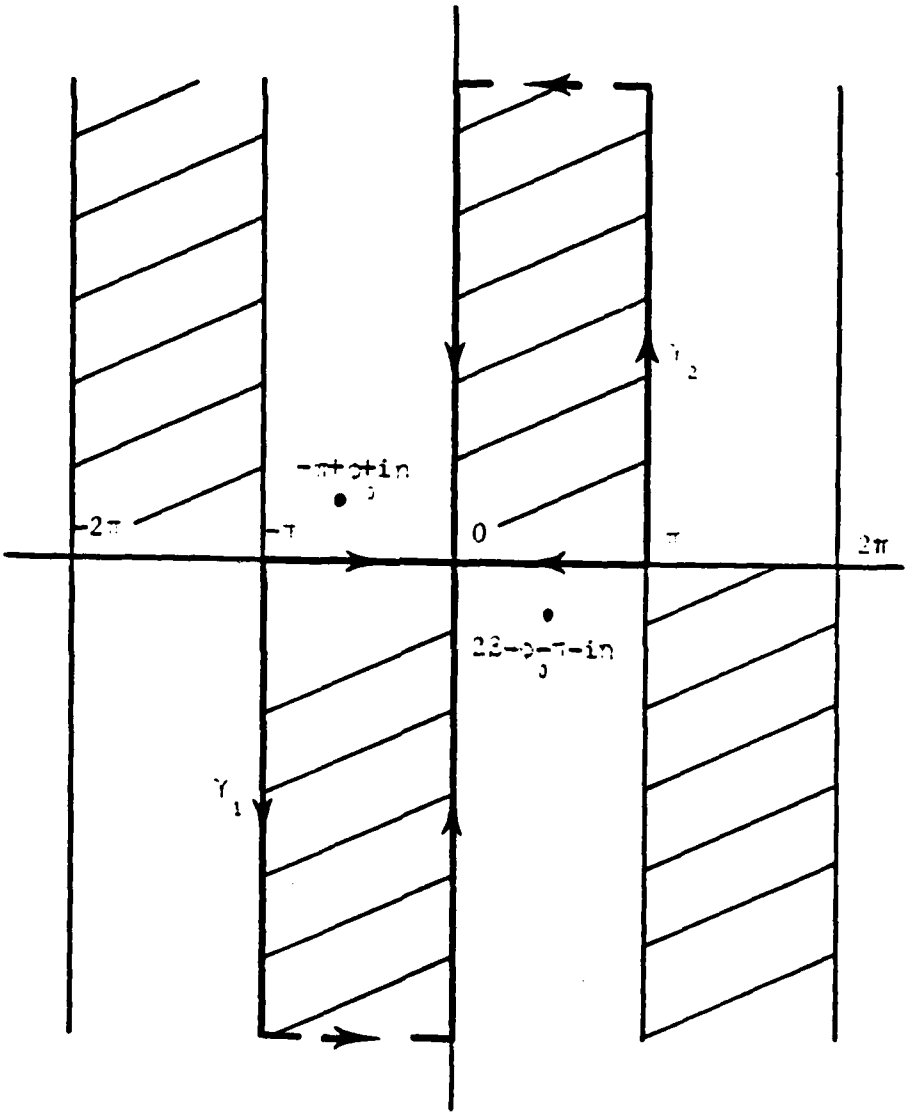

Fig. 2.9 Closure of path for satisfying continuity of velocity.

If the non-dimensional distance kr can be taken large enough then it is possible to get an asymptotic value of the integral by the steepest descent method. The method is one of finding the saddle point (or extremum point) and integrating along the exponentially decaying steepest descent path which passes through the saddle point. The path of integration should be chosen such that $Re(-ikrcos(\phi-\alpha))$ has a maximum value at some point. Therefore the function has an extremum if

$$\frac{\partial}{\partial\alpha}\,(-ikrcos(\phi-\alpha)) = 0\ . \tag{2.53}$$

Then the saddle points are located at

$$\alpha = \phi \pm 2n\pi \tag{2.54}$$

and the corresponding steepest descent paths are defined by:

$$Im(-ikrcos(\phi-\alpha)) = -kr = const \tag{2.55}$$

or

$$cos(\phi-\alpha_r)cosh\alpha_i = 1 \tag{2.56}$$

The above expression is the equation of the steepest descent path which passes through points $\alpha_r = \phi \pm 2n\pi$. It is helpful to know the slope at the saddle points and asymptotes as $\alpha_i \to \pm\infty$. The

slope and the asymptotes are determined from Eq. (2.56) as follows:

$$\frac{\partial \alpha_i}{\partial \alpha_r} = \pm \cosh\alpha_i = \pm 1 \text{ at } \alpha_i = 0 \tag{2.57}$$

and

$$\cos(\phi - \alpha_r) = 0 \quad \text{as} \quad \alpha_i = \pm \infty \tag{2.58}$$

or

$$\alpha_r = \phi \pm (2n-1)\frac{\pi}{2} . \tag{2.59}$$

For the observer angles $0 \leq \phi \leq \beta$, the steepest descent path is sketched in Fig. 2.10 by the use of Eqs. (2.54), (2.57) and (2.59).

After completely defining the saddle point and the steepest descent path, an approximation of the integral in Eq. (2.52) is written as [31],

$$\int_{SDP} P(\cos\alpha)\, e^{-ikr\cos(\phi-\alpha)} d\alpha$$

$$= \sqrt{\frac{2\pi}{kr}}\, e^{i\pi/4}\, e^{-ikr}\, P(\cos\phi) \tag{2.60}$$

It should be noted that the solution in Eq. (2.60) is valid for large values of kr and an observer angle ϕ not close to the incident and reflection shadow boundaries where the function $P(\cos\phi)$ becomes unbounded.

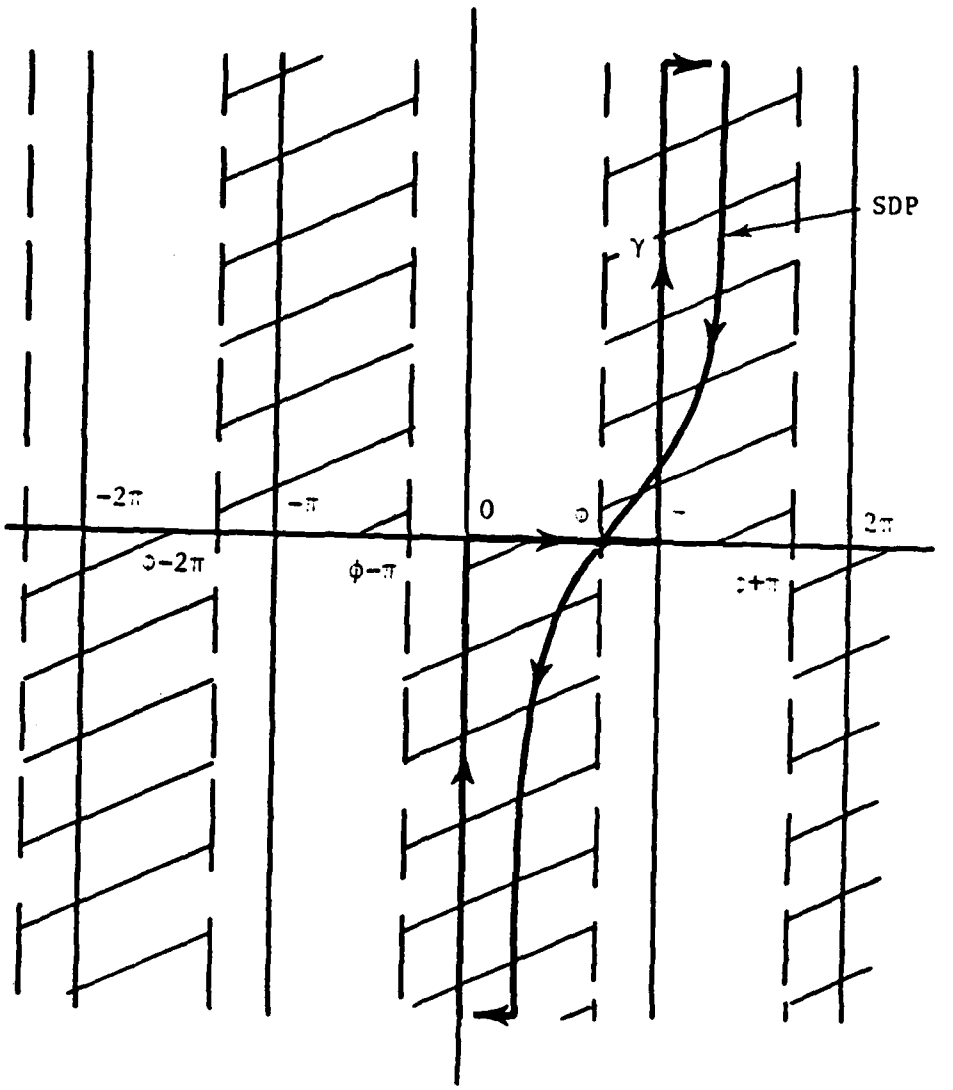

Fig. 2.10 Path of steepest descent.

2.7 Geometric Acoustics

The acoustic scattering by a wedge can be presented in two parts, a diffracted part and a geometric part. The steepest descent path contributes the diffracted part which is given in Eq. (2.60) for large kr. While the pole that is surrounded by the closed path contributes the geometric part.

Consider the case where the receiver angle ϕ is in the region $2\beta - \phi_o - \pi < \phi < \beta$. The path can be closed by the γ-path and the steepest descent path so that the pole is surrounded as shown in Fig. (2.11). Then the solution in this region becomes:

$$p(r,\phi) = \frac{p_o}{2} C_r e^{ikr\cos(\phi-\phi_o)} + p_d(r,\phi) \tag{2.61}$$

where p_d when kr is large is given by Eq. (2.60) and C_r is the reflection coefficient defined as:

$$C_r = \frac{\sin(\beta-\phi_o)-\sin\theta^+}{\sin(\beta-\phi_o)+\sin\theta^+} \quad . \tag{2.62}$$

If the receiver is placed at $0 > \phi > 2\beta - \phi_o - \pi$ (see Fig. 2.12) the solution is given by:

$$p(r,\phi) = -\frac{p_o}{2} C_r e^{ikr\cos(\phi-\phi_o)} + p_d(r,\phi) \tag{2.63}$$

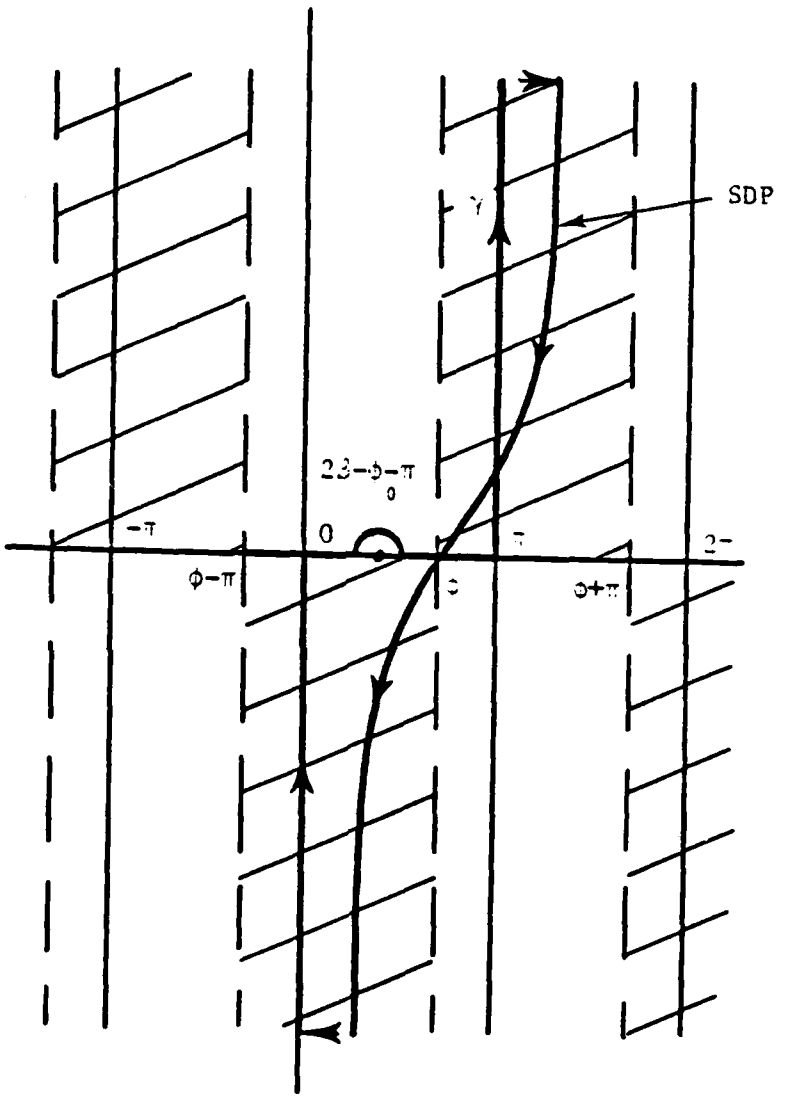

Fig. 2.11 Path of integration for the far-field with $2\beta - \phi_0 - \pi < \phi < \beta$.

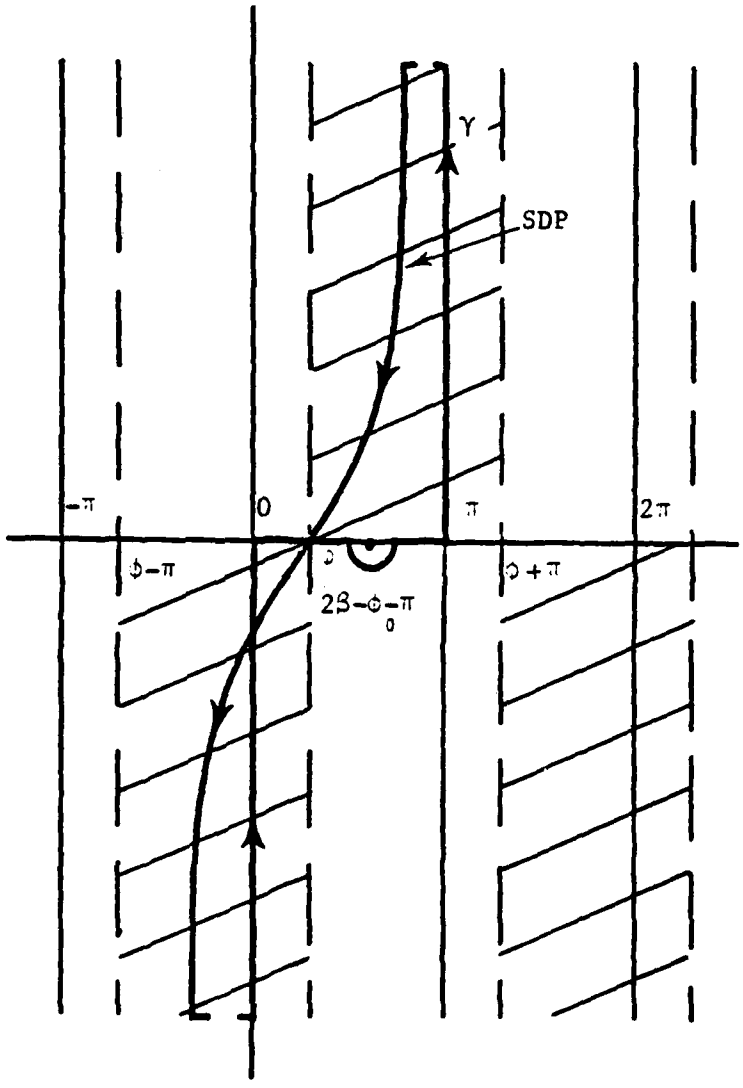

Fig. 2.12 Path of integration for the far-field with $0 > \phi > 2\beta - \phi_0 - \pi$.

The change in sign between Eqs. (2.61) and (2.63) represents the sudden transition across the reflection shadow boundary. Thus, the total field in the different regions shown in Fig. 2.13 can be written as:

$$
\begin{aligned}
p_t &= p_d + p_i + p_r && \text{Region (I)} \\
&= p_d + p_i && \text{Region (II)} \\
&= p_d && \text{Region (III)}
\end{aligned}
\qquad (2.64)
$$

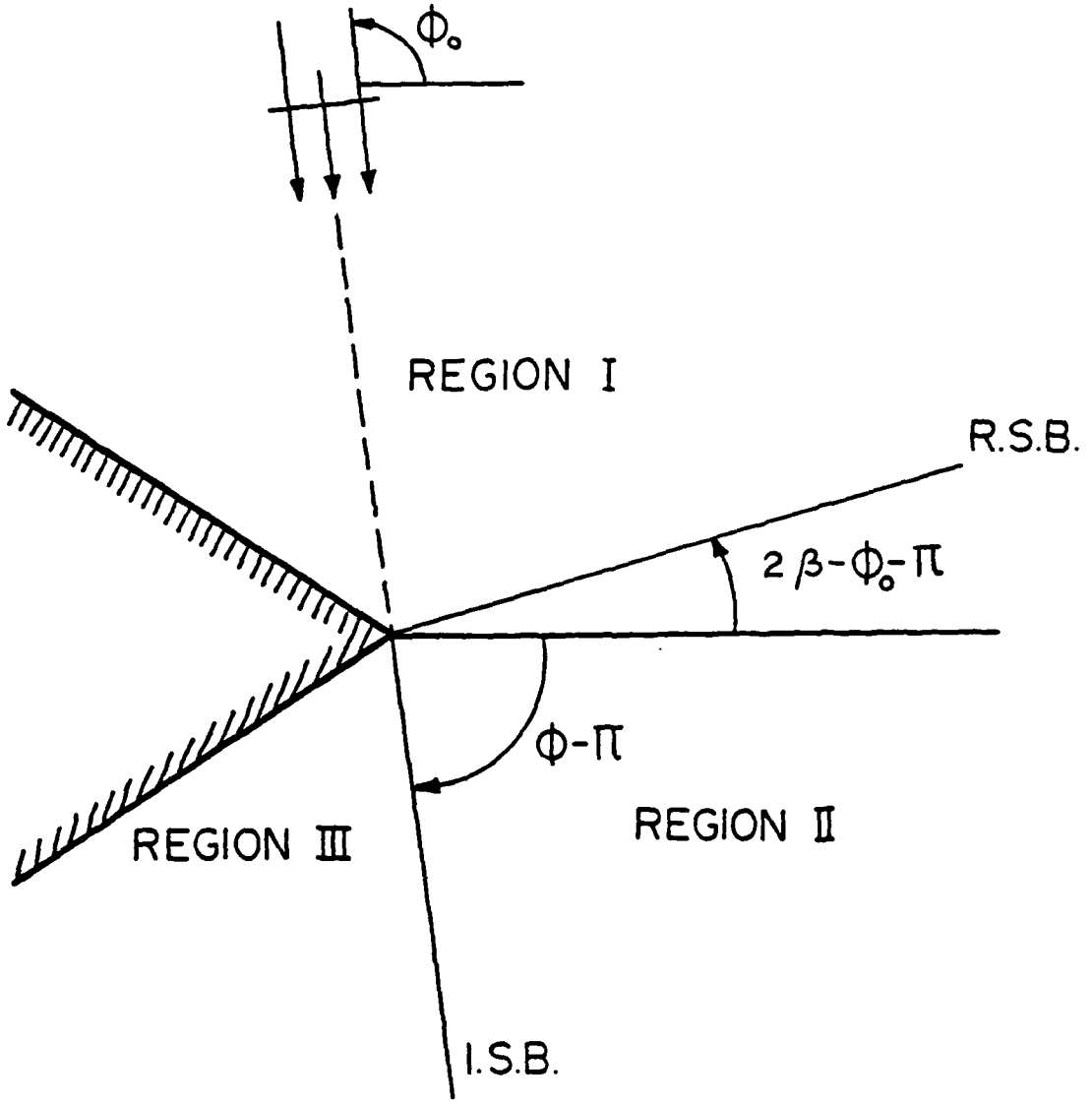

Fig. 2.13 Regions of validity of the solution (Eq. 2.64).

CHAPTER III

SOLUTIONS VALID FOR MID-RANGE AND AT SHADOW BOUNDARIES

3.1 Mid-range Solution for a Plane Wave Source

In the asymptotic solution for the far-field there are discontinuities near the shadow boundaries, because the coefficients $M_1(\alpha)$ and $M_2(\alpha)$ are singular at these angles. These regions are referred to as transition regions. To have a continuous total field, one has to derive a more exact solution which is bounded across these transition regions. A method was first proposed by Pauli [18] to achieve this task.

First, the spectrum function $P(\cos\alpha)$ in Eq. (2.45) can be manipulated to have the following convenient form.

$$P(\cos\alpha) = M_1(\alpha)\psi_1(\alpha) - M_2(\alpha)\psi_2(\alpha)$$

$$= \frac{1}{2}\{[\cot\frac{\pi}{4\beta}(\pi + (\alpha-\varphi_0)) + \tan\frac{\pi}{4\beta}(\pi+(\alpha+\varphi_0))]\psi_1(\alpha)$$

$$+ [\cot\frac{\pi}{4\beta}(\pi-(\alpha-\phi_0)) + \tan\frac{\pi}{4\beta}(\pi-(\alpha+\varphi_0))]\psi_2(\alpha)\} \qquad (3.1)$$

The integral for the pressure can now be treated as four separate integrals, each of which contains one simple pole. The first of these can be written as

$$p_1 = \frac{1}{2}\int_\gamma \psi_1(\alpha)\cot\frac{\pi}{4\beta}(\pi+(\alpha-\varphi_0))e^{-ikr\cos(\varphi-\alpha)}d\alpha \qquad (3.2)$$

By replacing α by $\varphi-\alpha$ and changing the limits of integration correspondingly (Fig. 3.1) the dependence of the exponential on the observer angle can be removed.

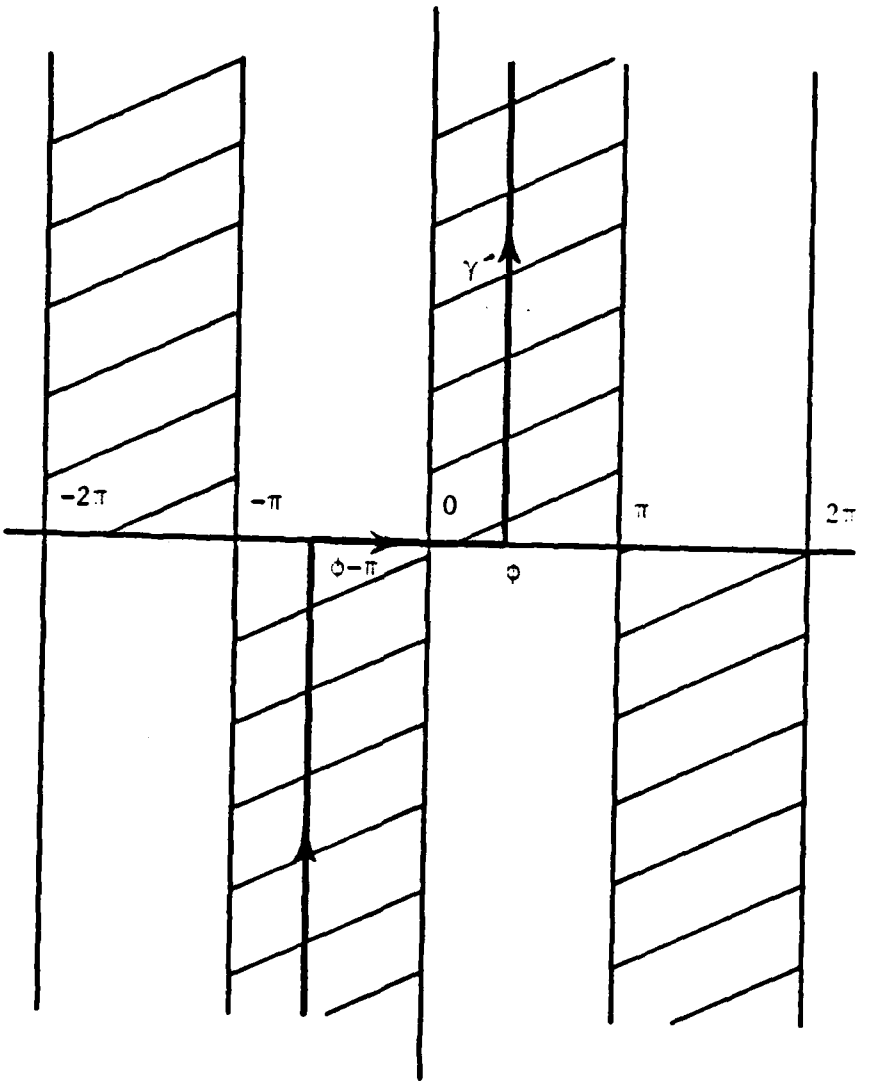

Fig. 3.1 Regions of convergence of the γ'-path.

$$P_1 = \frac{1}{2} \int_{\gamma'} \psi_1(\alpha-\phi)\cot\left(\frac{\pi+(\phi-\alpha-\phi_0)}{2n}\right) e^{-ikr\cos\alpha} d\alpha \tag{3.3}$$

where

$$n = \frac{2\beta}{\pi} \tag{3.4}$$

The singularity of the integrand can be separated by extracting the singularity explicitly, i.e., multiplying and dividing the integrand by a factor

$$\cos\alpha + \cos(2n\pi N^- + (\phi-\phi_0)) \tag{3.5}$$

Then Eq. (3.3) becomes

$$P_1 = \frac{1}{2} \int_{\gamma'} \psi_1(\alpha-\phi_0)\cot\left(\frac{\pi+(\phi-\alpha-\phi_0)}{2n}\right) \frac{\cos\alpha + \cos(2n\pi N^- + (\phi-\alpha-\phi_0))}{\cos\alpha + \cos(2n\pi N^- + (\phi-\alpha-\phi_0))} e^{-ikr\cos\alpha} d\alpha \tag{3.6}$$

where N^- is an integer which nearly satisfies the equation

$$2n\pi N^- - (\phi-\alpha-\phi_0) = -\pi \ . \tag{3.7}$$

This condition ensures that only one pole is generated and the other poles of the periodic functions of Eq. (3.5) are excluded.

In the method of steepest descent for the far-field approximation mentioned in the previous chapter, the saddle point is taken as the main contributor. The solution valid in the mid-range and at the shadow boundaries consists of evaluating the integral along the entire length of the steepest descent path.

Letting the conformal transformation

$$x^2 = ikr(\cos\alpha - 1);\quad x = \sqrt{2kr}\ e^{-i\pi/4} \sin\frac{\alpha}{2} \tag{3.8}$$

so that

$$\frac{d\alpha}{dx} = \sqrt{\frac{2}{kr}}\ e^{i\pi/4}/\cos\frac{\alpha}{2} \tag{3.9}$$

and substituting Eqs. (3.8) and (3.9) into (3.6) with limits $-\infty$ to ∞, it follows that:

$$p_1 = i\sqrt{\frac{kr}{2}}\, e^{i\pi/4}\, e^{-ikr} \int_{-\infty}^{\infty} \psi_1(\phi-\alpha)\cot\left(\frac{\pi+(\phi-\alpha-\varphi_o)}{2n}\right)$$

$$\frac{\cos\alpha+\cos(2n\pi N^- +(\phi-\alpha-\phi_o))}{x^2+ikr(\cos(2n\pi N^- +(\phi-\alpha-\phi_o)))}\ \frac{e^{-x^2}}{\cos\alpha/2}\ dx \tag{3.10}$$

By expanding the integrand in a Taylor series about the transformed saddle point $\alpha = 0$ and retaining only the leading term, Eq. (3.10) reduces to

$$p_1 = i\sqrt{\frac{kr}{2}}\ e^{i\pi/4}\, e^{-ikr}\, \psi_1(\phi)a^-(\phi-\varphi_o) \int_{-\infty}^{\infty} \frac{e^{-x^2}}{x^2+ikra^-(\varphi-\varphi_o)}\, dx \tag{3.11}$$

where

$$a^-(\varphi-\varphi_o) = 2\cos^2\left(\frac{2n\pi N^- + (\phi-\varphi_o)}{2}\right) \tag{3.12}$$

The real integrand in Eq. (3.11) can be expressed in terms of the complex Fresnel integrals [26].

$$b\int_{-\infty}^{\infty} \frac{e^{-\tau^2}}{\tau^2 + ib^2}\, d\tau = 2\sqrt{\pi}\ F(b) \tag{3.13}$$

where

$$F(b) = e^{ib^2} \int_b^\infty e^{-i\tau^2} d\tau \tag{3.14}$$

Another form of Fresnel function is given by:

$$F_o(b) = e^{ib^2} \int_o^b e^{-i\tau^2}\, d\tau. \tag{3.15}$$

Since

$$\int_{-\infty}^{\infty} e^{-i\tau^2}\, d\tau = 2 \int_o^\infty e^{-i\tau^2}\, d\tau = \sqrt{\pi}\, e^{-i\pi/4}, \tag{3.16}$$

and

$$F(b) + F_o(b) = \frac{1}{2} \sqrt{\pi}\, e^{-i\pi/4}\, e^{ib^2}\ , \tag{3.17}$$

then

$$F(b) = \frac{1}{2} \sqrt{\pi}\, e^{-i\pi/4}\, e^{ib^2} - F_o(b). \tag{3.18}$$

F(b) can be expressed in terms of C(b) and S(b)

$$F(b) = \frac{\sqrt{\pi}}{2}\ e^{ib^2}\ e^{-i\pi/4}$$

$$[1 - \sqrt{2}\ e^{i\pi/4}(C(b)-iS(b))] \tag{3.19}$$

where

$$C(b) = \sqrt{\frac{2}{\pi}} \int_o^b \cos\tau^2 d\tau, \tag{3.20}$$

and

$$S(b) = \sqrt{\frac{2}{\pi}} \int_o^b \sin\tau^2 d\tau. \tag{3.21}$$

Using Eqs. (3.19), (3.20) and (3.21), Eq. (3.11) can be rewritten as

$$p_1 = i \frac{\pi}{\sqrt{2}} \psi_1(\phi) \cot\left(\frac{\pi+(\phi-\phi_o)}{2n}\right) e^{-ikr} e^{ikra^-(\phi-\phi_o)}$$

$$\sqrt{a^-(\phi-\phi_o)} \left(1 - \sqrt{2}\, e^{i\pi/4} \left(C\left(\sqrt{kra^-(\phi-\phi_o)}\right) - iS\left(\sqrt{kra^-(\phi-\phi_o)}\right)\right)\right) \quad (3.22)$$

Similarly, expressions can be written for the remaining three terms of Eq. (3.1). Then the total diffraction field which behaves smoothly in the transition regions is given by :

$$p = i \frac{\pi}{\sqrt{2}} e^{-ikr}$$

$$\{\psi_1(\phi)\left[\cot\left(\frac{\pi+(\phi-\phi_o)}{2n}\right)F_-^1(\phi-\phi_o)\right.$$

$$\left. + \tan\left(\frac{\pi+(\phi+\phi_o)}{2n}\right)F_+^1(\phi+\phi_o-2\beta)\right]$$

$$+ \psi_2(\phi)\left[\cot\left(\frac{\pi-(\phi-\phi_o)}{2n}\right)F_-^1(\phi-\phi_o)\right.$$

$$\left. + \tan\left(\frac{\pi-(\phi+\phi_o)}{2n}\right)F_+^1(\phi+\phi_o+2\beta)\right]\} \quad (3.23)$$

where

$$F_\pm^1(x) = e^{ikra^\pm(x)} \sqrt{a^\pm(x)}$$

$$\left(1 - \sqrt{2}\, e^{i\pi/4} \left(C\left(\sqrt{kra^\pm(x)}\right) - iS\left(\sqrt{kra^\pm(x)}\right)\right)\right) \quad (3.24)$$

and

$$a^\pm(x) = 2\cos^2\left(\frac{2n\pi N^\pm - x}{2}\right) \quad (3.25)$$

in which $N^\pm$ are the integers which most nearly satisfy the following conditions [17]:

$$2n\pi N^{+}-x = \pi \tag{3.26a}$$

$$2n\pi N^{-}-x = -\pi \tag{3.26b}$$

3.2 Mid-range Solution for a Line Source

The diffraction field generated by a line source can be written by integrating the plane wave spectrum over two dimensional space, i.e.,

$$p(r,\phi) = \frac{e^{-i\pi/4}}{\sqrt{2\pi}} \int_{\gamma}\int_{\gamma} P(\alpha,\sigma)e^{-ikrcos(\phi-\alpha)}e^{-ikr_{o}cos(\phi_{o}-\sigma)}d\sigma d\alpha \tag{3.27}$$

Using the transformation $\phi - \alpha$ to α and $\phi_o - \alpha$ to σ and changing the limits correspondingly, one obtains:

$$p(r,\phi) = \frac{e^{-i\pi/4}}{\sqrt{2\pi}} \int_{\gamma_1}\int_{\gamma_2} P(\phi-\alpha,\phi_{o}-\sigma)e^{-ikrcos\alpha}\, e^{-ikr_{o}cos\sigma}d\sigma d\alpha \tag{3.28}$$

Consider the second term of the modified form of P(cosα) from Eq. (3.1)

$$P_2(\alpha,\sigma) = \frac{1}{2}\tan\frac{\pi}{4\beta}(\pi+(\alpha-\sigma))\psi_1(\alpha,\sigma) \tag{3.29}$$

where ϕ_o is replaced by σ and n denotes $2\beta/\pi$.

Substituting Eq. (3.29) into Eq. (3.28) leads to

$$p_2 = \frac{e^{-i\pi/4}}{2\sqrt{2\pi}} \int_{\gamma_1}\int_{\gamma_2} \psi_1(\phi-\alpha,\phi_{o}-\sigma)\tan\left(\frac{\pi+\phi-\alpha+\phi_{o}-\sigma}{2n}\right) e^{-ikrcos\alpha}\, e^{-ikr_{o}cos\sigma}d\sigma d\alpha \tag{3.30}$$

Then multiplying both the numerator and the denominator by the factor

$$\cos\tfrac{1}{2}(\phi+\phi_{o}-\alpha-\sigma+2n\pi N^{+})\cos\tfrac{1}{2}((\phi+\phi_{o}-\alpha+\sigma+2n\pi N^{+})$$

Eq. (3.30) becomes

$$p_2 = \frac{e^{-i\pi/4}}{4\sqrt{2\pi}} \int_{\gamma_1}\int_{\gamma_2} \{ \frac{\psi_1'(\phi-\alpha,\phi_o-\sigma)}{[\cos(\frac{\phi+\phi_o-\alpha-h}{2})-\sin\frac{\sigma}{2}]}$$

$$+ \frac{\psi_1(\phi-\alpha,\phi_o-\sigma)}{[\cos(\frac{\varphi+\phi_o-\sigma-h}{2})+\sin\frac{\alpha}{2}]} \} e^{-ikr\cos\alpha} e^{-ikr_o\cos\sigma} d\sigma d\alpha \quad (3.31)$$

where

$$h = 2\beta + 2n\pi N^+ \quad (3.32)$$

and

$$\psi_1'(\phi-\alpha,\phi_o-\sigma) = \psi_1(\phi-\alpha,\phi_o-\sigma)\tan(\frac{\pi+\phi-\alpha+\phi_o-\sigma}{2n})$$

$$\cos(\frac{\varphi+\phi_o-\alpha-\sigma-h}{2}) \quad . \quad (3.33)$$

In the first term of the Eq. (3.31) changing α by $-\alpha$, then

$$p_2 = \frac{e^{-i\pi/4}}{4\sqrt{2\pi}} \int_{\gamma_1}\int_{\gamma_2} \{ \frac{\psi_1'(\phi+\alpha,\phi_o-\sigma)}{[\cos(\frac{\phi+\phi_o+\alpha-h}{2})-\sin\frac{\sigma}{2}]}$$

$$+ \frac{\psi_1'(\phi-\alpha,\phi_o-\sigma)}{[\cos(\frac{\varphi+\phi_o-\alpha-h}{2})+\sin\frac{\sigma}{2}]} \} e^{-ikr\cos\alpha} e^{-ikr_o\cos\sigma} d\sigma d\alpha \quad (3.34)$$

$$= \frac{e^{-i\pi/4}}{2\sqrt{2\pi}} \int_{\gamma_1} \int_{\gamma_2}$$

$$\{\psi_1'(\phi+\alpha,\phi_o-\sigma)[\cos(\frac{\phi+\phi_o-\alpha-h}{2})+\sin\frac{\sigma}{2}]+\psi_1'(\phi-\alpha,\phi_o-\sigma)[\cos(\frac{\phi+\phi_o+\alpha-h}{2})-\sin\frac{\sigma}{2}] /$$

$$[\cos\alpha+\cos\sigma-4\sin(\frac{\phi+\phi_o-h}{2})\sin\frac{\sigma}{2}\sin\frac{\alpha}{2}+2\cos^2(\frac{\phi+\phi_o-h}{2})]\}e^{ikr\cos\alpha}e^{-ikr\cos\sigma}d\sigma d\alpha \tag{3.35}$$

After introducing new variables,

$$\sin\frac{\alpha}{2} = \frac{1}{\sqrt{2}} e^{i\pi/4}\xi \tag{3.36}$$

$$\sin\frac{\sigma}{2} = \frac{1}{\sqrt{2}} e^{i\pi/4}\eta \tag{3.37}$$

and expanding the numerator of Eq. (3.35) around the saddle point $\alpha = 0$ leads to

$$p_2 = \frac{2e^{-i\pi/4}}{\sqrt{2\pi}} \psi'(\phi,\phi_o)\cos(\frac{\phi+\phi_o-h}{2})$$

$$i\int_{-\infty}^{\infty}\int_{-\infty}^{\infty} - \frac{e^{-ikr\xi^2}\, e^{-ikr_o\eta^2}\, d\eta d\xi}{[\xi^2+\eta^2+2\sin(\frac{\phi+\phi_o-h}{2})\eta\xi+2i\cos^2(\frac{\phi+\phi_o-h}{2})]} \tag{3.38}$$

in which only the leading term of the Taylor series is retained.

Furthermore changing ξ and η to ρ and γ through

$$\xi = \sqrt{\frac{R_1}{r}}\,\rho\cos\gamma \tag{3.39}$$

and

$$\eta = \sqrt{\frac{R_1}{r_o}}\,\rho\sin\gamma \tag{3.40}$$

where

$$R_1 = r_o + r \tag{3.41}$$

yields

$$p_2 = \frac{i2e^{-i\pi/4}}{\sqrt{2\pi}} e^{-ik(r+r_o)} \psi_1(\phi,\phi_o)\cos^2\left(\frac{\phi+\phi o-h}{2}\right)$$

$$\int_o^\infty \rho K(\rho)\, e^{-kR_1\rho^2} d\rho \tag{3.42}$$

with

$$K(\rho)= \int_o^{2\pi} \frac{d\gamma}{\rho^2[\sqrt{r/r_o}\cos^2\gamma+\sqrt{r_o/r}\sin^2\gamma+\sin\left(\frac{\phi+\phi_o-h}{2}\right)\sin 2\gamma]+2i\sqrt{rr_o/R_1}\cos^2\left(\frac{\phi-\phi_o-h}{2}\right)]} \tag{3.43}$$

$K(\rho)$ can be integrated by putting

$$z = e^{i\gamma} \tag{3.44}$$

so that

$$K(\rho) = -4i\int_{\substack{\text{UNIT}\\ \text{CIRCLE}}} \frac{z\, dz}{Az^4 + 2Bz^2 + C} \tag{3.45}$$

where

$$A = \rho^2[\sqrt{\frac{r}{r_o}} - \sqrt{\frac{r_o}{r}} - i2\sin\left(\frac{\phi+\phi_o-h}{2}\right)] , \tag{3.46}$$

$$B = \sqrt{\frac{rr_o}{R_1}}\ \rho^2 + 4i\sqrt{\frac{rr_o}{R_1}}\ \cos^2\left(\frac{\phi+\phi_o-h}{2}\right), \tag{3.47}$$

and

$$C = \rho^2\left[\sqrt{\frac{r}{r_o}} - \sqrt{\frac{r_o}{r}} + i2\sin\left(\frac{\phi+\phi_o-h}{2}\right)\right]. \tag{3.48}$$

It can be easily confirmed that only two of the four poles of Eq. (3.45) are inside the unit circle. By Cauchy integral theorem $K(\rho)$ is evaluated as [26]

$$K(\rho) = 2\pi\left|\sec\left(\frac{\phi+\phi_o-h}{2}\right)\right| \Big/ \sqrt{\rho^4+2i\rho^2-\frac{4rr_o}{R_1^2}\cos^2\left(\frac{\phi+\phi_o-h}{2}\right)} \tag{3.49}$$

Substituting Eq. (3.49) into the integral in Eq. (3.43) yields

$$\int_0^\infty \rho K(\rho)\ e^{-kR_1\rho^2}d\rho = 2\pi\left|\sec\left(\frac{\phi+\phi_o-h}{2}\right)\right| \int_0^\infty \frac{\rho\ e^{-ikR_1\rho^2}}{\sqrt{(\rho^2+i(\frac{R_1-S}{R_1}))(\rho^2+i(\frac{R_1+S}{R_1}))}}\ d\rho \tag{3.50}$$

with

$$S = \sqrt{r^2 + r_o^2 - 2rr_o\cos(\varphi+\varphi_o-h)}$$

$$= \sqrt{(r+r_o)^2 - 4rr_o\cos^2\left(\frac{\varphi+\varphi_o-h}{2}\right)} \tag{3.51}$$

Again introducing a new variable λ

$$i\lambda^2 = ik(R_1-S) + kR_1\rho^2 \tag{3.52}$$

Then the integral in Eq. (3.50) becomes

$$\int_{\sqrt{k(R_1-S)}}^{\infty} \frac{i\lambda/kR_1 \; e^{-i\lambda^2} \; e^{ik(R_1-S)}}{\sqrt{(\frac{i\lambda^2}{kR_1})(\frac{i\lambda^2}{kR_1} + 2i\,\frac{S}{R_1})}}\, d\lambda$$

$$= \int_{\sqrt{k(R_1-S)}}^{\infty} \frac{e^{ik(R_1-S)}}{\sqrt{\lambda^2 + 2Sk}}\; e^{-i\lambda^2} d\lambda \qquad (3.53)$$

A Fresnel approximation of Eq. (3.53) can be obtained when $kR_1 >> 1$ by replacing the non-exponential part of the integrand by its value at the lower limit, to give the approximation

$$\frac{e^{ik(R_1-S)}}{\sqrt{k(R_1+S)}} \int_{\sqrt{k(R_1-S)}}^{\infty} e^{-i\lambda^2} d\lambda = \frac{1}{\sqrt{k(R_1+S)}}\; F(\sqrt{k(R_1-S)}) \qquad (3.54)$$

where F(b) is given in Eq. (3.19).

Finally, the integration of Eq. (3.30) is reached

$$P_2 = \sqrt{\frac{\pi}{2}}\; 4ie^{-i\pi/4} e^{-ikR_1} \psi_1'(\phi,\varphi_0) \frac{1}{\sqrt{k(R_1+S)}}\; F(\sqrt{k(R_1-S)})$$

$$= 2\,\frac{\pi}{\sqrt{2}}\; \psi_1'(\phi,\varphi_0) \frac{e^{-ikS}}{\sqrt{k(R_1+S)}}\; (1 - \sqrt{2}\; e^{i\pi/4}(C(\sqrt{k(R_1-S)}) - iS(\sqrt{k(R_1-S)})) \qquad (3.55)$$

with

$$h = 2\beta + 2n\pi N^+$$

and

$$S = \sqrt{(r+r_0)^2 - 4rr_0\cos^2(\frac{\phi+\varphi_0-h}{2})}$$

Similar expressions can be found for the other three terms of the Eq. (3.27). Then the total solution for a line source when $k(r+r_o) >> 1$ is

$$p = \pi\{\psi_1(\phi,\phi_o)[\cot(\frac{\pi+(\phi-\phi_o)}{2n}) F_-^2(\phi-\phi_o) + \tan(\frac{\pi+(\phi+\phi_o)}{2n})F_+^2 (\phi+\phi_o-2\beta)]$$

$$+ \psi_2(\phi,\phi_o)[\cot(\frac{\pi-(\phi-\phi_o)}{2n})F_+^2(\phi-\phi_o) + \tan(\frac{\pi-(\phi+\phi_o)}{2n})F_-^2 (\phi+\phi_o+2\beta)]\} \tag{3.56}$$

where

$$F_\pm^2(x) = \frac{e^{-ikS_\pm^*(x)}}{\sqrt{k(R_1+S_\pm^*(x)}} \sqrt{a^\pm(x)}$$

$$(1 - \sqrt{2}\, e^{i\pi/4}(C(\sqrt{k(R_1+S_\pm^*(x))}) - iS(\sqrt{k(R_1+S_\pm^*(x))}) \tag{3.57}$$

$$S_\pm^* = \sqrt{(r+r_o)^2 - 2rr_o a^\pm(x)} \tag{3.58}$$

and

$$a^\pm(x) = 2\cos^2(\frac{2n\pi N^\pm - x}{2}) \tag{3.59}$$

$N^\pm$ is given in Eqs. (3.26a) and (3.26b).

3.3 Mid-range Solution for a Point Source

The diffracted pressure for a point source can be written in the form

$$p = \int_\gamma \frac{P(\cos\alpha)}{kR(\alpha)} e^{-ikR(\alpha)} d\alpha \tag{3.60}$$

where

$$R(\alpha) = \sqrt{r^2 + r_o^2 + 2rr_o\cos(\phi-\alpha) + (z-z_o)^2} \tag{3.61}$$

and $P(\cos\alpha)$ is defined in Eq. (2.45).

The function is not single valued, so the branch cuts are located at

$$R(\alpha) = 0 \tag{3.62}$$

i.e.,

$$\frac{r^2 + r_o^2 + (z-z_o)^2}{2rr_o} = -\cos(\phi-\alpha)$$

$$= -\cos(\phi-\alpha_r)\cosh\alpha_i \tag{3.63}$$

Since $(r-r_o)^2 = r^2 + r_o^2 - 2rr_o > 0$, then $r^2 + r_o^2 > 2rr_o$ which implies that

$$\left| \frac{r^2 + r_o^2 + (z-z_o)^2}{2rr_o} \right| > 1 \quad . \tag{3.64}$$

As a result, the branch points are located by

$$\cos(\phi-\alpha_r) < 1 \tag{3.65}$$

and

$$\cosh\alpha_i = \frac{r^2+r_o^2+(z-z_o)^2}{2rr_o} \tag{3.66}$$

or

$$\alpha_r = (2n-1)\pi+\phi \tag{3.67}$$

and

$$\alpha_i = \pm \cosh^{-1}\left(\frac{r^2+r_o^2+(z-z_o)^2}{2rr_o}\right) \quad . \tag{3.68}$$

The regions of convergence of the integral in Eq. (3.60) are determined by the real part of the exponential power,

$$\mathrm{Re}(-ikR(\alpha)) < 0 \tag{3.69}$$

or

$$\mathrm{Im}(R(\alpha)) < 0 \tag{3.70}$$

The function $R(\alpha)$ can be written in polar form as

$$R(\alpha) = |R|^{1/2} e^{i\psi} = |R|^{1/2} (\cos\psi + i\sin\psi) \tag{3.71}$$

From Eq. (3.70) the condition of convergence reduces to $\sin\psi < 0$. Then the regions of convergence are governed by:

$$\pi + \phi < \alpha_r < \phi \quad \text{when} \quad \alpha_i < 0, \tag{3.72}$$

and

$$\pi + \phi > \alpha_r > \phi \quad \text{when} \quad \alpha_i > 0. \tag{3.73}$$

From Eqs. (3.67), (3.68), (3.72) and (3.73) the branch cuts and regions of convergence are illustrated in Fig. 3.2.

To obtain the solution to the integral in Eq. (3.60), a procedure is employed similar to the plane-wave and line source incidences. The solution is divided into subintegrals and poles are extracted explicitly. First of these subintegrals (using Eq. (3.1)) is

$$p_1 = \frac{1}{2} \int_\gamma \psi_1(\alpha) \cot\left(\frac{\pi+(\alpha-\varphi_o)}{2n}\right) \frac{e^{-ikR(\alpha)}}{k\,R(\alpha)}\, d\alpha. \tag{3.74}$$

One can avoid the singularity again by multiplying and dividing the integrand by a factor

$$\cos\left(\frac{2n\pi N^- - (\alpha-\varphi_o)}{2}\right) \tag{3.75}$$

Consider closing the γ-path along $\varphi + i\infty$ to $\varphi - i\infty$. Then p_1 is given by

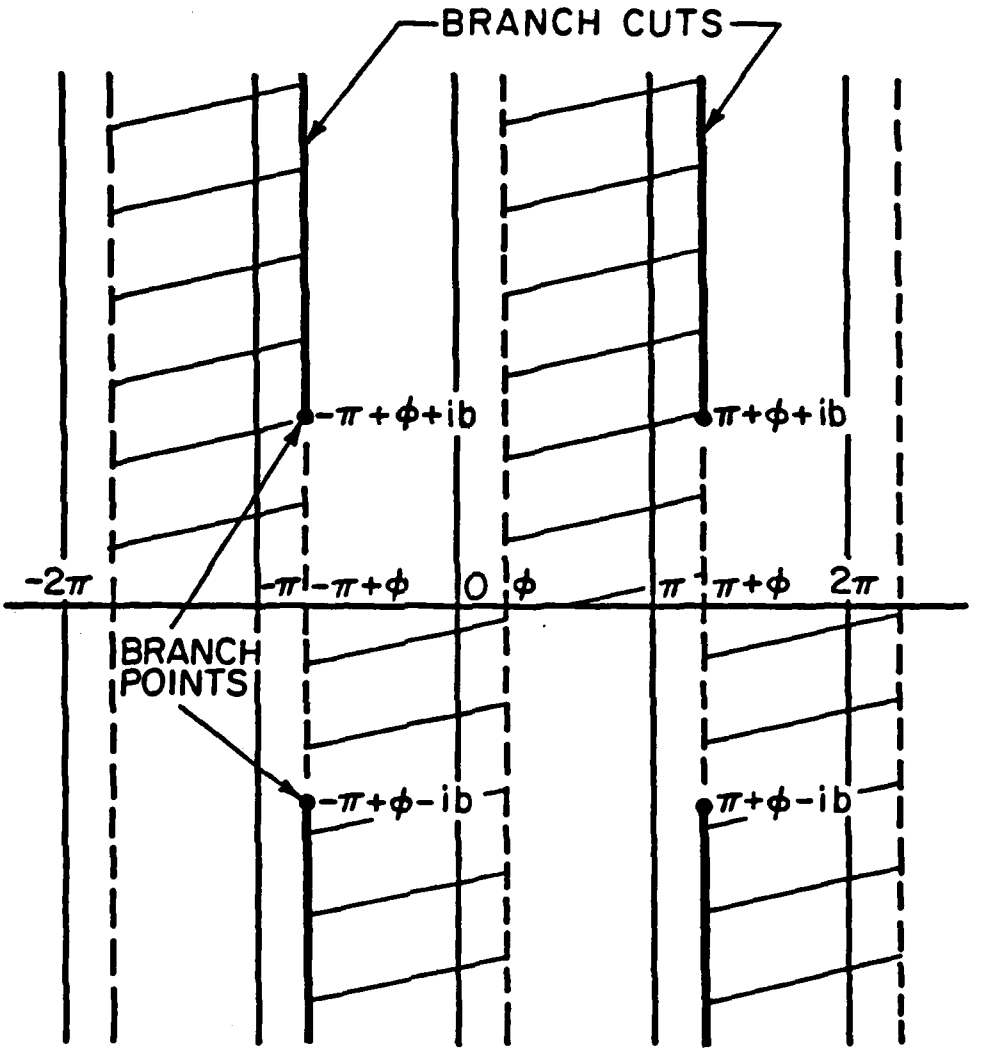

Fig. 3.2 Regions of convergence and branch cuts for a point source.

$$P_1 = -\frac{i}{2}\int_{-\infty}^{\infty} \psi_1'((\phi+i\alpha_i)\ \frac{1}{\cos(\frac{2n\pi N^- - (\phi+i\alpha_i-\varphi_o)}{2})}$$

$$\frac{e^{-ik\sqrt{r^2+r_o^2+2rr_o\cosh\alpha_i+(z-z_o)^2}}}{k\sqrt{r^2+r_o^2+2rr_o\cosh\alpha_i+(z-z_o)^2}}\ d\alpha_i \qquad (3.76)$$

where

$$\psi_1'(\phi+i\alpha_i) = \psi_1(\phi+i\alpha_i)\cot(\frac{\pi+\phi+i\alpha_i-\phi_o}{2n})\ \cos(\frac{2n\pi N^- -(\phi+i\alpha_i-\phi_o)}{2}) \qquad (3.77)$$

Using the fact that $p_1(\alpha) = p_1(-\alpha)$

$$p_1 = -i\int_{-\infty}^{\infty}[\psi_1'(\phi+i\alpha_i)+\psi_1'(\phi-i\alpha_i)]$$

$$\{\frac{\cos(\frac{2n\pi N^- -(\phi-\phi_o)}{2})\ \cosh\frac{\alpha_i}{2}}{[\cosh\alpha_i+\cos(2n\pi N^- -(\phi-\phi_o))]}\ \frac{e^{-ik\sqrt{r^2+r_o^2+2rr_o\cosh\alpha_i+(z-z_o)^2}}}{\sqrt{r^2+r_o^2+2rr_o\cosh\alpha i+(z-z_o)^2}}\}d\alpha_i$$

(3.78)

An asymptotic expression for the integral in Eq. (3.77) can be obtained by letting

$$\tau = \frac{2\sqrt{rr_o}}{R_1}\ e^{-i\pi/4}\ \sinh\alpha_i/2 \qquad (3.79)$$

where $R_1 = \sqrt{(r+r_o)^2 + (z-z_o)^2}$

Then

$$R(\alpha) = \sqrt{(r+r_o)^2 + (z-z_o)^2\ (1+\frac{4rr_o\sinh^2\alpha_i/2}{(r+r_o)^2+(z-z_o)^2})}$$

$$= R_1\sqrt{1-i\tau^2}$$

Rewriting Eq. (3.78) with new variables

$$p_1 = \frac{\sqrt{rr_o}}{kR_1^2} e^{-i\pi/4} \int_{-\infty}^{\infty} \frac{[\psi_1'(\phi+i\alpha_i)+\psi_1'(\phi-i\alpha_i)]}{\sqrt{1-i\tau^2}} \cos\left(\frac{2n\pi N^- -(\phi-\phi_o)}{2}\right)$$

$$\int_{-\infty}^{\infty} \frac{e^{-ikR_1\sqrt{1-i\tau^2}}}{\tau^2+i\frac{4rr_o}{R_1^2}\cos^2\left(\frac{2n\pi N^- -(\phi-\phi_o)}{2}\right)} d\tau \qquad (3.81)$$

Expanding $[\psi_1'(\phi+i\alpha_i)+\psi_1'(\phi-i\alpha_i)]/\sqrt{1-i\tau^2}$ in a Taylor series about $\alpha_i = 0$ and retaining the leading term, Eq. (3.81) becomes:

$$p_1 = \frac{4\sqrt{rr_o}}{kR_1^2} e^{-i\pi/4} \psi_1'(\phi) \cos\left(\frac{2n\pi N^- -(\phi-\phi_o)}{2}\right)$$

$$\int_{-\infty}^{\infty} \frac{e^{-ikR_1\sqrt{1-i\tau^2}}}{\tau^2+i\frac{4rr_o}{R_1^2}\cos^2\left(\frac{2n\pi N^- -(\phi-\phi_o)}{2n}\right)} d\tau \qquad (3.82)$$

In order to integrate the integral in Eq. (3.82) consider the case $kR_1 > 1$, then $\sqrt{1-i\tau^2} \cong 1-i\tau^2/2$ and

$$p_1 = \frac{2}{kR_1}\psi_1'(\phi)e^{-i\pi/4} e^{-ikR_1} \sqrt{\frac{2rr_o}{R_1^2}\, a^-(x)}$$

$$\int_{-\infty}^{\infty} \frac{e^{-kR_1\tau^2/2}}{\tau^2 + i\frac{2rr_o}{R_1^2}\, a^-(x)} d\tau \qquad (3.83)$$

with $x = \phi-\phi_o$

where

$$a^{-}(x) = 2\cos^2\left(\frac{2n\pi N^{-}-x}{2}\right) \tag{3.84}$$

which has a similar form to Eq. (3.11).

Defining Fresnel integral of the form

$$b\int_{-\infty}^{\infty} \frac{e^{-t\tau^2}}{\tau^2+ib^2}\, d\tau = 2\sqrt{\pi}\, F(b\sqrt{t}) \tag{3.85}$$

and using Eqs. (3.13) through (3.15) the final form is obtained:

$$p_1 = i\,\frac{2\pi}{\sqrt{2}kR_1}\,\psi(\phi)\cot\left(\frac{\pi+(\phi-\phi_o)}{2n}\right)\, e^{-ikR_1}\, e^{ikrr_o/R_1}\, a^{-}(x)$$

$$\sqrt{a^{-}(x)}\,\left(1 - \sqrt{2}\, e^{i\pi/4}\left(C\left(\sqrt{(krr_o/R_1)a^{-}(x)}\right) - iS\left(\sqrt{(krr_o/R_1)a^{-}(x)}\right)\right)\right. \tag{3.86}$$

There are similar expressions for the other three terms; then the total solution becomes:

$$\begin{aligned} p_1 = -\frac{i2\pi}{\sqrt{2}kR_1}\, e^{-ikR_1}\, \{ & \psi_1(\phi)\left[\cot\left(\frac{\pi+(\phi-\phi_o)}{2n}\right) F_{-}^{3}(\phi-\phi_o)\right. \\ & \left. + \tan\left(\frac{\pi+(\phi+\phi_o)}{2n}\right) F_{+}^{3}(\phi+\phi_o-2\beta)\right] \\ & + \psi_2(\phi)\left[\cot\left(\frac{\pi-(\phi-\phi_o)}{2n}\right) F_{+}^{3}(\phi-\phi_o)\right. \\ & \left. + \tan\left(\frac{\pi-(\phi+\phi_o)}{2n}\right) F_{-}^{3}(\phi+\phi_o+2\beta)\right]\} \end{aligned} \tag{3.87}$$

where

$$F_{\pm}^{3}(x) = e^{ikrr_o/R_1}\, a^{\pm}(x)\, \sqrt{a^{\pm}(x)}$$

$$\left(1 - \sqrt{2}\, e^{i\pi/4}\left(C\left(\sqrt{(krr_o/R_1)a^{\pm}(x)}\right) - iS\left(\sqrt{(krr_o/R_1 a^{-}(x)}\right)\right)\right.$$

and

$$a^{\pm}(x) = 2\cos^2\left(\frac{2n\pi N^{\pm} - x}{2}\right) \tag{3.89}$$

CHAPTER IV

NUMERICAL RESULTS

The solution for the acoustic diffraction from impedance covered wedges is a function of several physical and geometric parameters; the surface impedances θ^+ and θ^-, the source angle ϕ_o, the non-dimensional wave numbers kr and kr_o and the wedge angle β. In this chapter, diffracted and backscattered pressures are plotted for different values of these parameters. In order to assess the influence of one of the parameters, the others are kept constant. Most of the graphs shown in this section are polar plots of the angular distribution of the diffracted pressure in decibels relative to the amplitude of the incident pressure.

The mid-range solution of diffraction of a plane wave in Eq. (3.23) diminishes at a rate proportional to $\sqrt{kr}$ because of the factor $\sqrt{kr}$ in the argument of the Fresnel integrals. To study the influences of the wedge angle and the surface impedances on the angular variation of the pressure, it is advantageous to remove the geometric spreading factor ($\sqrt{kr}$) from the expression for the diffracted pressure for plane wave incidence. Thus, henceforth only the product of $\sqrt{kr} \cdot p_d(r,\varphi)$ is plotted. By the same reasoning, the diffracted pressure for a point source is normalized by the incident pressure at the edge due to a point source e^{-ikr_o}/kr_o and multiplied by $\sqrt{kr}$ in order to facilitate comparisons between the different plots. For all the plots for a point source, the source and the receiver are placed in the z=0 plane. Because of limitations of the plotter the following symbols are used for labeling:

$kr = KR$	$\theta^+ = BAT$	$\phi_o = SA$
$kr_o = KRO$	$\theta^- = BAB$	$\beta = WA$

4.1 Dependence on Surface Impedances

In the derivation of the solution, the Brewster angles θ^+ and θ^- were used instead of complex impedance $Z^{\pm}$. Rewriting the relation between $Z^{\pm}$ and $\theta^{\pm}$ as

$$\sin\theta^{\pm} = \frac{\rho c}{Z^{\pm}} \quad ,$$

various impedance conditions ranging from pressure release to rigid are considered. The list of impedances and their corresponding Brewster angles are listed below

	Z (Impedance)	θ (Brewster Angle)
Rigid	∞	0°
	2.00 ρc	30°
	1.16 ρc	60°
Matched	ρc	90°
Pressure Release	0	90°-i5

The influence of the impedance of the insonified (source-facing) and uninsonified surfaces are considered in the first five plots. These figures are plotted by employing Eq. (3.23) for the following parameters:

1. Fig. 4.1 presents results for the diffracted pressure for the impedances $\theta^+ = 30°$, 60° and 90° on the insonified surface,

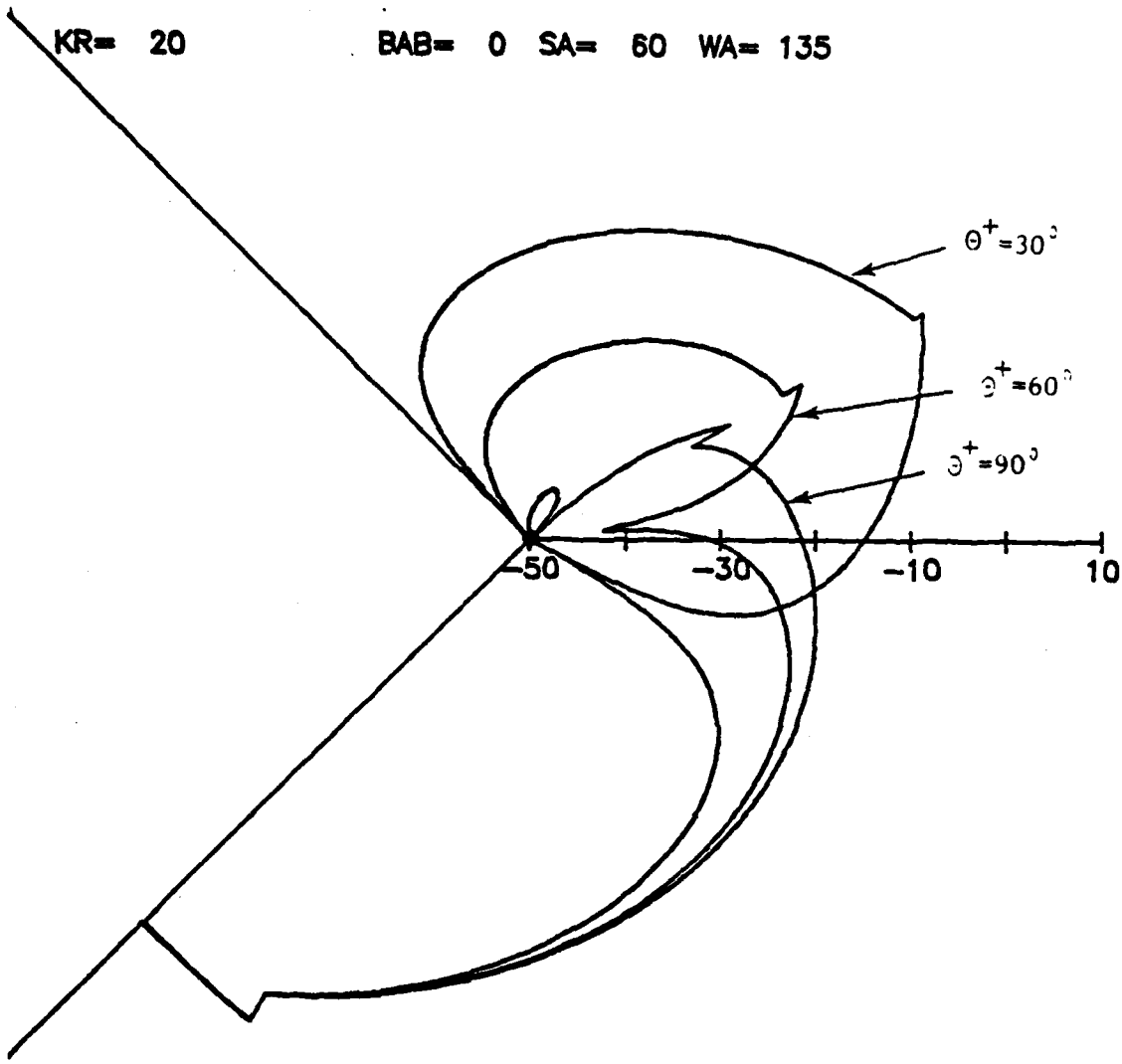

Fig. 4.1 Diffraction of plane wave with impedance cover on the insonified surface with kr = 20, $\Theta^- = 0°$, $\Theta_o = 60°$ and $\beta = 135°$.

while $\theta^- = 0°$ (rigid) remains the same on the uninsonified surface with kr = 20, $\phi_0 = 60°$ and $\beta = 135°$.

2. Fig. 4.2 presents plots of the diffracted pressure for the source angle $\phi_0 = -60°$ to show the influence of the impedances of the uninsonified surface. All other parameters are the same as in Fig. 4.1.
3. The influence of an imaginary component of impedance is considered in Figs. 4.3 and 4.4 where $\theta^+ = 90° - i5$ and $\theta^- = 0°$. The angle of incidence is $\phi_0 = 105°$ in Fig. 4.3, while $\phi_0 = -105°$ in Fig. 4.4 and kr = 20 in both figures.
4. The diffraction by a wedge covered by absorbent surfaces with $\theta^+ = 60°$ and $\theta^- = 30°$ are shown in Fig. 4.5. The values for kr is 20, ϕ_0 is 105° and β is 135°.

4.2 Dependence on the Wedge Angle

To facilitate comparisons of diffraction from different wedge geometries, plots for four wedge angles are made by using Eq. (3.23). Since the diffracted field is mainly controlled by the shadow boundaries and nulls, for each wedge angle two different source angles are used to demonstrate their influence. In Figs. 4.6 through 4.9 the angle of incidence is $\phi_0 = 110°$, whereas in Figs. 4.10 through 4.13, $\phi_0 = 30°$. The values of other parameters are kr = 20, $\theta^+ = 30°$ and $\theta^- = 0°$.

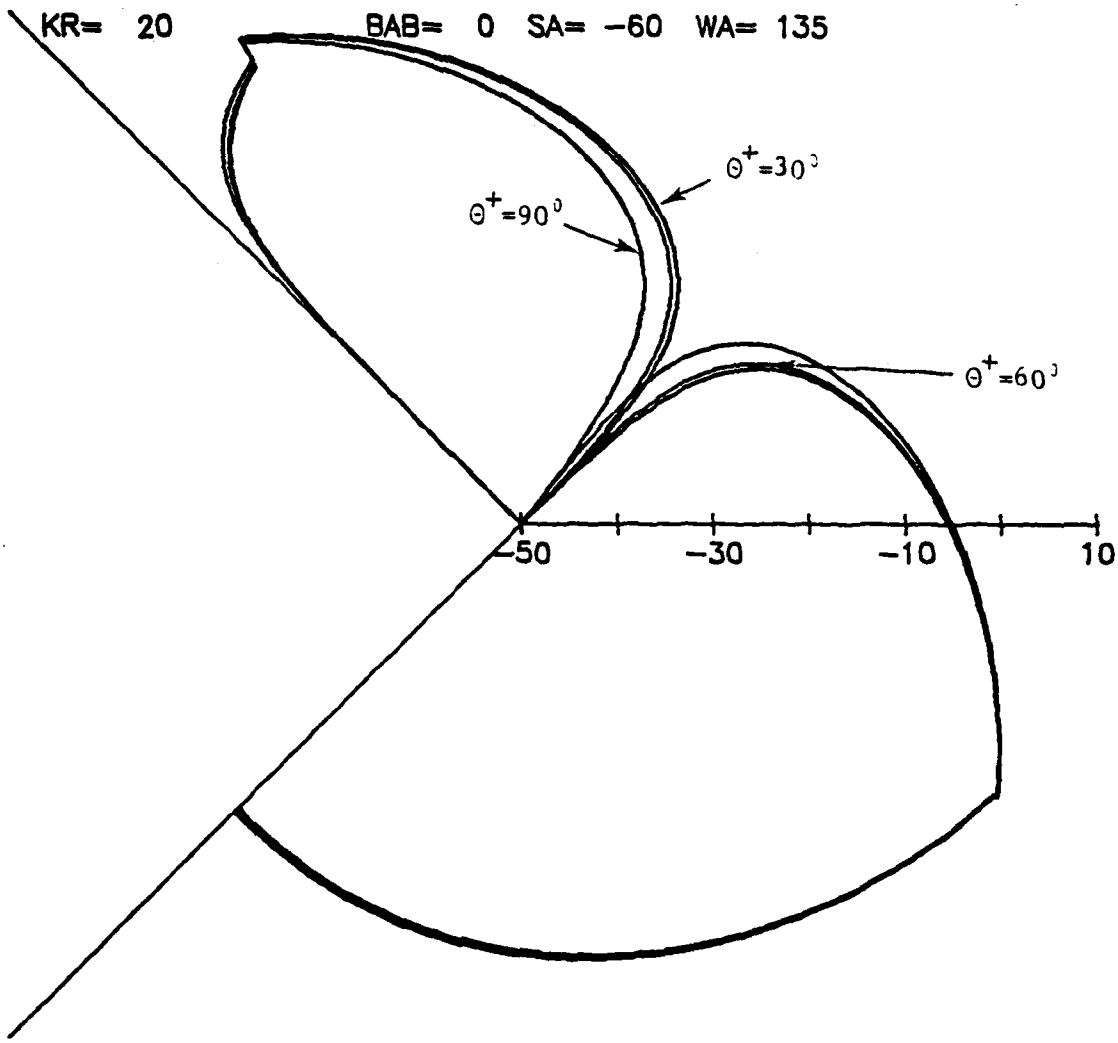

Fig. 4.2 Diffraction of plane wave with impedance cover on the uninsonified surface with kr = 20, $\theta^- = 0°$, $\theta_o = -60°$ and $\beta = 135°$.

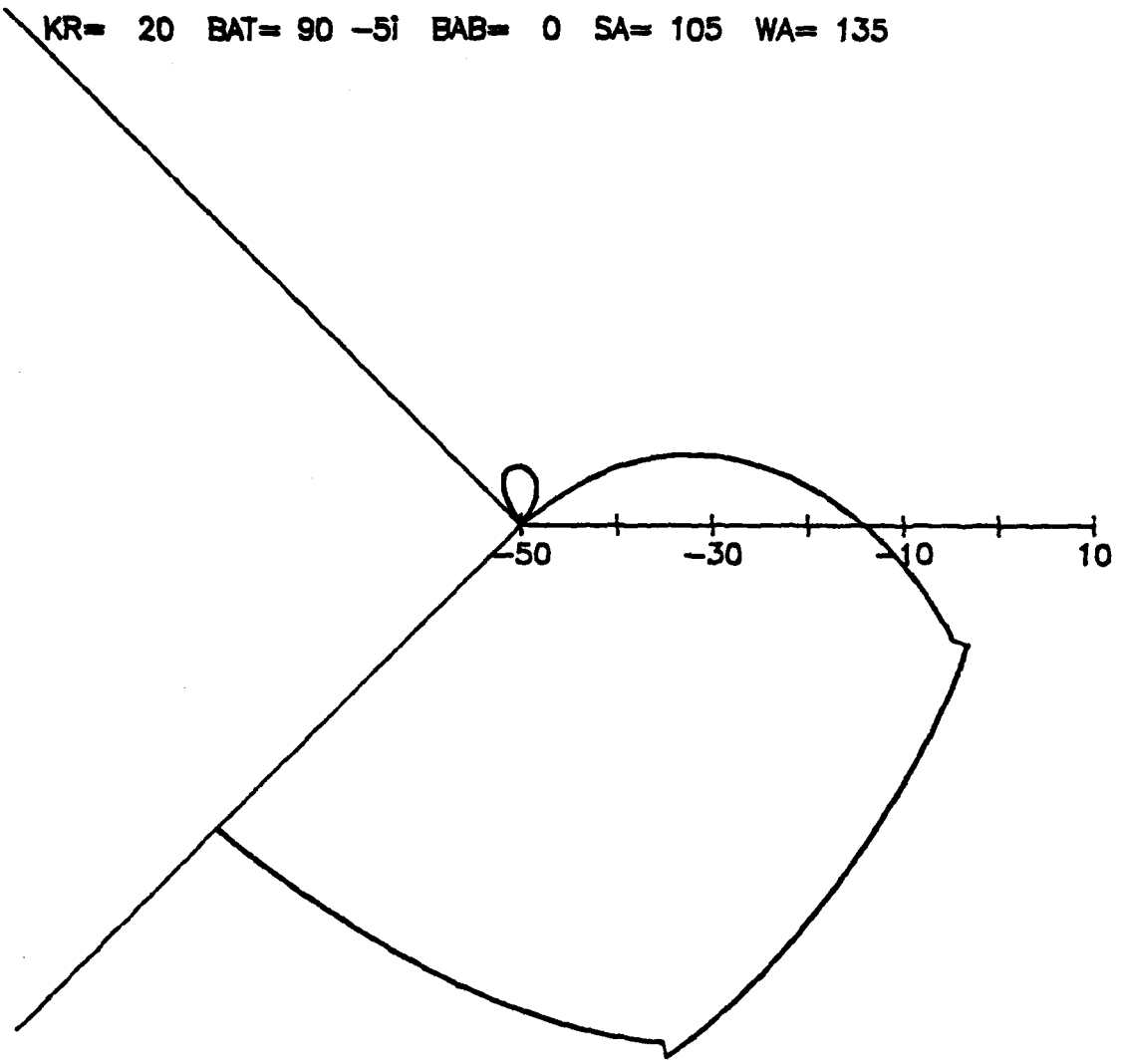

Fig. 4.3 Diffraction of plane wave with total absorption on the insonified surface with kr = 20, $\theta^+ = 90-i5$, $\theta^- = 0°$, $\phi_o = 105$ and $\beta = 135°$.

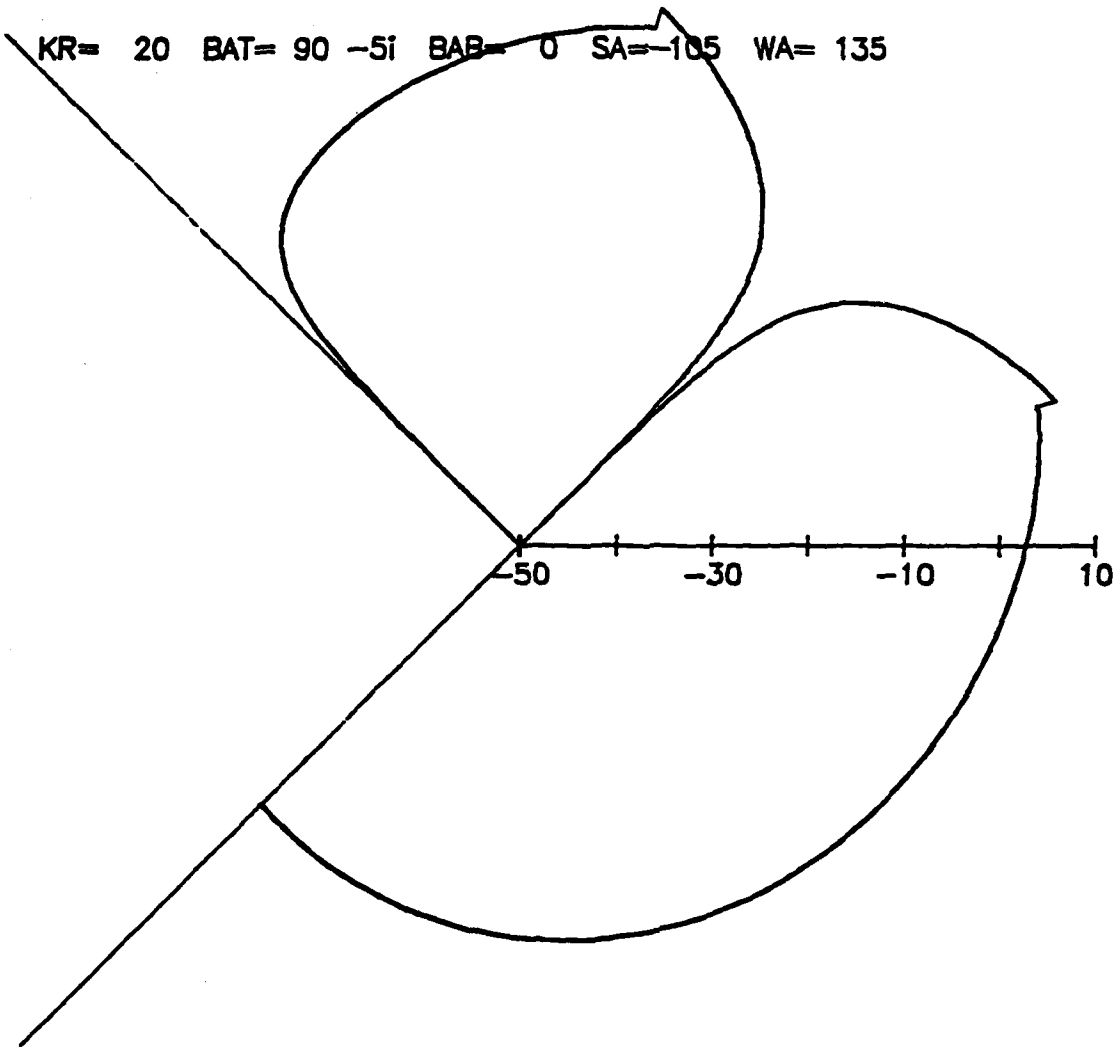

Fig. 4.4 Diffraction of plane wave with total absorption on the uninsonified surface with kr = 20, $\theta^+ = 90°-i5$, $\theta^- = 0°$, $\phi_o = -105°$ and $\beta = 135°$.

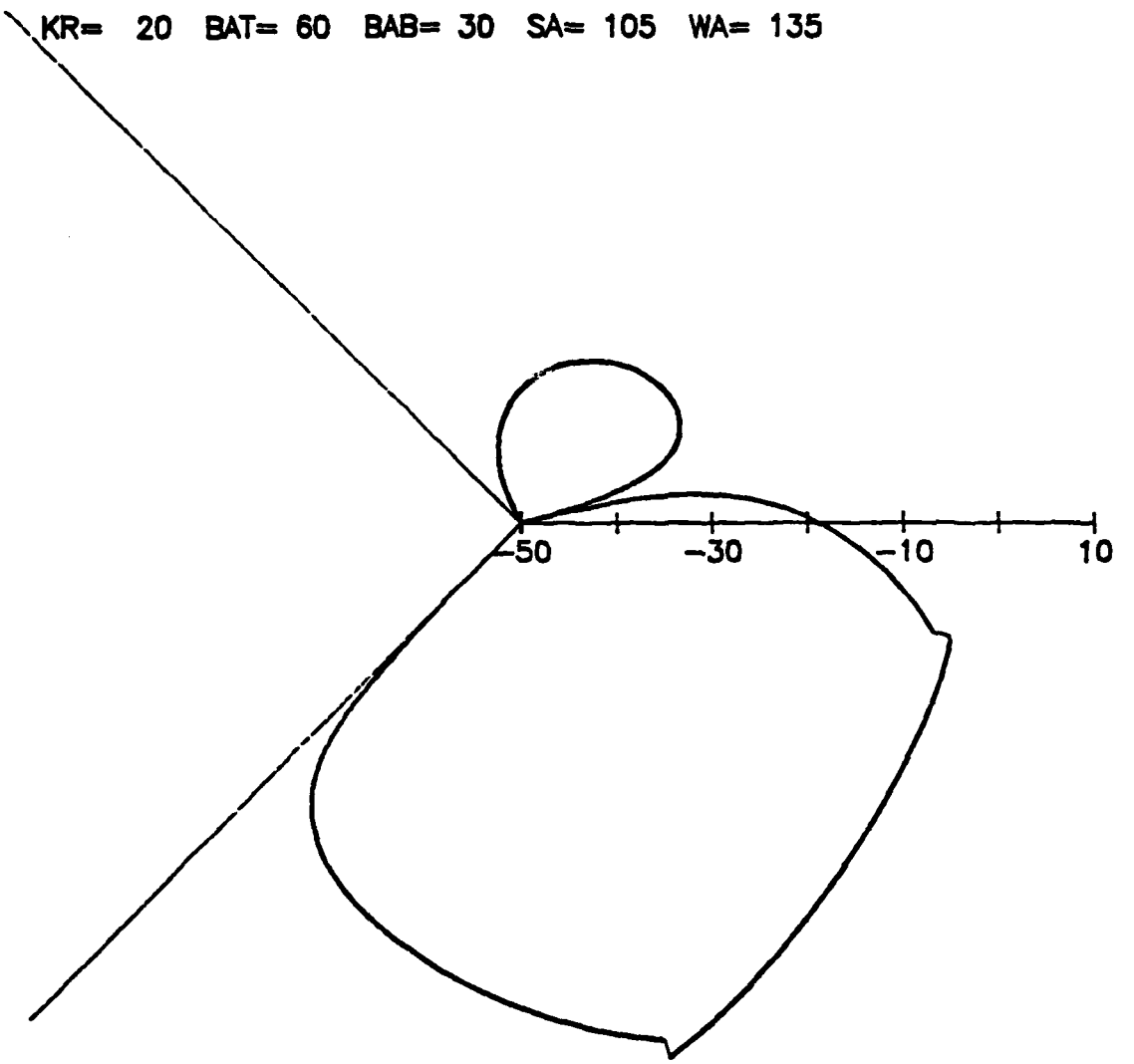

Fig. 4.5 Diffraction of plane wave with impedance cover on both surfaces with kr = 20, θ^+ = 60°, θ^- = 30°, ϕ_o = 105° and β = 135°.

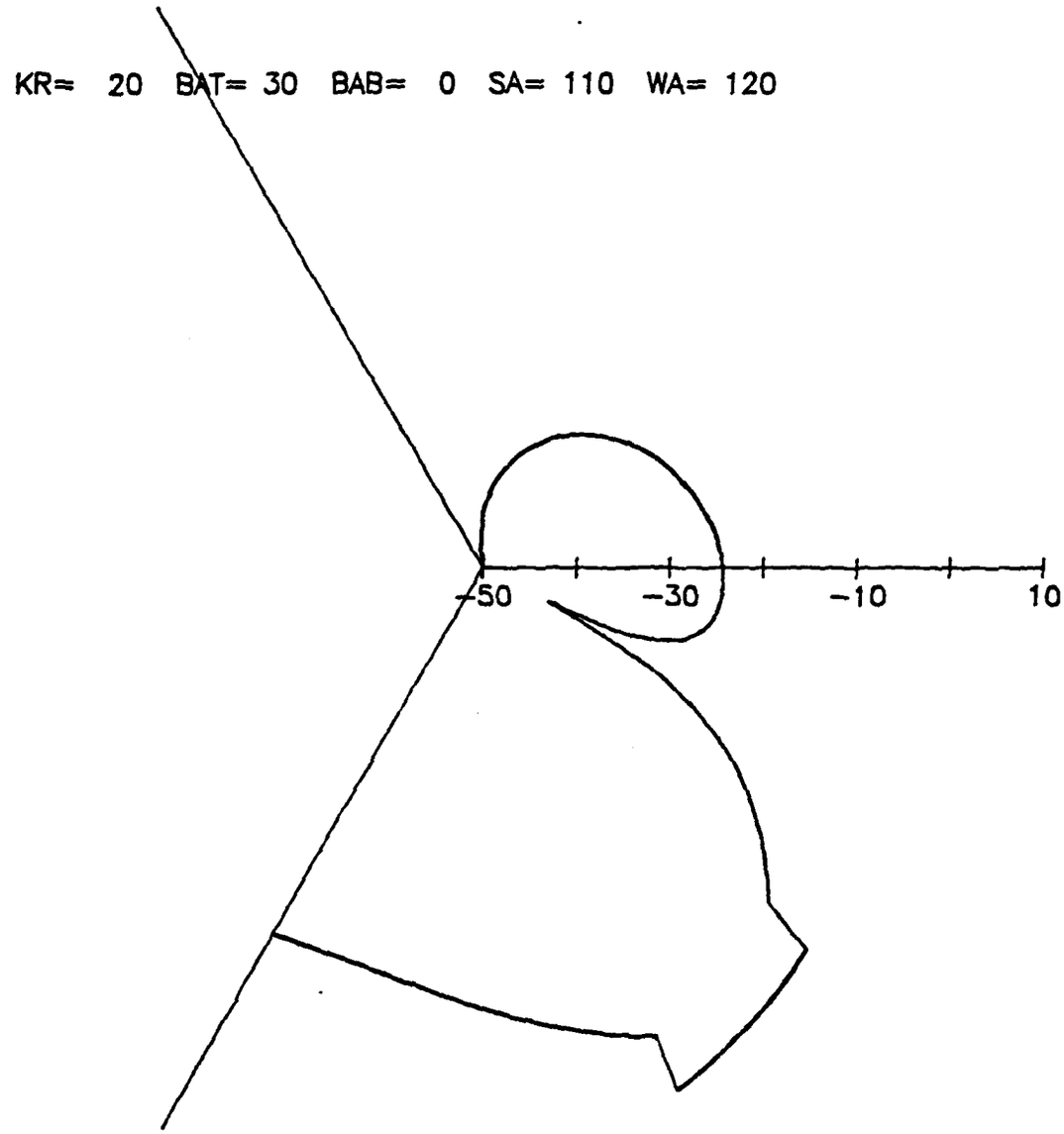

Fig. 4.6 Diffraction of plane wave from a 120° wedge with $\phi_o = 110°$, $\theta^+ = 30°$, $\theta^- = 0°$ and kr = 20.

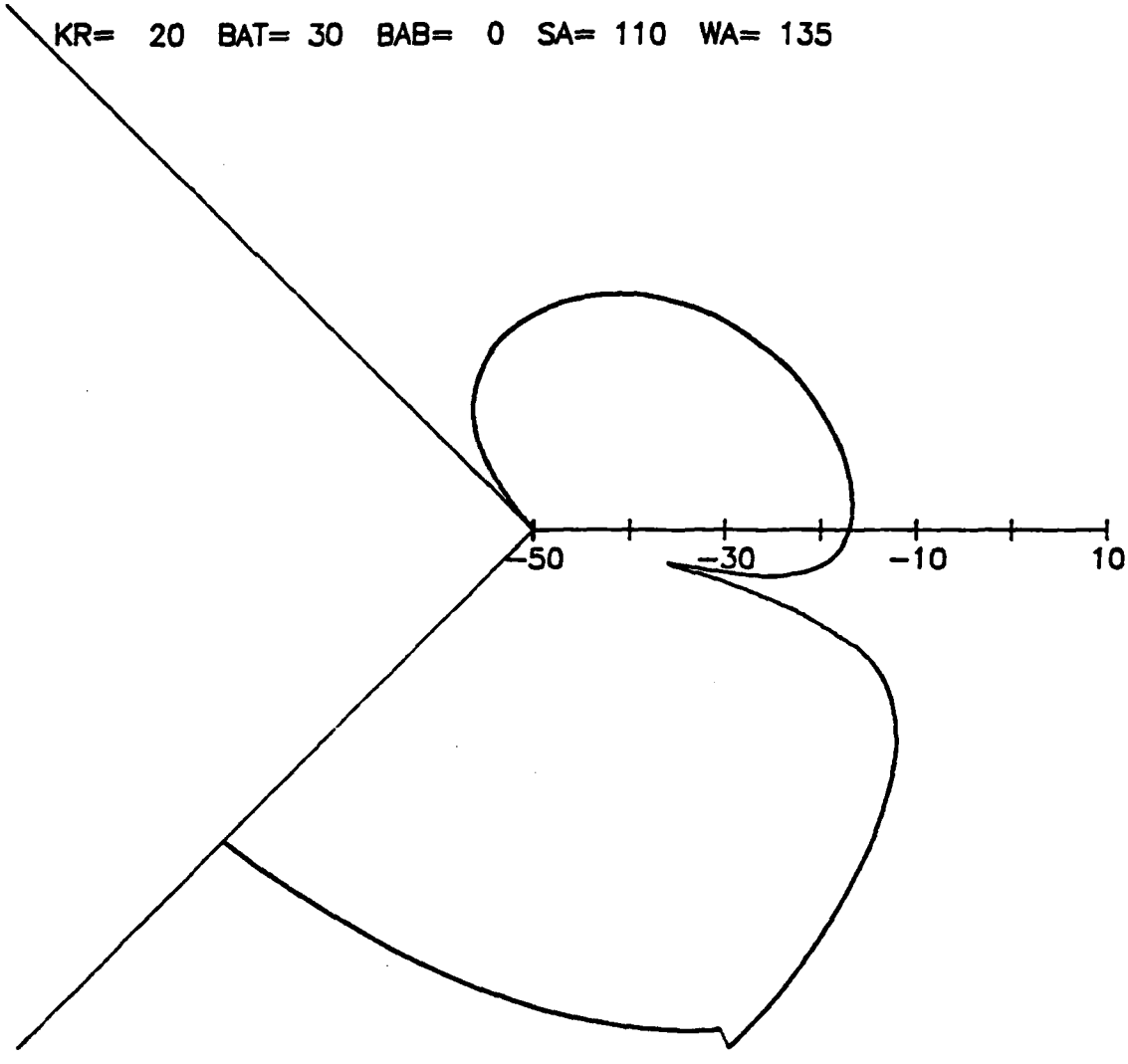

Fig. 4.7 Diffraction of plane wave from a 135° wedge with $\phi_o = 110°$, $\theta^+ = 30°$, $\theta^- = 0$ and kr = 20.

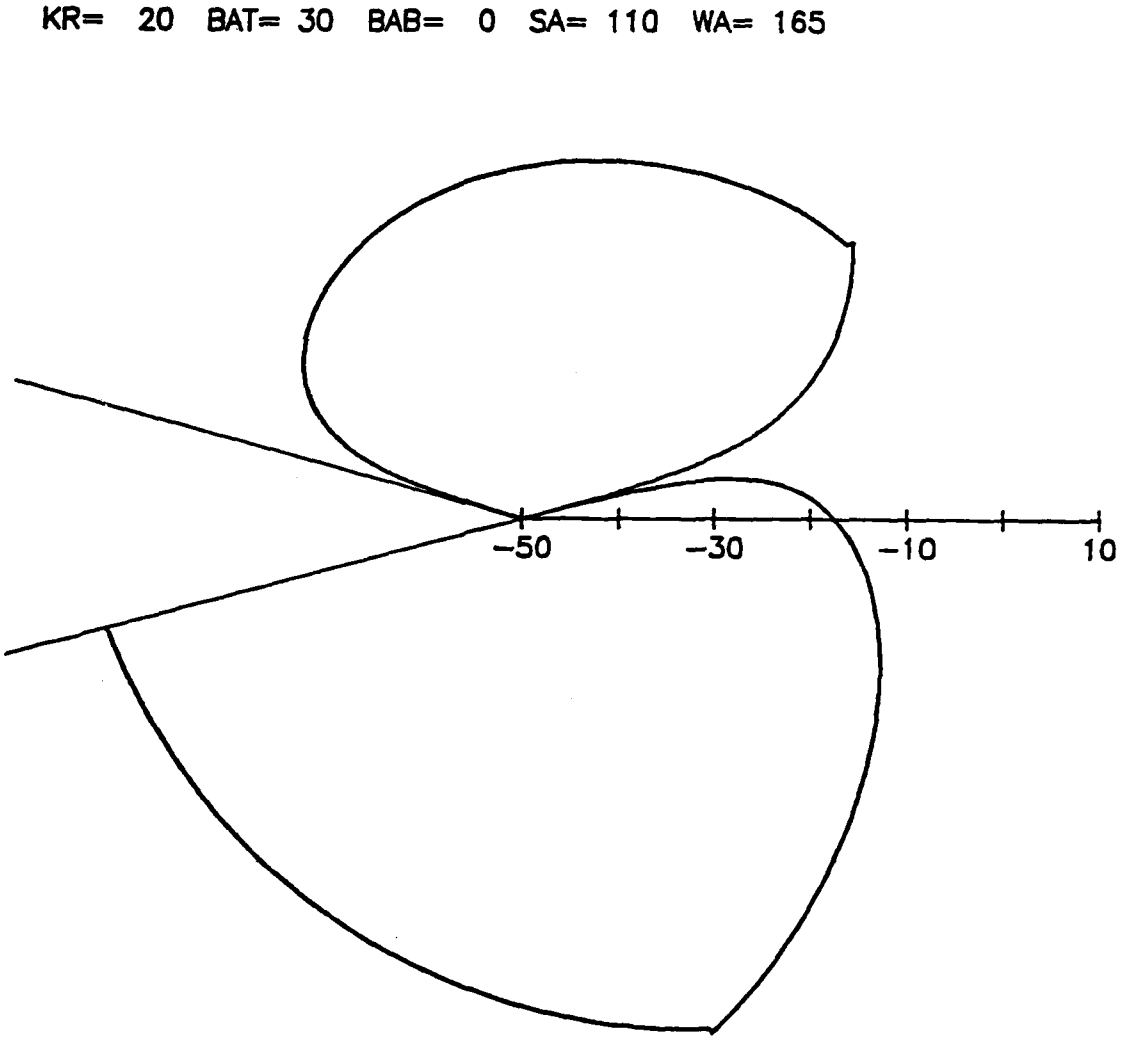

Fig. 4.8 Diffraction of plane wave from a 165° wedge with $\phi_o = 110°$, $\theta^+ = 30°$, $\theta^- = 0°$ and kr = 20.

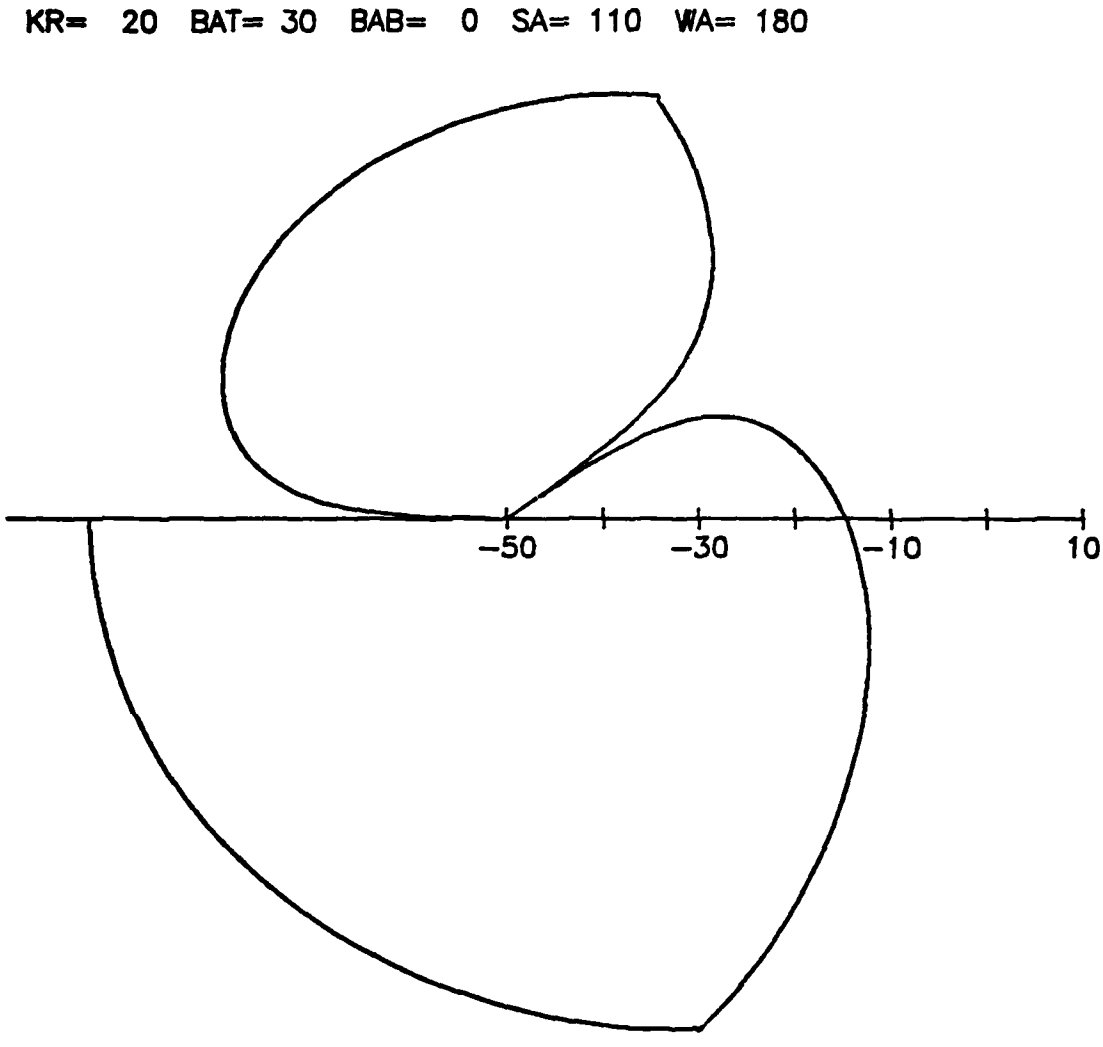

Fig. 4.9 Diffraction of plane wave from a 180° wedge with $\phi_o = 110°$, $\theta^+ = 30°$, $\theta^- = 0°$ and $kr = 20$.

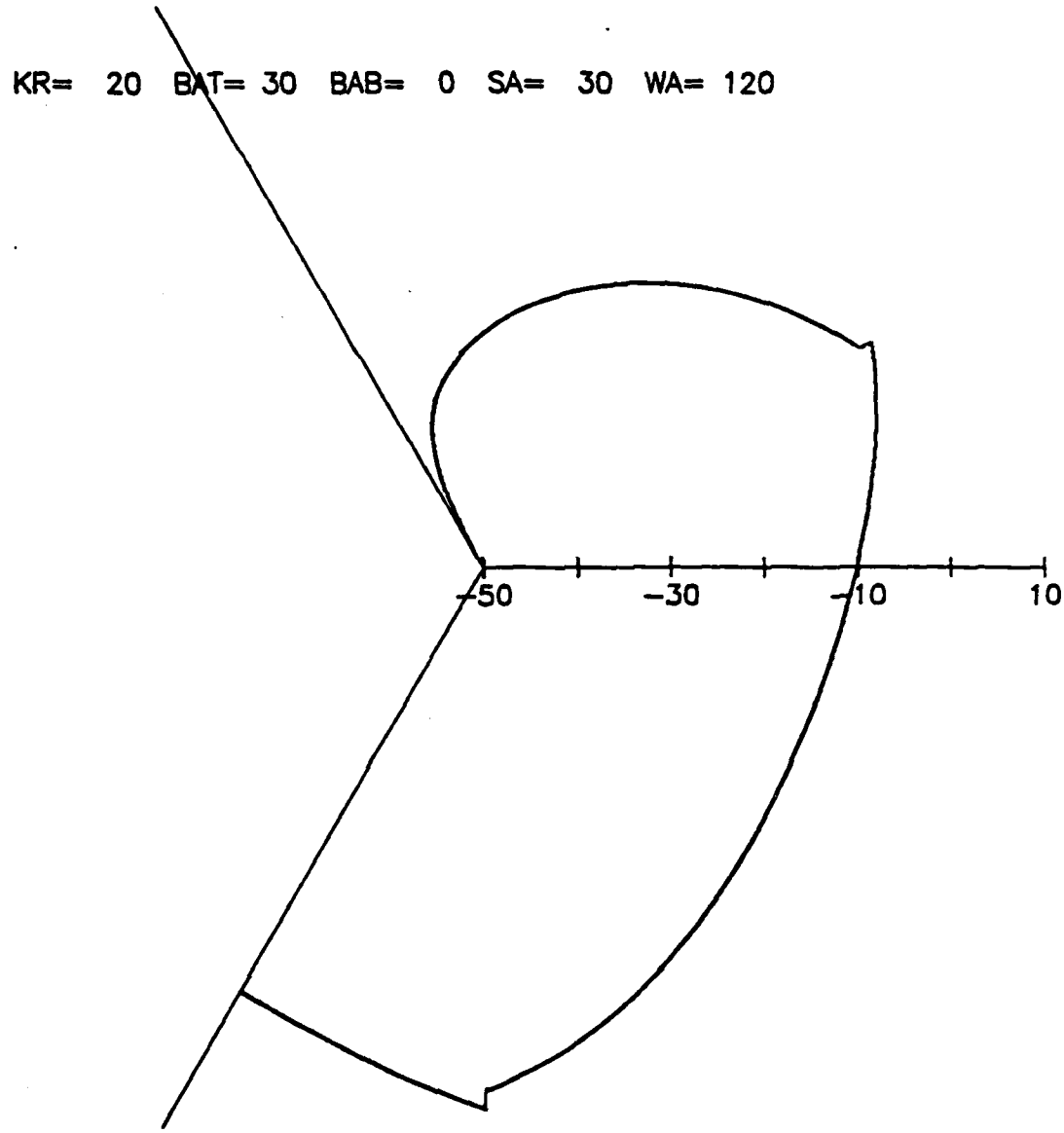

Fig. 4.10 Diffraction of plane wave from a 120° wedge with ϕ_o = 30°, θ^+ = 30°, θ^- = [illegible] and kr = 20.

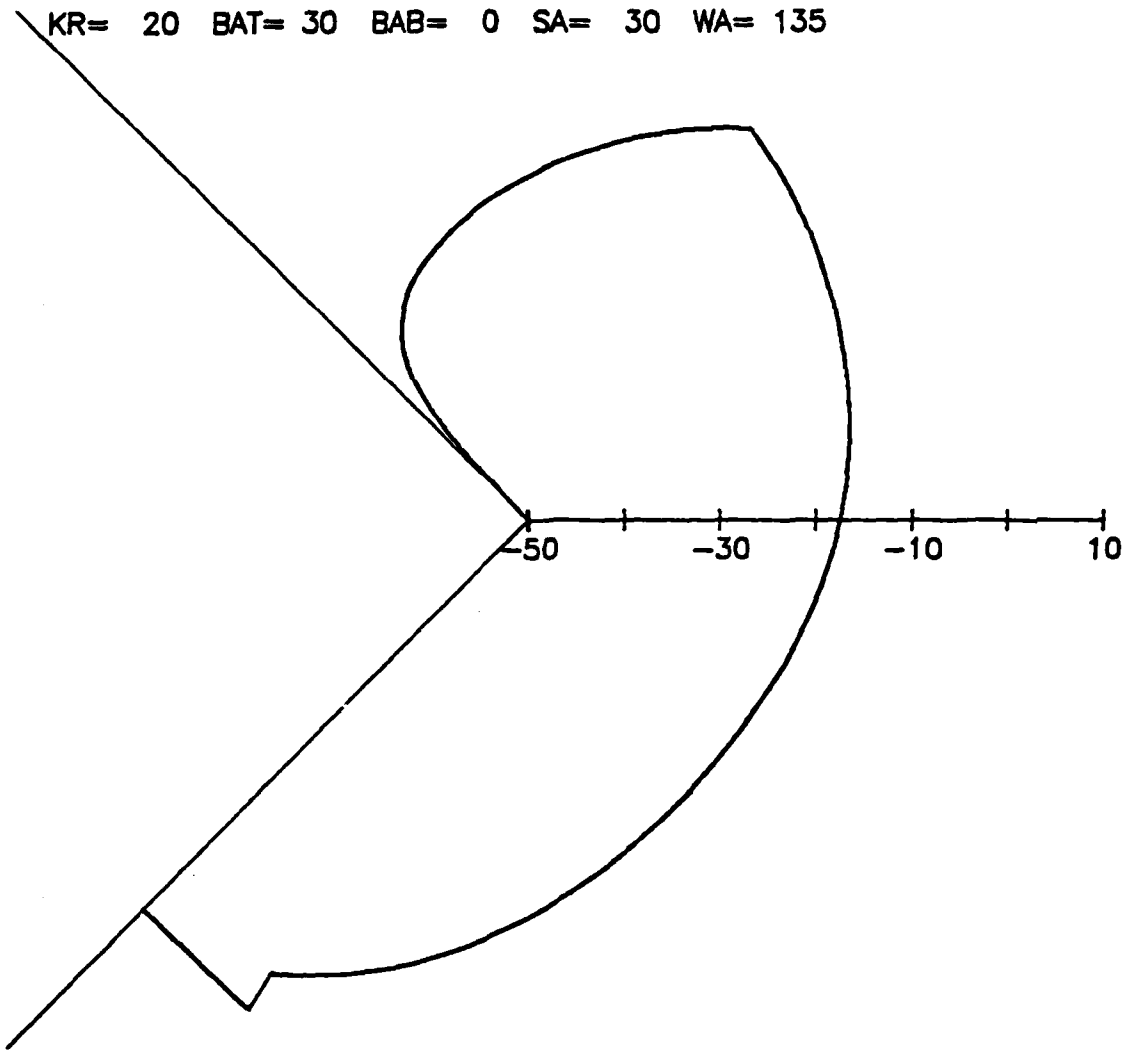

Fig. 4.11 Diffraction of plane wave from a 135° wedge with $\phi_o = 30°$, $\theta^+ = 30°$, $\theta^- = 0°$ and $\beta = 135°$.

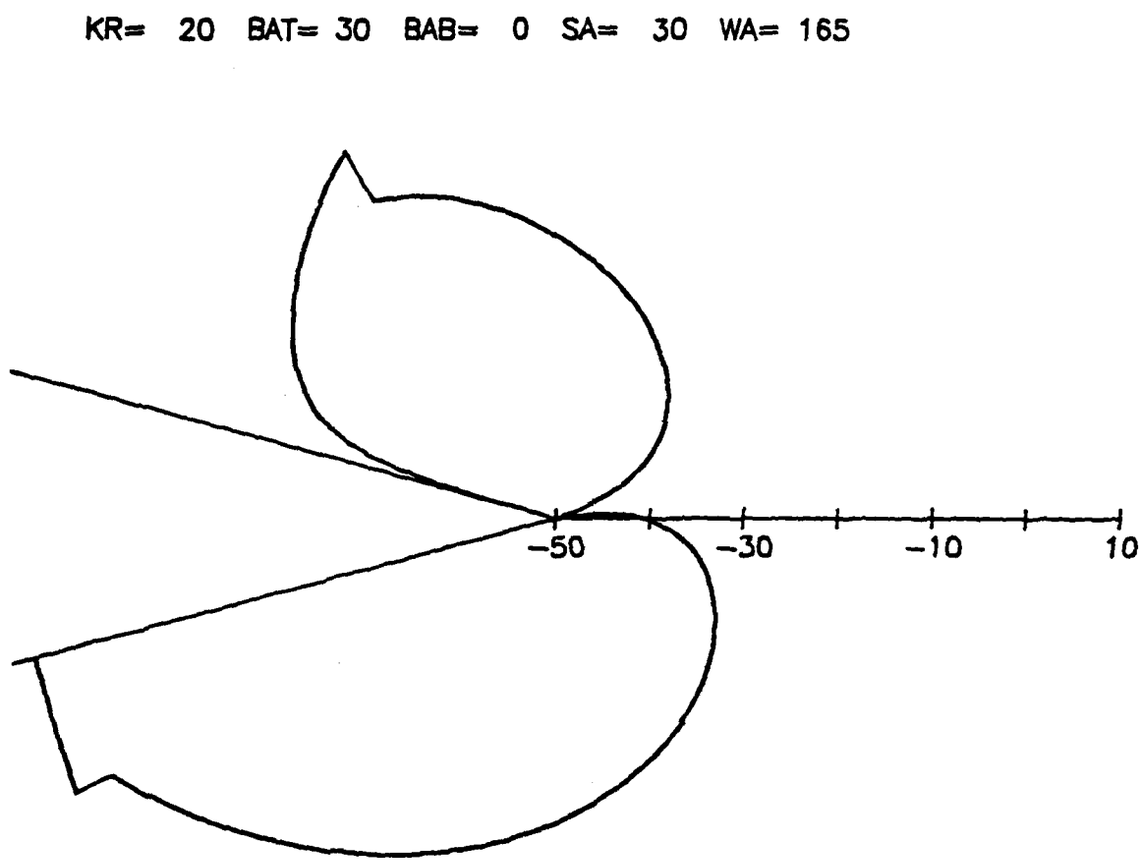

Fig. 4.12 Diffraction of plane wave from a 165° wedge with $\phi_o = 30°$, $\theta^+ = 30°$, $\theta^- = 0°$ and kr = 20.

KR= 20 BAT= 30 BAB= 0 SA= 30 WA= 180

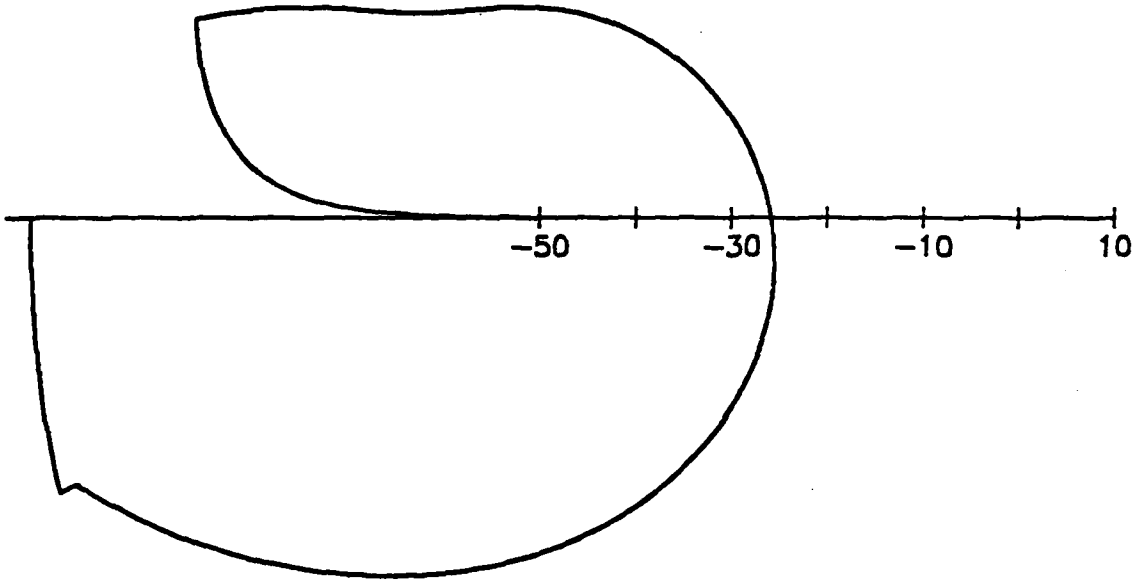

Fig. 4.13 Diffraction of plane wave from a 180° wedge with ϕ_o = 30°, θ^+ = 30°, θ^- = 0° and kr = 20.

4.3 Dependence on kr_o

When the incident pressure field is due to a point source, another parameter kr_o is introduced which is the direct distance from the tip of the wedge to the location of the source. As the source is moved away from the wedge, the incoming spherical waves impinging on the wedge look like plane waves. To demonstrate the influence of kr_o on the diffracted field, five plots are made using Eq. (3.87) with impedances $\theta^+ = 60°$, $\theta^- = 30°$, $kr = 20$, $\phi_o = 60°$ and $\beta = 135°$. The non-dimensional parameter kr_o takes the values 5,10, 20, 200, 2000 in Figs. 4.14 through 4.18.

4.4 Excess Attenuation

It is practical to model the diffracted field from a point source as that due to a plane wave with a correction factor for spherical spreading. This model assumes that there is a geometric-optic relationship between spherical and plane waves. Fig. 4.19 is plotted to explore this relationship. The veritcal axis of Fig. 4.19 is in terms of excess attenuation, defined as

$$\text{Excess Attenuation} = -20 \log_{10} \left| \frac{P_d}{P_{dir}} \right| \text{ dB}, \qquad (4.1)$$

where p_d is the diffracted field from Eq. (3.87) and p_{dir} is the direct field (e^{ikr_2}/kr_2) at the receiver in the absence of a wedge. The horizontal axis is the $\log_{10}$ of non-dimensional distance kr from the tip of the wedge to a receiver located at $\phi_o = -90°$ from the x-axis.

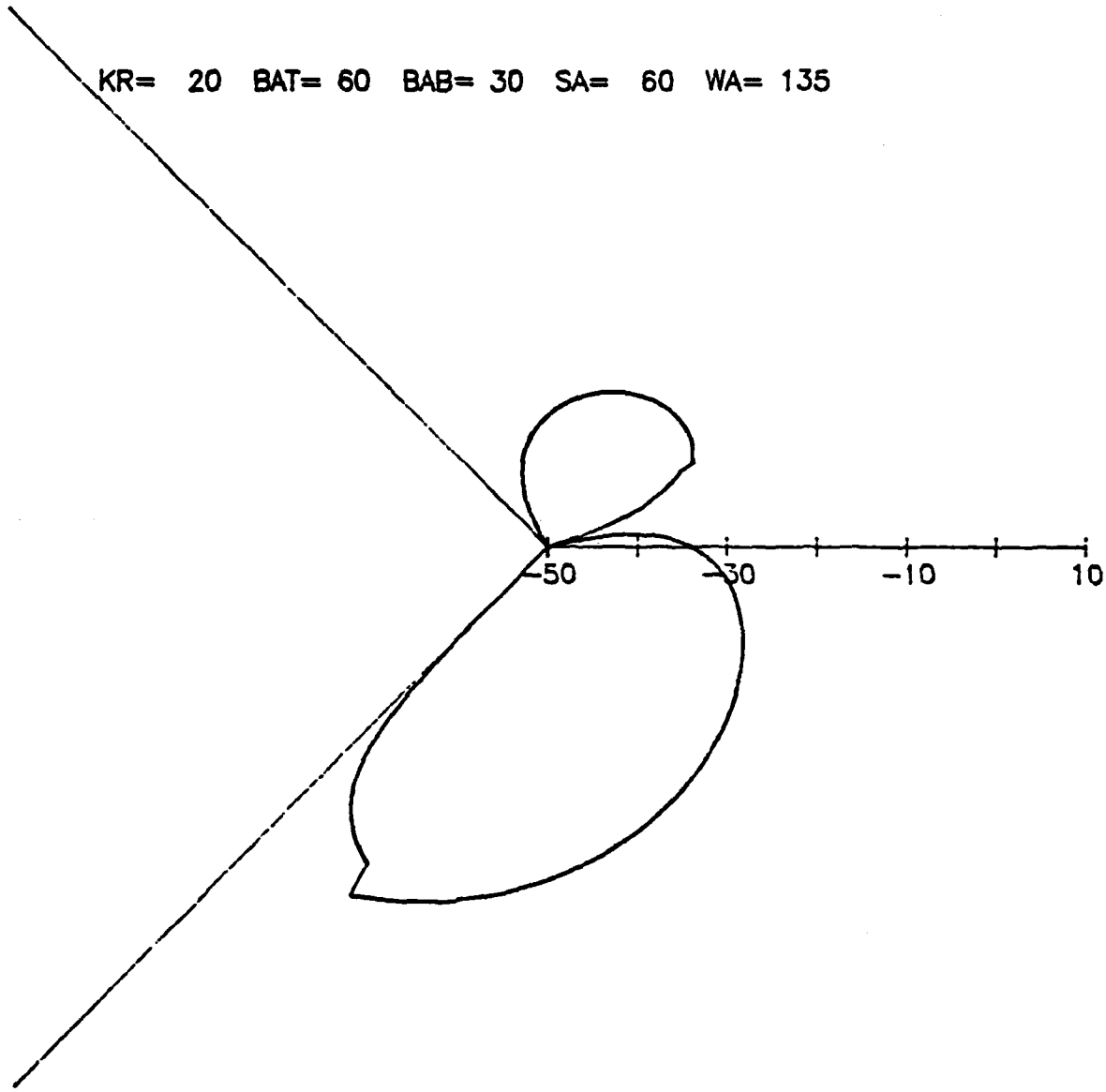

Fig. 4.14 Diffraction of point source radiation with $kr_o = 5$ $\theta^+ = 60°$, $\theta^- = 30°$, $\phi_o = 60°$ and $\beta = 135°$.

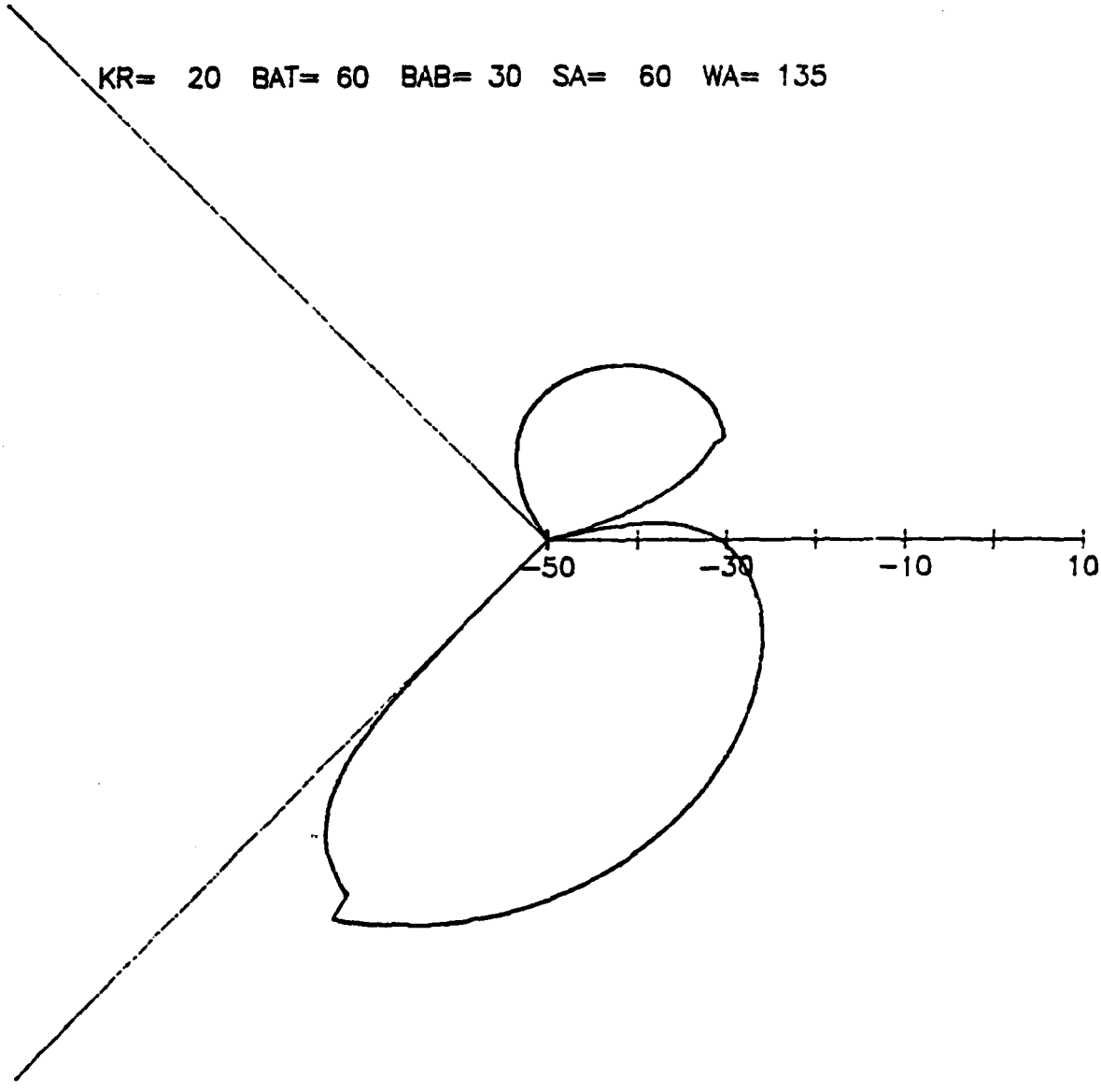

Fig. 4.15 Diffraction of point source radiation with $kr_o = 10$, $\theta^+ = 60°$, $\theta^- = 30°$, $\phi_o = 60°$ and $\beta = 135°$.

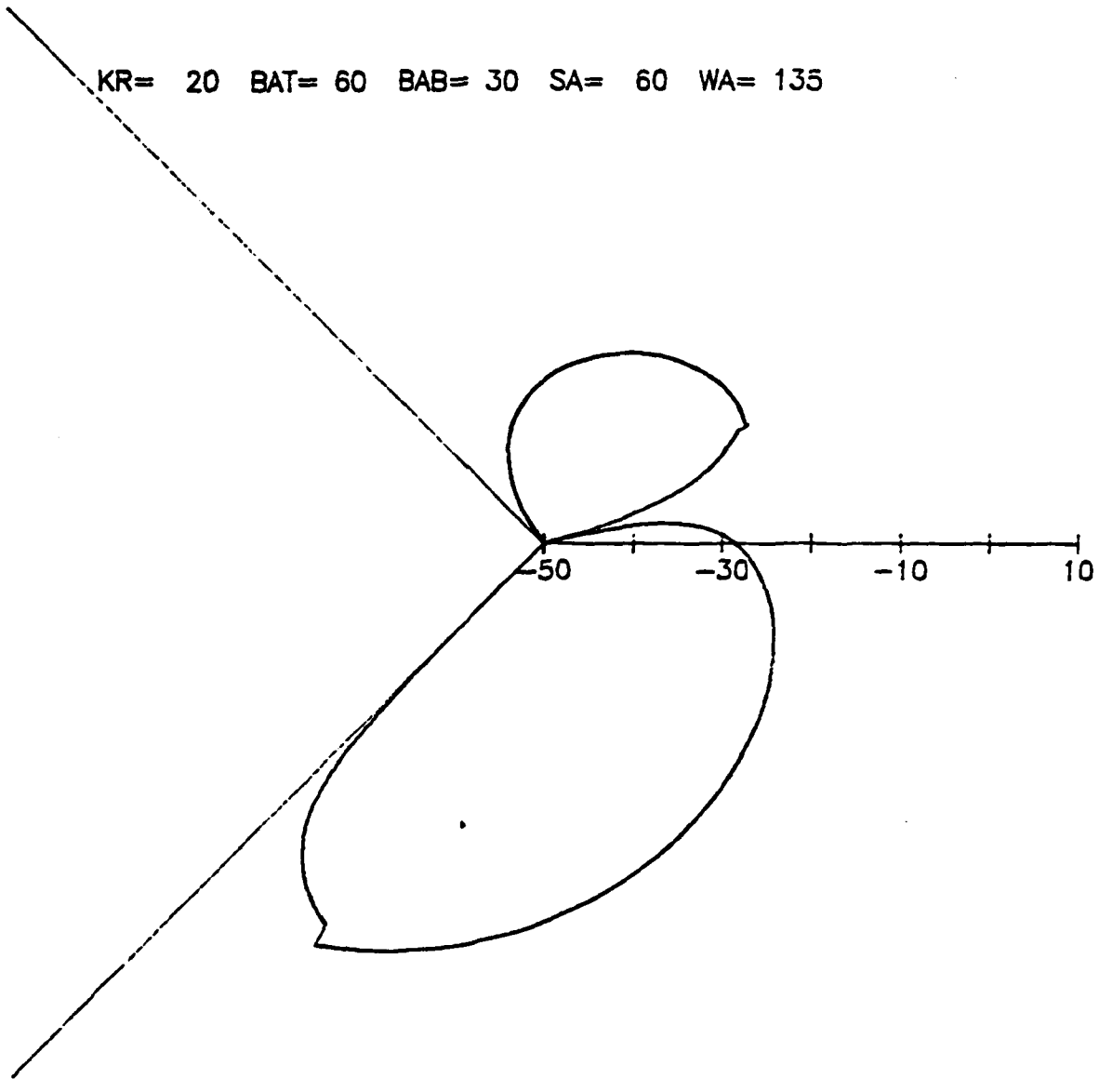

Fig. 4.16 Diffraction of point source radiation with $kr_o = 20$, $\beta^+ = 60°$, $\beta^- = 30°$, $\beta_o = 60°$ and $\beta_o = 135°$.

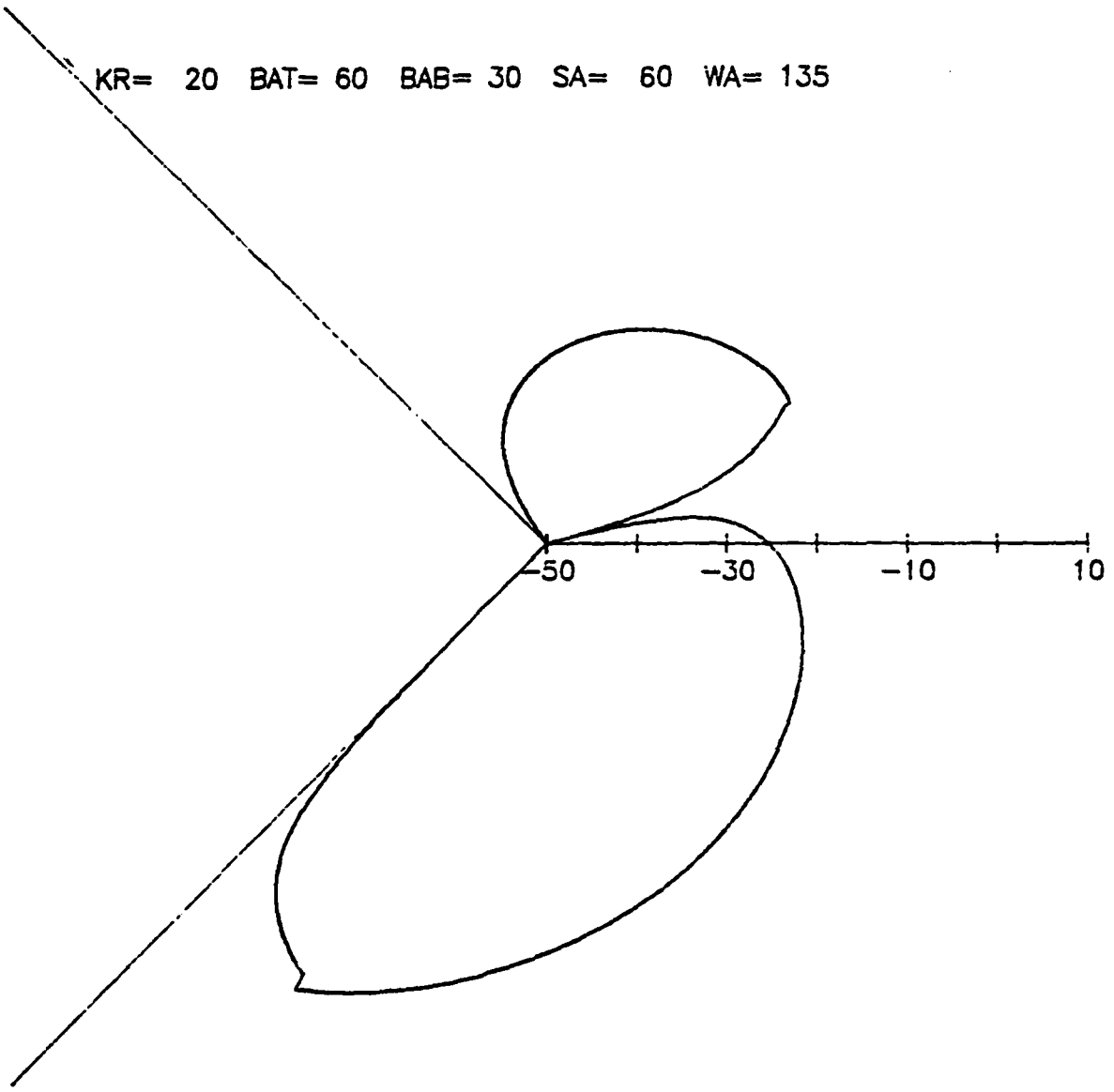

Fig. 4.17 Diffraction of point source radiation with $kr_o = 200$, $\theta^+ = 60°$, $\theta^- = 30°$, $\theta_o = 60°$ and $\beta = 135°$.

D-A133 266 ACOUSTIC DIFFRACTION BY AN IMPEDANCE-COVERED EDGE(U) 2/2
PENNSYLVANIA STATE UNIV UNIVERSITY PARK APPLIED
RESEARCH LAB M MARSAN 15 JUN 83 ARL/PSU/TM-83-95
UNCLASSIFIED N00024-79-C-6043 F/G 20/1 NL

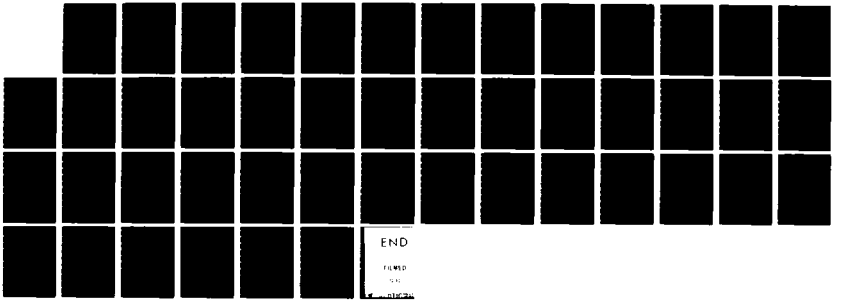

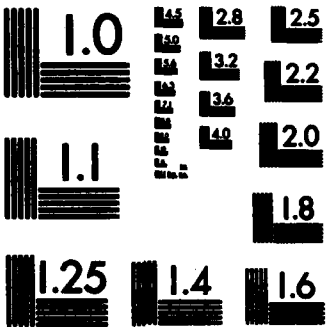

MICROCOPY RESOLUTION TEST CHART
NATIONAL BUREAU OF STANDARDS-1963-A

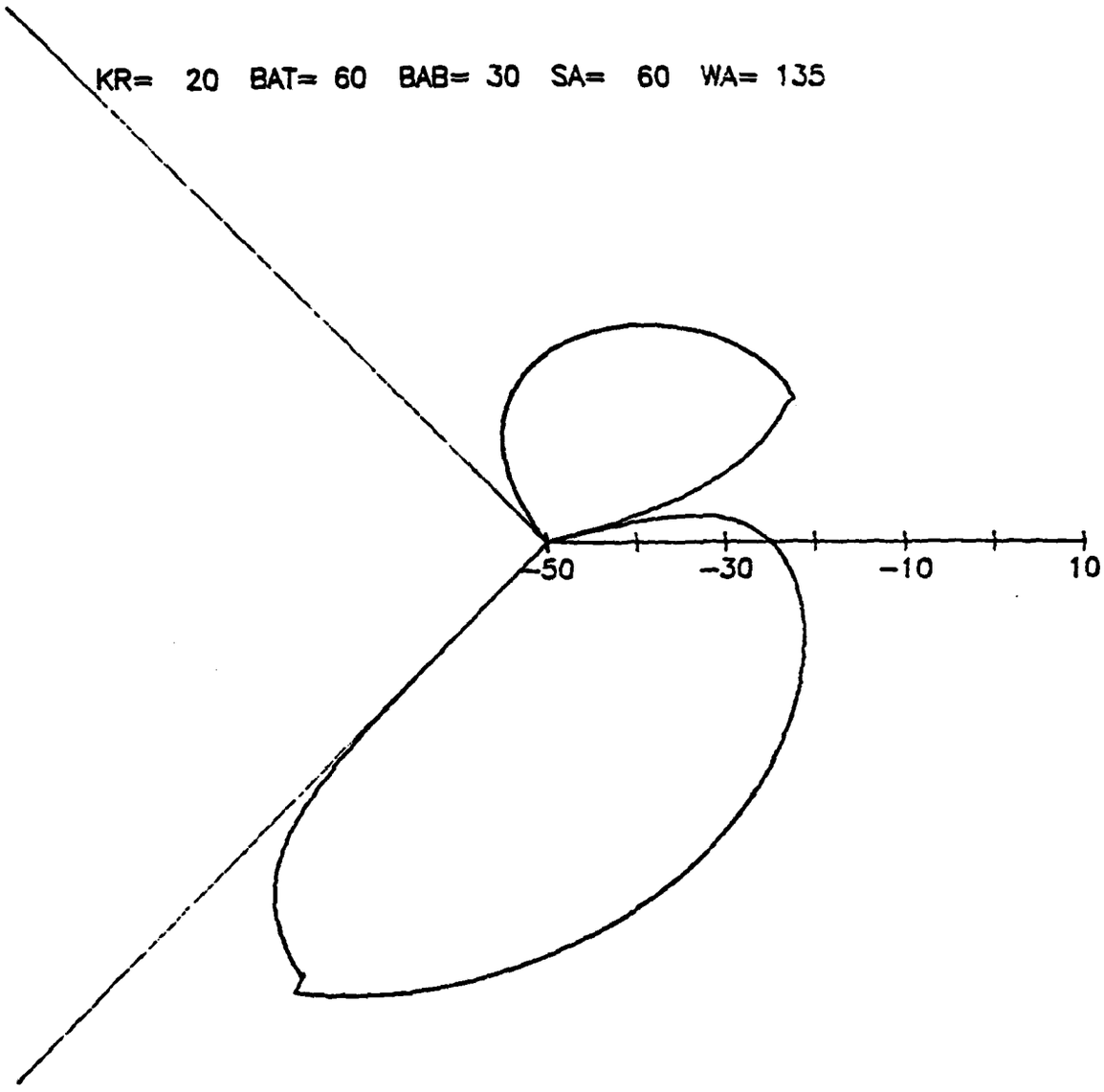

Fig. 4.18 Diffraction of point source radiation with $kr_o = 2000$, $\vartheta^+ = 60°$, $\vartheta^- = 30°$, $\vartheta_o = 60°$ and $\beta = 135°$.

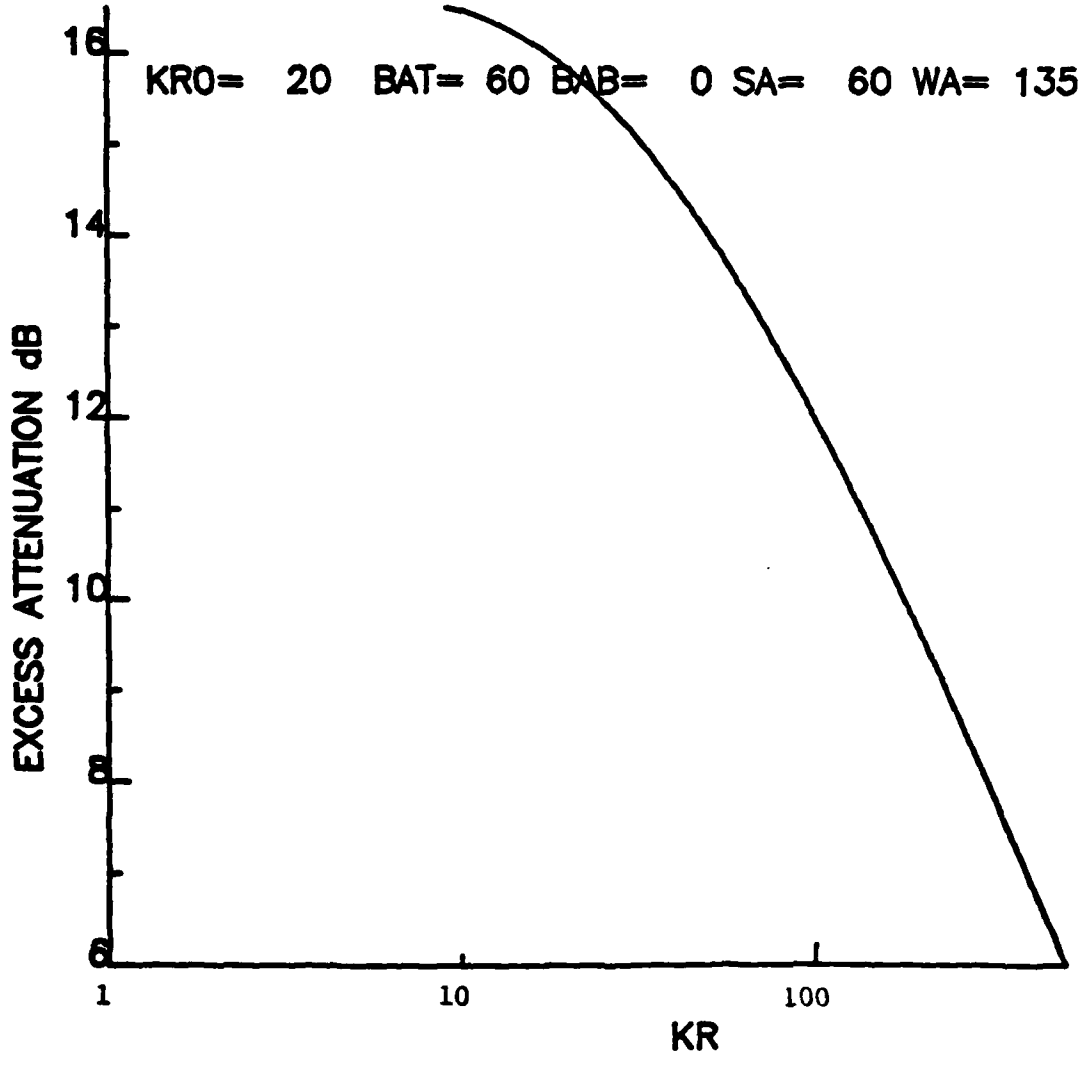

Fig. 4.19 Excess attenuation as a function of kr (Eq. 4.1).

4.5 Backscattering from a Wedge

For many applications, it is imperative to calculate the diffracted pressure at the source location, the so called monostatic diffraction. The next six plots exhibit this backscattered pressure. For this situation, the source and the observer are at the same location, i.e., $\phi = \phi_0$ in Eq. (3.23). In Figs. 4.20 through 4.23, the backscattered pressure is calculated for wedges whose surface impedances are $\theta^+ = 60°$ and $\theta^- = 30°$ with $kr = 20$. In the next two plots the impedances on the two surfaces are equal $\theta^+ = \theta^- = 30°$, while $kr = 20$ in Fig. 4.24 and $kr = 200$ in Fig. 4.25.

4.6 Comparison with the Maliuzhinets Solution

To conclude this section, plots comparing results of Maliuzhinets and results from Chapter II are presented in Figs. 4.26 and 4.27. The plots are for the far-field diffracted pressure of plane waves derived from Eq. (3.23). Two wedge angles, namely, $\beta = 135°$ and $\beta = 165°$, are used in the plots because, for these special wedge angles, the complicated Maliuzhinets functions reduce to a finite product form. The resulting solution is adapted from Skudrzyk [7]. In both figures $\theta^+ = 60°$, $\theta^- = 30°$, $kr = 20$ and $\phi_0 = 60°$.

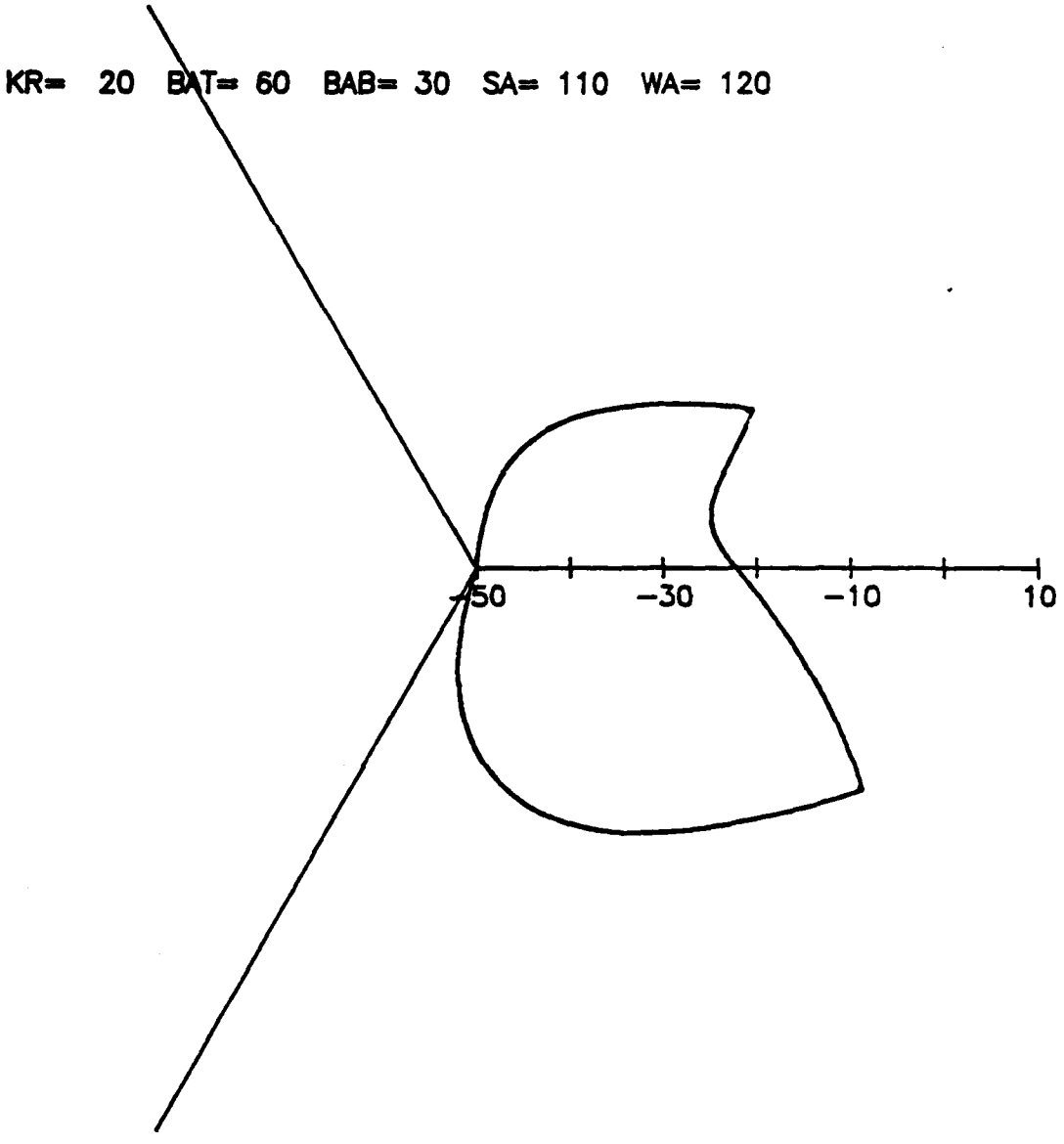

Fig. 4.20 Backscattering of plane wave from a 120° wedge with $\theta^{+} = 60°$, $\theta^{-} = 30°$, $kr = 20$ and $\phi_o = 110°$.

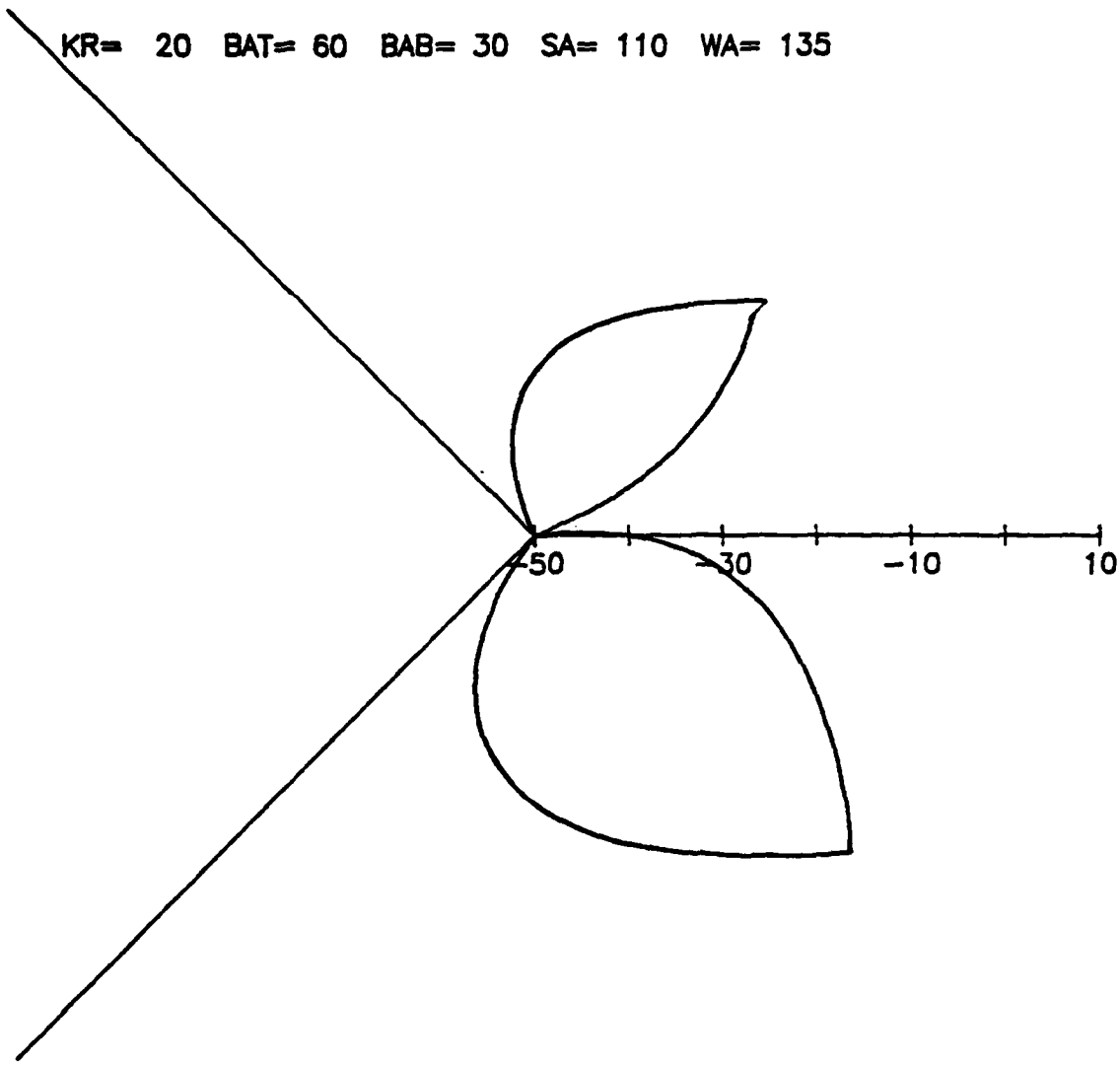

Fig. 4.21 Backscattering of plane wave from a 135° wedge with $\vartheta^+ = 60°$, $\vartheta^- = 30°$, kr = 20 and $\phi_o = 110°$.

KR= 20 BAT= 60 BAB= 30 SA= 110 WA= 165

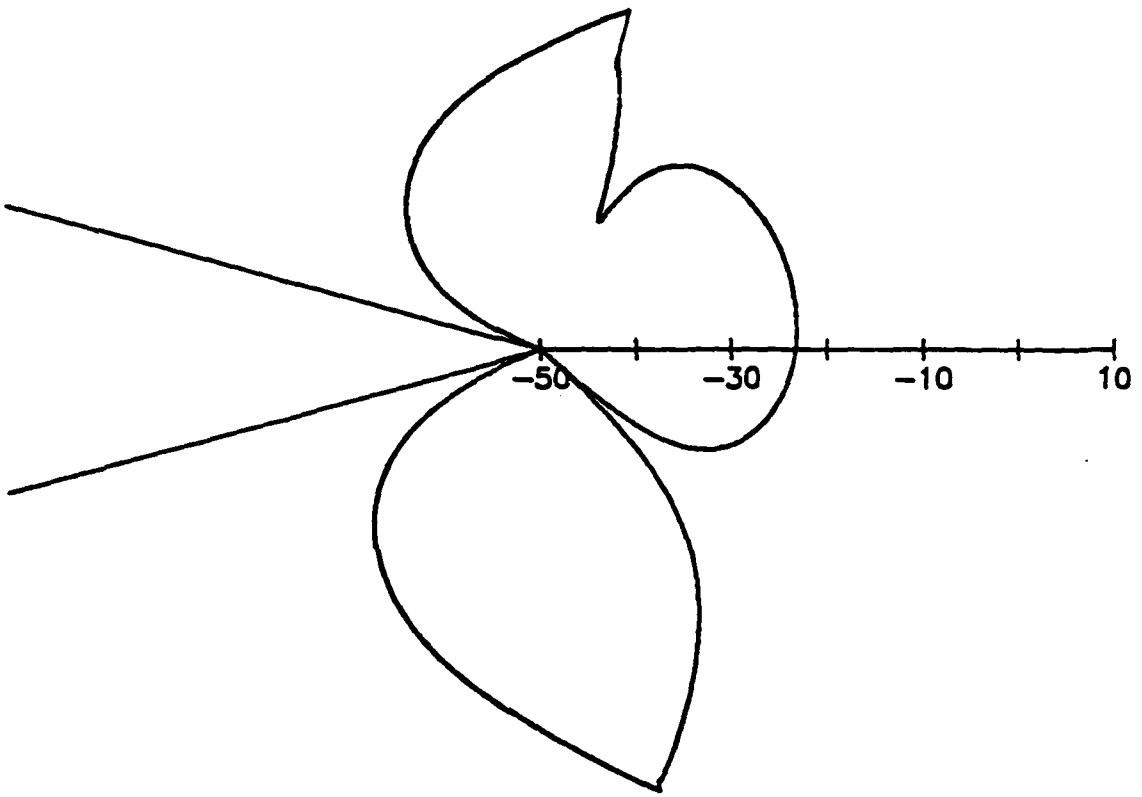

Fig. 4.22 Backscattering of plane wave from a 165° wedge with $\theta^+ = 60°$, $\theta^- = 30°$, kr = 20 and $\phi_o = 110°$.

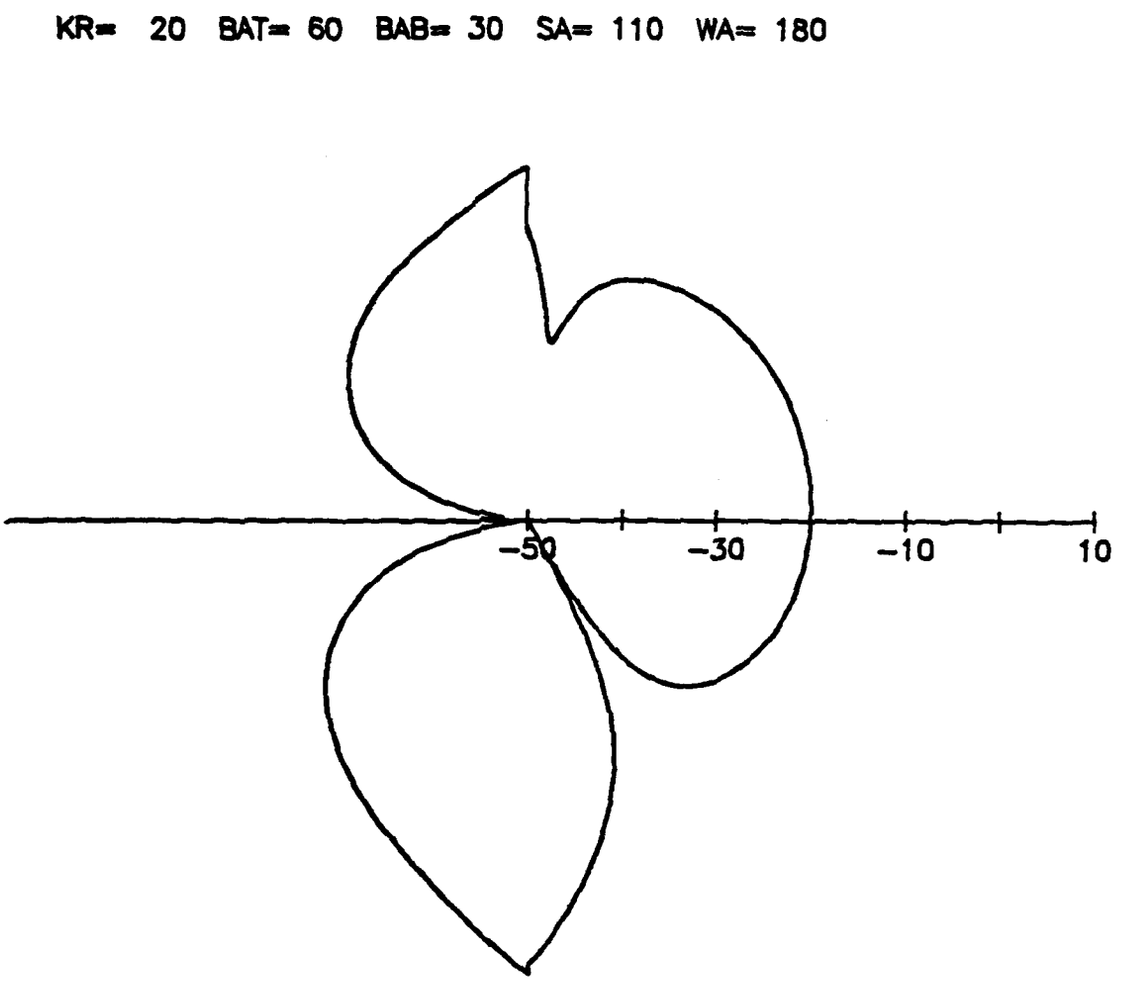

Fig. 4.23 Backscattering of plane wave from a 180° wedge with $\theta^+ = 60°$, $\theta^- = 30°$, kr = 20 and $\phi_o = 110°$.

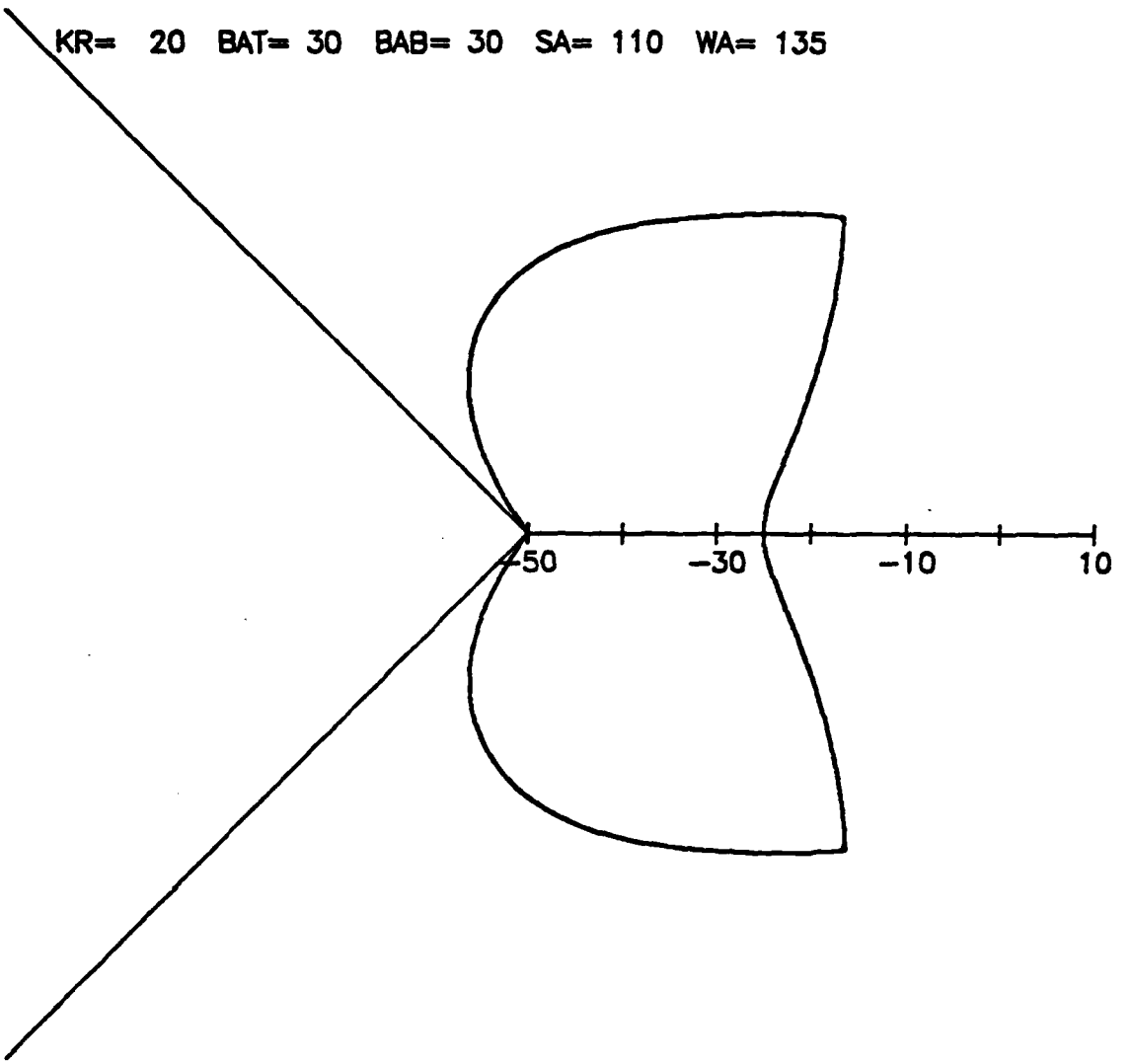

Fig. 4.24 Backscattering of plane wave from a 135° wedge with $\theta^+ = 30°$, $\theta^- = 30°$, kr = 20 and $\phi_o = 110°$.

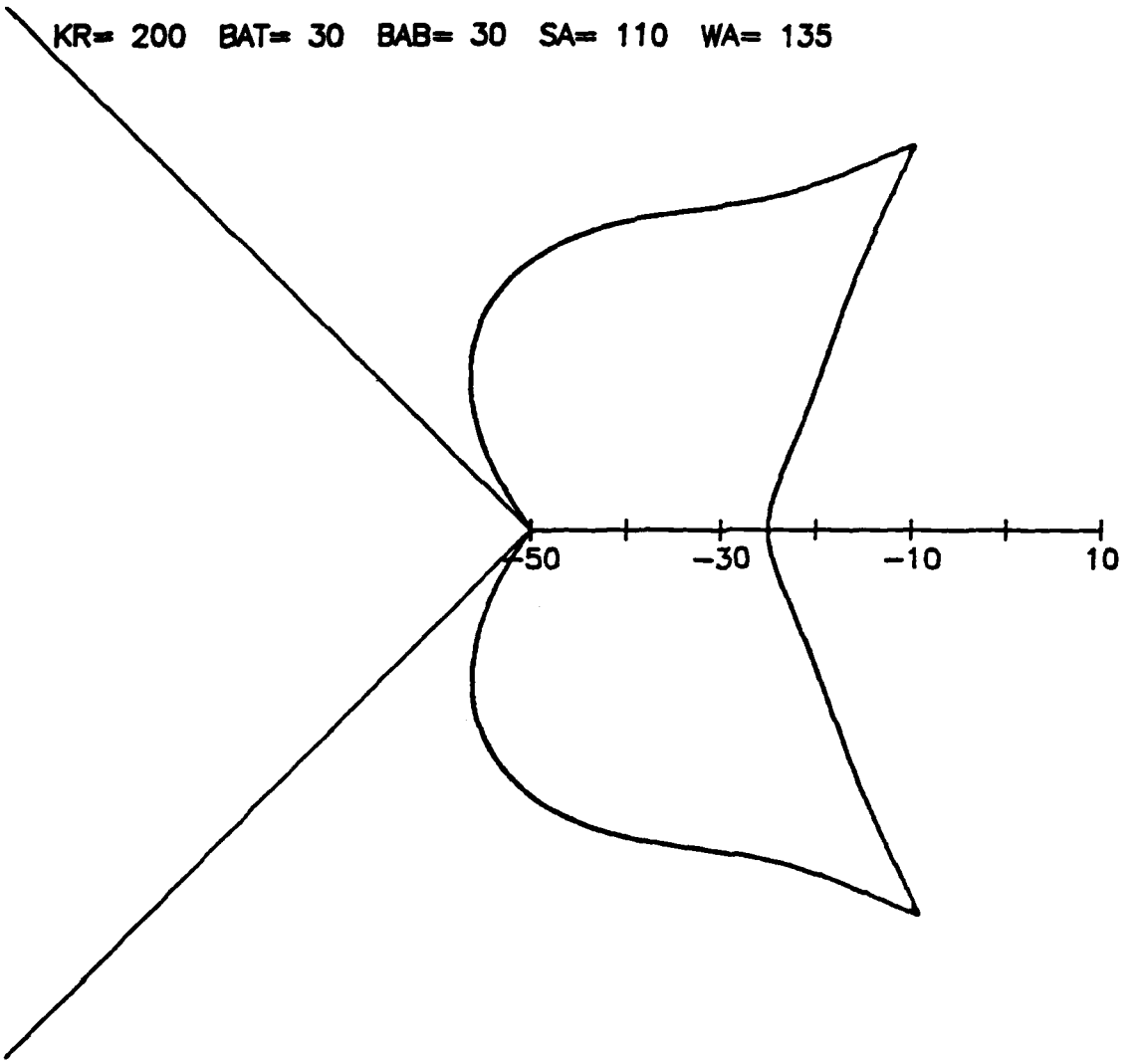

Fig. 4.25 Backscattering of plane wave from a 135° wedge with $\theta^+ = 30°$, $\theta^- = 30°$, $kr = 200$ and $\phi_o = 110°$.

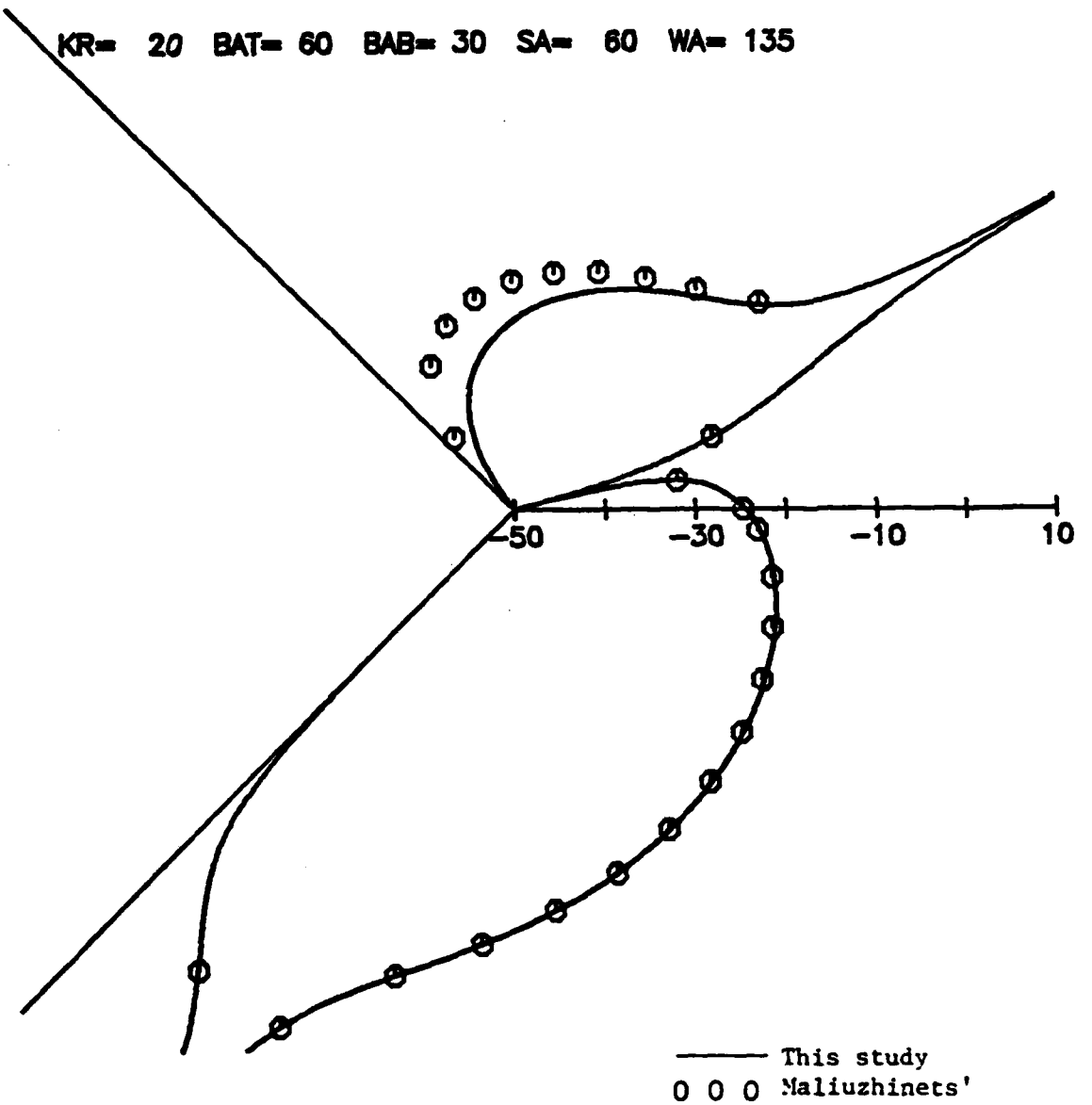

Fig. 4.26 Comparison of far-field diffracted pressure predicted by t' is study with Maliuzhinets'.

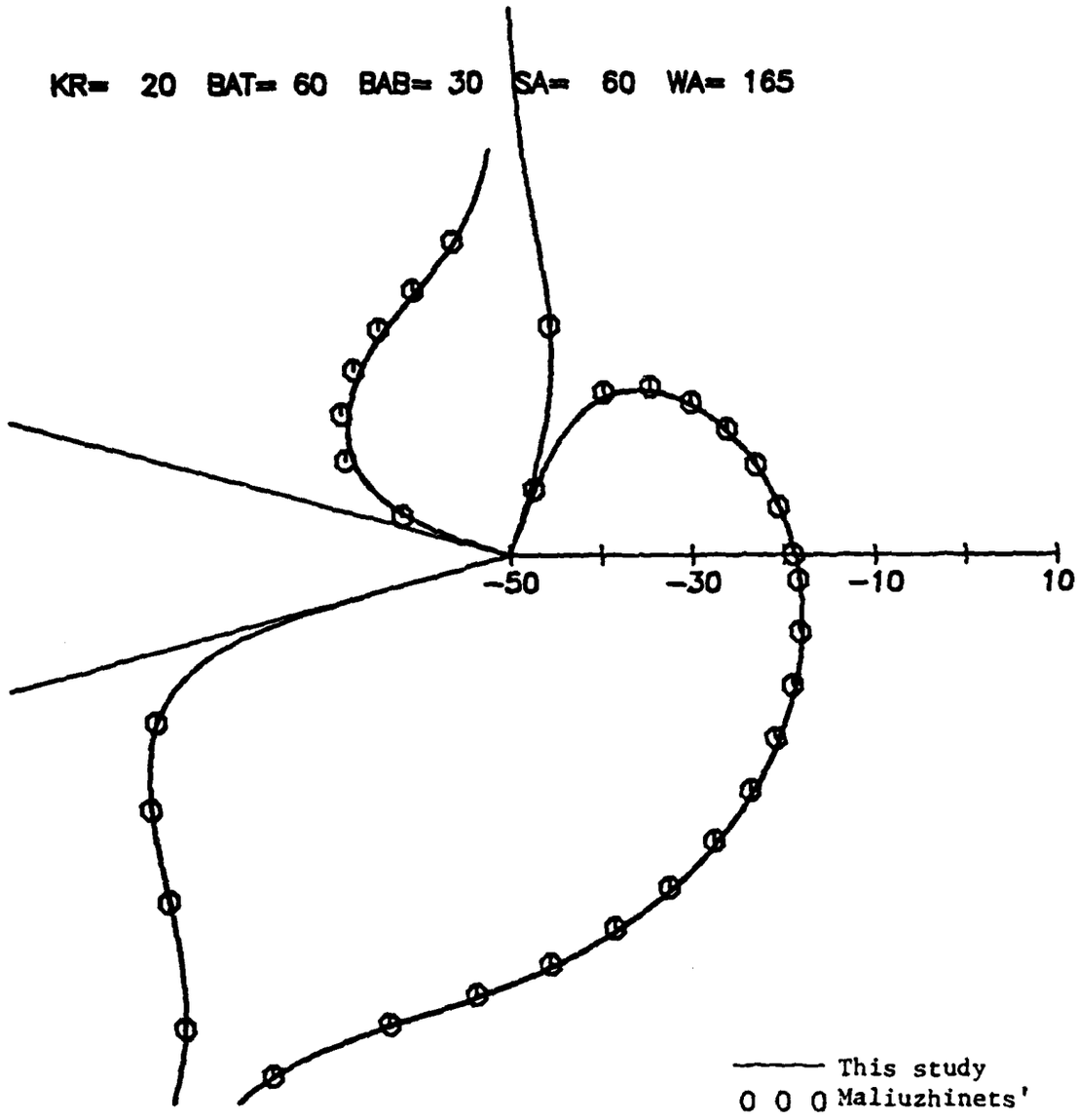

Fig. 4.27 Comparison of far-field diffracted pressure predicted by this study with Maliuzhinets'.

CHAPTER V

DISCUSSION OF NUMERICAL RESULTS AND CONCLUSIONS

5.1 Introduction

The primary objective of this study is to develop a solution for diffraction of acoustic waves by a locally reacting impedance covered wedge. This objective is achieved by constructing a spectrum function from the physical interpretation of the singularities. The resulting solution from this analysis is a closed form solution, which is a significant improvement on the Maliuzhinets solution.

In this chapter discussions of the physical interpretation of the diffraction problem solved in Chapter II and the numerical results that were compiled in Chapter IV, using the mid-range solutions from Chapter III, are presented.

5.2 Physical Interpretation of P(cosα)

The spectrum function P(cosα) (see Eq. (2.45)) consists of two parts; the two angle factors $M_1(\alpha)$ and $M_2(\alpha)$ multiplied by two diffraction factors $\psi_1(\alpha)$ and $\psi_2(\alpha)$, respectively. The geometrical shadow boundaries are represented in P(cosα) and are contained in $M_1(\alpha)$ and $M_2(\alpha)$. Although they are different from the Sommerfeld angle factors, they possess identical poles. Four of these poles represent the following geometrical boundaries:

a. $2\beta - \phi_0 - \pi$ represents the angle of specular reflection from the upper surface ($+\beta$).

b. $+\phi_0 - \pi$ represents the angle of the incident shadow boundary.

c. $-2\beta - \phi_0 + \pi$ represents the angle of specular reflection from the lower surface ($-\beta$).

d. $+\phi_0 + \pi$ represents the angle of the incident shadow boundary.

The functions $\psi_1(\alpha)$ and $\psi_2(\alpha)$ are relatively insensitive to the argument α except when α is close to the zeros and poles of $P(\cos\alpha)$. For example, when α approaches $2\beta - \phi_0 - \pi$, representing the reflection angle from the upper surface, $\psi_1(\alpha)$ approaches the reflection coefficient C_r (see Eq. 2.62). Although $\psi_1(\alpha)$ and $\psi_2(\alpha)$ do not have any poles in the region $\mathrm{Re}|\alpha| < \beta$, they have two zeros each when the exit angle is equal to one of two Brewster angles of an impedance covered surface. The nulls α_z of the functions can be given in terms of the grazing Brewster angles θ^+, and θ^- as follows:

For $\psi_1(\alpha)$

$$\alpha_z = \beta - \theta^+ \tag{5.1}$$

and

$$\alpha_z = \beta - \pi + \theta^+ \tag{5.2}$$

and for $\psi_2(\alpha)$

$$\alpha_z = -\beta + \theta^- \tag{5.3}$$

and

$$\alpha_z = -\beta + \pi - \theta^- \quad . \tag{5.4}$$

The function $P(\cos\alpha)$ has another property; the term $M_1(\alpha)\ \psi_1(\alpha)$ interchanges with $M_2(\alpha)\ \psi_2(\alpha)$ when the signs of α, representing the observer angle ϕ, and ϕ_0 are interchanged as well as θ^+ by θ^-. This is expected, since the chosen coordinate system is symmetric about the axis x=0.

The conditions of evenness, Eqs. (2.40) and (2.42) can be written in difference equation form as:

$$P(\beta-\alpha-\pi)[\sin\theta^{+}-\sin\alpha] = P(\beta+\alpha-\pi)[\sin\theta^{+}+\sin\alpha] \tag{5.5}$$

$$P(-\beta+\alpha+\pi)[\sin\theta^{-}-\sin\alpha] = P(-\beta-\alpha+\pi)[\sin\theta^{-}+\sin\alpha] \tag{5.6}$$

or

$$P(\alpha) = P(2\beta-\alpha)\,\frac{[\sin\theta^{+}-\sin(\beta-\alpha)]}{[\sin\theta^{+}+\sin(\beta-\alpha)]} \tag{5.7}$$

$$P(\alpha) = P(-2\beta-\alpha)\,\frac{[\sin\theta^{-}-\sin(\beta+\alpha)]}{[\sin\theta^{-}+\sin(\beta+\alpha)]} \tag{5.8}$$

It is apparent from Eqs. (5.7) and (5.8) that only wedges with rigid-rigid or soft-soft boundary conditions have spectrum functions $P(\cos\alpha)$ with periodicity 4β.

5.3 Discussion of Numerical Results

5.3.1 Transition Regions

The mid-range solutions (Eqs. (3.23), (3.56) and (3.87)) for diffraction of an acoustic plane wave consist of two terms; each term having two $F_{\pm}(x)$ terms defined by Eqs. (3.24), (3.57) and (3.88). At the incident and reflection shadow boundaries, the far-field solution (Eq. 2.58) becomes unbounded. This discontinuity in the geometric-optics field is compensated separately by one of the four $F_{\pm}(x)$ terms in the mid-range solution.

The $F_{\pm}(x)$ functions contain an argument

$$a^{\pm}(x) = 2\cos^{2}\left(\frac{2n\pi N^{\pm}-x}{2}\right)$$

which is a measure of the angular separation between the field point and the incident or the reflection shadow boundaries which are listed in section 5.2. At one such boundary, one of the cotangent or tangent functions in the mid-range solution becomes singular. The integers N^+ and N^-, which are defined by Eqs. (3.26a) and (3.26b), assure that the argument of $a^{\pm}(x)$ becomes zero at that boundary. Since the $a^{\pm}(x)$ function appears as a multiplier in $F_{\pm}(x)$, the corresponding term of the solution vanishes but the other three remaining terms are bounded. Because the $F_{\pm}(x)$ functions cause the solution to become smooth across these boundaries, they are called transition functions.

For example consider Fig. 4.1 with $kr = 20$, $\theta^+ = 60°$, $\theta^- = 0°$, $\phi_o = 60°$ and $\beta = 135°$. The complex values of pressure on either side of the reflection shadow boundary at $2\beta - \phi_o - \pi = 30°$ are:

$$p_d = 0.0092 - i0.0295, \quad \phi = 30°^-,$$

$$= -0.0128 + i0.0202, \quad \phi = 30°^+.$$

Using Eqs. (2.61) and (2.63) the reflected pressures at either side of the reflection shadow boundary are:

$$p_r = -0.0111 + i0.0249, \quad \phi = 30°^-,$$

$$= 0.0111 - i0.0249, \quad \phi = 30°^+$$

Addition of reflected and diffracted fields produce a continuous field as follows:

$$p_t = -0.0019 - i0.0046 + p_i, \quad \phi = 30°^-,$$

$$= -0.0017 - i0.0047 + p_i, \quad \phi = 30°^+.$$

If similar calculations are made for the incident shadow boundary at $-\pi + \phi_o = -120°$ the following continuous pressure field results across that boundary:

$$P_t = 0.1816 - i0.5725, \ \phi = -120°^-,$$

$$= 0.1874 - i0.5735, \ \phi = -120°^+.$$

5.3.2 Influence of Impedance Coverage

In Figs. 4.1 and 4.2 the source is placed above and below the wedge, respectively. When the impedance covered surface is insonified the magnitude of the impedance cover dramatically influences the diffraction field. As the impedance of the insonified surface is increased thereby increasing the absorption, the diffracted pressure in the illuminated zone decreases. However, the impedance cover of the surface in the shadow zone has very little effect on the diffracted pressure in the entire field.

If the upper surface of the wedge has a pressure release cover and the bottom surface is rigid, and the angle of incidence is on the pressure release side and close to the grazing angle, Fig. 4.3, the diffracted pressure in the insonified zone is negligible because the diffracted energy is primarily absorbed by the pressure release surface. The opposite is true when the rigid surface is insonified (Fig. 4.4), the diffracted pressure is significant over the entire space. Fig. 4.5 demonstrates how the impedance cover on both surfaces influences the diffracted pressure. Since the upper surface is more absorbent than the lower surface, the diffracted pressure is higher in the lower region.

5.3.3 Influence of the Wedge Angle

The diffracted field is controlled by the position of the observer with respect to the incident and reflected shadow boundaries and the

nulls. Their effects are demonstrated in Figs. 4.6 through 4.13 by changing the wedge angle for different source locations. For any one geometric configuration, there can be only two geometric-optics boundaries; one incident and one reflected shadow boundary or two reflected shadow boundaries. Figs. 4.10 and 4.11 are examples of two reflection shadow boundaries. The relative position of the zeros of $\psi_1(\alpha)$ and $\psi_2(\alpha)$ with respect to the angle of incidence causes sharp minima shown in these figures.

5.3.4 Influence of the Sphericity of the Point Source Field

The diffraction solution for a point source is given by Eq. (3.87). The parameter R_1 which appears in the solution is the shortest path the wave travels from the source to the edge of the wedge and from there to the receiver. It can be seen that the reciprocity theorem is satisfied in this solution. If the values for kr and kr_o and ϕ and ϕ_o are interchanged in Eq. (3.87), which is essentially interchanging the positions of the source and the receiver, there is no change in the solution. Figs. 4.14 through 4.18 illustrates that, as the source is placed farther away from the wedge, the normalized diffracted pressure field approaches to a plane wave incidence except near the shadow boundaries.

The next plot (Fig. 4.19) shows the excess attenuation (see Eq. 4.1) versus non-dimensional distance from the wedge. The curve almost becomes a straight line for observer distance kr over 50, i.e., the diffracted pressure approaches its asymptotic approximation of $1/\sqrt{kr}$. This means that the asymptotic solution can be used for observers located at least 8 wavelengths away.

5.3.5 Backscattered Field

The plots of the backscattered pressure field show clearly defined maxima. The maxima are located where the reflection coefficient C_r reaches its maximum such that

$$C_r = \frac{1-\sin\theta^+}{1+\sin\theta^+} \text{ , i.e., at } \phi = \beta - \pi/2 \text{ ,}$$

and

$$C_r = \frac{1-\sin\theta^-}{1+\sin\theta^-} \text{ , i.e., at } \phi = -\beta + \pi/2.$$

Also at these locations the angle factors $M_1(\alpha)$ and $M_2(\alpha)$ become infinite, so the impedance cover only controls the magnitude of the maxima, but not the location.

In the backscattering from a rigid-rigid wedge there is no return if the source is located at $\phi = 0°$, whereas Figs. 4.20 through 4.25 illustrate that the nulls are dependent on the impedance cover.

5.4 Conclusions

In the discussion of the closed form solution and the numerical results for the diffracted pressure from impedance covered wedges, many significant factors affecting the diffraction are pointed out.

It is evident from the plots that the impedance of the surface lying in the shadow zone has little effect on the diffracted pressure while the impedance cover on the insonified surface has a significant effect on the diffracted pressure in the entire space. The impedance coverage of the insonified surface has similarly a dominant influence on the behavior of the backscattered pressure.

The location of the maxima and the minima of the diffracted field may be adjusted by changing the impedance of the insonified surface and the wedge angle. It was also shown that the plane wave asymptotic solution for an observer in the far-field with the correction factor for a point source is a good approximation for kr > 50 except near the shadow boundaries.

In the derivation of the mid-range solutions, only the first term of the Taylor series expansion is included in the solution. It has been previosly established by the author that in the integration for the asymptotic series, the odd terms vanish and the high order even terms have very little contributions except for receivers located very close to the absorbent wedge surfaces. The first term in the series was found to provide sufficient accuracy.

5.5 Suggestions for Further Research

In the mid-range solutions, although the first term in the asymptotic series provides sufficient accuracy, an investigation of higher terms near the wedge surfaces can be studied. The higher order terms in the Taylor expansion contributes the surface waves.

The problem of diffraction of acoustic waves from a wedge with locally reacting boundary conditions can be expended to diffraction from elastic wedges made of plates or solid bodies.

Furthermore, the solutions obtained in this study may be adapted for problems of diffraction of sound over a wedge located on a rigid plane.

REFERENCES

[1] Sommerfeld, A. Mathematische theorie der diffraction. Mathematische Annalen, 1896, 47, 317-374.

[2] MacDonald, H.M. Elastic waves. Cambridge, England: Cambridge University Press, 1902.

[3] Senior, T.B.A. Diffraction of a plane wave by an imperfectly conducting wedge. Commun. Pure and Applied Math., 1959, 337-372.

[4] Williams, W.E. Diffraction of an E-polarized plane wave by an imperfectly conducting wedge. Proceedings of the Royal Society of London, 1959, A252, 376-393.

[5] Barnes, E.W. Messinger Math. 1899, 29, 64.

[6] Maliuzhinets, G.D. Conversion formula for Sommerfeld integral. Dokl. Adad. Nauk S.S.S.R., 1958, 118(6), 1099,1102.

[7] Skudrzyk, E.J. Acoustic scattering from the impedance covered straight edge and wedge; the exact theory. The Penn State University, Applied Research Lab., TM 75-01, 1975.

[8] VanLennep, A.G.R. The kernal of Sommerfeld's transform as solution to difference equations for a class of diffraction problems. Journal of Acoustic Society of America, 1974, 45 4401-4405.

[9] Maliuzhinets, G.D. Sound radiation by vibrating sides of an arbitrary wedge. Akus. Zh., 1955, 1(2), 144-163.

[10] Maliuzhinets, G.D. Audio radiation by the oscillating boundaries of an arbitrary wedge-Part II, Akust. Zh., 1955, 1(3), 226-234.

[11] Maliuzhinets, G.D. The excitation, reflection, and emission of surface waves with given impedances of faces. Dokl. Adad. Nauk. S.S.S.R., 1958, 121(3), 436-439.

[12] Sakharova, M.P. Influence of the edge of a wedge with vibrating faces on the radiation of acoustic power. Dokl. Akad. Nauk. S.S.S.R., 1966, 12, 121-125.

[13] Tuzhilin, A.A. New representation of diffraction fields in wedge-shaped regions with ideal boundaries. Soviet Physics-Acoustics, 1963, 9, No. 2.

[14] Zavadskii, Yu and Sakharova, M.P. Application of the special function $\chi(z)$ in problems of wave diffraction in wedge-shaped regions. Soviet Physics-Acoustics, 1967, 13, 487.

[15] Zavadskii, Yu and Sakharova, M.P. Tables of the special function $\psi(z)$. Report of the Institute of Acoustics, Acadamy of Science of the USSR, 1960, Moskow.

[16] Pierce, A.D. Diffraction of sound around corners and over wide barriers. Journal of Acoustic Society of America, 1974, 55, 941-955.

[17] Kouyoumjian, R.G. and Patnak, P.H. A uniform geometrical theory of diffraction for an edge in a perfectly conducting surface. Proceedings of the Institute of Electronic and Electrical Engineers, 1974, 62(11), 1448-1461.

[18] Pauli, W. On asymptotic series for functions in the theory of diffraction of light. Physics Review, 1938, 54, 924-931.

[19] Oberhettinger, F. On asymptotic series for functions occurring in the theory of diffraction of wave by wedges. Journal of Mathematical Physics, 1956, 34, 245-255.

[20] Hayek, S.I., Lawther, J.M., Kendig, R.P., and Simowitz, K.T. Investigation of selected noise barrier acoustic parameters. Final Report, National Cooperative Highway Research Program 3-26, Transportation Research Board, National Research Council, 1978.

[21] Rawlins, A.D. Diffraction by an absorbing wedge. Journal of Sound and Vibration, 1975, 41(3), 391-393.

[22] Carslaw, H.S. Some multiform solutions of the partial differential equations of physics and mathematics and their applications. Proceedings of London Mathematical Society, 1899, 30, 121-163.

[23] MacDonald, H.M. A class of diffraction problems. Proceedings of the London Mathematical Society, 1915, 14, 410-427.

[24] Rawlins, A.D. The solution of a mixed boundary value problem in the theory of diffraction by a semi-infinite plane. Proceedings of the Roval Society of London, 1975, A346, 469-484.

[25] Senior, T.B.A. Diffraction by a semi-infinite metalic sheet. Proceedings of the Roval Society of London, 1952, A213, 436-458.

[26] Clemmow, P.C. The plane wave spectrum representation of electromagnetic waves. London: Pergammon Press, 1966.

[27] Kendig, R.P., and Hayek, S.I. Diffraction by a hard-soft barrier. Journal of Acoustic Society of America, 1981, 70, 1156-1165.

[28] Kendig, R.P. Acoustic diffraction by an impedance covered half plane (Doctoral dissertation, The Pennsylvania State University, 1977). Dissertation Abstract International, 1977, 38, 2264. (University Microfilms No. 77-23246).

[29] Bowman, J., Senior T.B.A., and Uslenghi, P.L.E. Electro-magnetic and acoustic scattering by simple shapes. Amsterdam: North-Holland, 1969.

[30] Christiansen, P.L. Comparison between edge diffraction processes. Proceedings of the IEEE, 1974, 62, 1462-1468.

[31] Skudrzyk, E.J. The foundations of acoustics. Vienna: Springer-Verlag, 1971.

APPENDIX A

CONDITION OF ZERO VALUE OF THE LOOP INTEGRAL

A loop integral is zero [7],

$$\int_{U_1+U_2} S(z)\, e^{-ikr\cos(z)}\, dz = 0,$$

if the function $S(z)$ is even, i.e., if $S(z) = S(-z)$

where

$$z = u + iv$$

Proof:

The path of integration is deformed into lines arbitrarily close to $u = -\pi$ and $u = +\pi$. Since $\cos(z) = \cos(-z)$ and $S(z) = S(-z)$ the integrands along the line $0 \geq v > -\infty$, $u = -\pi$ and $0 \leq v < \infty$, $u = \pi$ are equal. But since the directions of the two paths are opposite their total contribution is zero.

APPENDIX B

COMPUTER PROGRAM LISTINGS

```
C%%%%%FAR-FIELD SOLUTION FOR PLANE WAVE%%%%%%
      IMPLICIT REAL*8(A-H,O-Z)
      COMPLEX*16 C,CONST,THETAP,THETAM
      COMPLEX P,SD,PC
      REAL KR,PDB,SX,SY
      PI=3.141592
C%%%%%READ IN DATA%%%%%
C*    THETAP=COMPLEX IMPEDANCE OF THE TOP SURFACE
C*    THETAM=COMPLEX IMPEDANCE OF THE BOTTOM SURFACE
C*    PHI0=LOCATION OF THE SOURCE
C*    BETA=WEDGE ANGLE
      READ(3,500) THETAP,THETAM,PHI0,BETA
      KR=20.0
      P0=1.0
      N=BETA
500   FORMAT(6D10.5)
      WRITE(6,550) THETAP,THETAM,KR,PHI0,P0,BETA
550   FORMAT(10X,F10.5)
      RAD=PI/180.0
      THETAP=THETAP*RAD
      THETAM=THETAM*RAD
      PHI0=PHI0+0.0001
      PHI0=PHI0*RAD
      BETA=BETA*RAD
      C=CMPLX(0.0,1.0)
      R=PI/2.0/BETA
      CONST=-P0/4.0/BETA/C
      NN=10.0*N+1
      MM=2.0*NN
C
      WRITE(14,300) MM
300   FORMAT(1X,I10)
C
      DO 10 M=1,MM
      I=M-1
      IF(M.GT.NN) I=M-MM
```

```
      PHI=I*RAD/10.0
C
C*      CALCULATE THE DIFFRACTION FUNCTIONS
C
        C1=DTAN((2.0*BETA-PHI-PHI0-PI)/4.0)*DTAN((PHI-PHI0+PI)/4.0)
        C2=DTAN((2.0*BETA+PHI+PHI0-PI)/4.0)*DTAN((-PHI+PHI0+PI)/4.0)
        PS11=CDSIN(THETAP)-DSIN(BETA-PHI)
C
        PS12=CDSIN(THETAP)+2.0*DSIN((BETA-PHI)/2.0)*DSIN((BETA-PHI0)/2.0
     *)
C
        PS13=CDSIN(THETAM)+4.0*C1*(DSIN((BETA-PHI)/2.0)*C1+
     *DSIN((BETA+PHI)/4.0)*DCOS((3.0*BETA-PHI)/4.0)*DCOS(BETA))
C
        PS14=CDSIN(THETAM)+4.0*C1*(DSIN((BETA-PHI)/2.0)*C1-
     *DSIN((BETA+PHI)/4.0)*DCOS((3.0*BETA-PHI)/4.0)*DSIN((BETA+PHI0)/2.0
     *))
C
        PS21=CDSIN(THETAM)-DSIN(BETA+PHI)
C
        PS22=CDSIN(THETAM)+2.0*DSIN((BETA+PHI)/2.0)*DSIN((BETA+PHI0)
     */2.0)
C
        PS23=CDSIN(THETAP)+4.0*C2*(DSIN((BETA+PHI)/2.0)*C2+
     *DSIN((BETA-PHI)/4.0)*DCOS((3.0*BETA+PHI)/4.0)*DCOS(BETA))
        PS24=CDSIN(THETAP)+4.0*C2*(DSIN((BETA+PHI)/2.0)*C2-
     *DSIN((BETA-PHI)/4.0)*DCOS((3.0*BETA+PHI)/4.0)*DSIN((BETA-PHI0)/2.0
     *))
C
C*      ANGLE FACTORS
C
        FM1=DCOS(R*PHI0)/(DSIN(R*(PHI+PI))-DSIN(R*PHI0))
C
        FM2=DCOS(R*PHI0)/(DSIN(R*(PHI-PI))-DSIN(R*PHI0))
```

```
      PC=CONST*(FM1*(PS11/PS12*PS13/PS14)-FM2*(PS21/PS22*PS23/PS24))
C
      P=DSQRT(2.0*PI/KR)*PC*CDEXP(-C*PI/4.0-C*KR)
C
      Z1=PS11/PS12*PS13/PS14
      Z2=PS21/PS22*PS23/PS24
      PDB=SD(P,KR)
      WRITE(6,600) I,P,PDB,Z1,Z2
600   FORMAT(10X,I5,2(F10.5,5X),F10.5,2X,2F10.5)
      PDB=PDB+50.0
      IF(PDB.LT.0.0) PDB=0.0
      SY=PDB*DSIN(PHI)
      SX=PDB*DCOS(PHI)
      WRITE(14,310) SX,SY
310   FORMAT(1X,2F15.5)
10    CONTINUE
      STOP
      END
C
C
      FUNCTION SD(SS,KR)
      COMPLEX SS,SD
      REAL KR
      AA=SQRT(KR)
      ASS=CABS(AA*SS)
      SD=20.0*ALOG10(ASS)
      RETURN
      END
```

```
C         PLANE WAVE
          IMPLICIT REAL*8(A-H,O-Z)
          COMPLEX*16 C,CONST,THETAP,THETAM
          COMPLEX P,P1,P2,SD,PC,F1,F2,F3,F4,CE,FRES1,FRES2,FRES3,FRES4
          REAL KR,PDR,SX,SY,A1,A2,A3,A4,C1,C2,C3,C4,S1,
     $     S2,S3,S4
          PI=3.141592
          XXX=1
          READ(3,500) THETAP,THETAM,PHI0,BETA,KR
C%%%%%READ IN DATA%%%%%
C*    THETAP=COMPLEX IMPEDANCE OF THE TOP SURFACE
C*    THETAM=COMPLEX IMPEDANCE OF THE BOTTOM SURFACE
C*    PHI0=LOCATION OF THE SOURCE
C*    BETA=WEDGE ANGLE
          P0=1.0
          N=BETA
500       FORMAT(6D10.5,F10.5)
          WRITE(6,550) THETAP,THETAM,KR,PHI0,P0,BETA
550       FORMAT(10X,F10.5)
          RAD=PI/180.0
          THETAP=THETAP*RAD
          THETAM=THETAM*RAD
          PHI0=PHI0+0.0001
          PHI0=PHI0*RAD
          BETA=BETA*RAD
          C=CMPLX(0.0,1.0)
          AN=2.0*BETA/PI
          O=2.0*AN
C
          PR1=2.0*BETA-PHI0-PI
          PI1=PHI0-PI
          PR2=-2.0*BETA-PHI0+PI
C
          CE=C*(-KR+PI/4.0)
          CONST=-P0*CEXP(CE)/AN/DSQRT(2.0*PI*KR)
```

```
      NN=10*N+1
      MM=2.0*NN
C
      WRITE(14,300) MM
300   FORMAT(1X,I10)
C
      DO 10 M=1,MM
      I=M-1
      IF(M.GT.NN) I=M-MM
      PHI=I*RAD/10.0
C
C*    CALCULATE THE DIFFRACTION FUNCTIONS
      C1=DTAN((2.0*BETA-PHI-PHI0-PI)/4.0)*DTAN((PHI-PHI0+PI)/4.0)
      C2=DTAN((2.0*BETA+PHI+PHI0-PI)/4.0)*DTAN((-PHI+PHI0+PI)/4.0)
C
      PS11=CDSIN(THETAP)-DSIN(BETA-PHI)
C
      PS12=CDSIN(THETAP)+2.0*DSIN((BETA-PHI)/2.0)*DSIN((BETA-PHI0)/2.0
     *)
C
      PS23=CDSIN(THETAP)+4.0*C2*(DSIN((BETA+PHI)/2.0)*C2+
     *DSIN((BETA-PHI)/4.0)*DCOS((3.0*BETA+PHI)/4.0)*DCOS(BETA))
C
      PS21=CDSIN(THETAM)-DSIN(BETA+PHI)
      PS22=CDSIN(THETAM)+2.0*DSIN((BETA+PHI)/2.0)*DSIN((BETA+PHI0)
     */2.0)
C
      PS13=CDSIN(THETAM)+4.0*C1*(DSIN((BETA-PHI)/2.0)*C1+
     *DSIN((BETA+PHI)/4.0)*DCOS((3.0*BETA-PHI)/4.0)*DCOS(BETA))
C
      PS14=CDSIN(THETAM)+4.0*C1*(DSIN((BETA-PHI)/2.0)*C1-
     *DSIN((BETA+PHI)/4.0)*DCOS((3.0*BETA-PHI)/4.0)*DSIN((BETA+PHI0)/2.0
     *))
```

```
      GO TO 199
99    PS21=-DCOS((BETA+PHI)/2.0)
      PS22=DSIN((BETA+PHI0)/2.0)
      PS13=DSIN((BETA-PHI)/2.0)+2.0*C1*
     $   DCOS(BETA)
C
      PS14=DSIN((BETA-PHI)/2.0)-4.0*C1*
     $   DSIN((2.0*BETA-PHI+PHI0)/4.0)*DCOS((PHI+PHI0)/4.0)
C
199   CONTINUE
      PS1=PS11/PS12*PS13/PS14
      PS2=PS21/PS22*PS23/PS24
C
      ARG1=-PHI+PHI0
      ARG2=-PHI+PHI0
      ARG3=PHI+PHI0-2.0*BETA
      ARG4=PHI+PHI0+2.0*BETA
C
C     SET N+ AND N- TO NEAREST INTEGER
C
      ANNEG1=(-PI+ARG1)/(2.0*AN*PI)
      ANPOS1=(PI+ARG2)/(2.0*AN*PI)
      ANPOS2=(PI+ARG3)/(2.0*AN*PI)
      ANNEG2=(-PI+ARG4)/(2.0*AN*PI)
C
      IF(ANPOS1) 1,2,2
1     ANPOS1=ANPOS1-0.5
      GO TO 9
2     ANPOS1=ANPOS1+0.5
9     IF(ANPOS2) 3,4,4
3     ANPOS2=ANPOS2-0.5
      GO TO 13
```

```
4       ANPOS2=ANPOS2+0.5
13      IF(ANNEG1) 5,6,6
5       ANNEG1=ANNEG1-0.5
        GO TO 11
6       ANNEG1=ANNEG1+0.5
11      IF(ANNEG2) 7,8,8
7       ANNEG2=ANNEG2-0.5
        GO TO 12
8       ANNEG2=ANNEG2+0.5
12      NPOS1=ANPOS1
        NPOS2=ANPOS2
        NNEG1=ANNEG1
        NNEG2=ANNEG2
C
C       CALCULATE THE ARGUMENTS OF FRESNELS
C
        SIGNN1=1.0
        SIGNP1=1.0
        SIGNP2=1.0
        SIGNN2=1.0
        AA1=DCOS((2.0*AN*NNEG1-ARG1)/2.0)
        IF(AA1.LT.0.0) SIGNN1=-1.0
        A1=SQRT(2.0*KR)*AA1*SIGNN1
        AA2=DCOS((2.0*AN*NPOS1-ARG2)/2.0)
        IF(AA2.LT.0.0) SIGNP1=-1.0
        A2=SQRT(2.0*KR)*AA2*SIGNP1
        AA3=DCOS((2.0*AN*NPOS2-ARG3)/2.0)
        IF(AA3.LT.0.0) SIGNP2=-1.0
        A3=SQRT(2.0*KR)*AA3*SIGNP2
        AA4=DCOS((2.0*AN*NNEG2-ARG4)/2.0)
        IF(AA4.LT.0.0) SIGNN2=-1.0
        A4=SQRT(2.0*KR)*AA4*SIGNN2
C
```

```
      A1S=A1*A1
      A2S=A2*A2
      A3S=A3*A3
      A4S=A4*A4
C     CALCULATE FRESNEL INTEGRALS
C
      CALL CS(C1,S1,A1S)
      F1=CMPLX(C1,-S1)
      CALL CS(C2,S2,A2S)
      F2=CMPLX(C2,-S2)
      CALL CS(C3,S3,A3S)
      F3=CMPLX(C3,-S3)
      CALL CS(C4,S4,A4S)
      F4=CMPLX(C4,-S4)
C
      FRES1=ABS(A1)*CDEXP(C*A1*A1)*DSQRT(PI)*CDEXP(-C*PI/4.0)/2.0*
     1  (1.0-SQRT(2.0)*CDEXP(C*PI/4.0)*F1)
      FRES2=ABS(A2)*CDEXP(C*A2*A2)*DSQRT(PI)*CDEXP(-C*PI/4.0)/2.0*
     2  (1.0-SQRT(2.0)*CDEXP(C*PI/4.0)*F2)
      FRES3=ABS(A3)*CDEXP(C*A3*A3)*DSQRT(PI)*CDEXP(-C*PI/4.0)/2.0*
     3  (1.0-SQRT(2.0)*CDEXP(C*PI/4.0)*F3)
      FRES4=ABS(A4)*CDEXP(C*A4*A4)*DSQRT(PI)*CDEXP(-C*PI/4.0)/2.0*
     4  (1.0-SQRT(2.0)*CDEXP(C*PI/4.0)*F4)
C     CALCULATE THE FUNCTIONS
C
      P1=PS1*(1.0/DTAN((PI+(PHI-PHI0))/Q)*FRES1
     &  +DTAN((PI+(PHI+PHI0))/Q)*FRES3)
      P2=PS2*(1.0/DTAN((PI-(PHI-PHI0))/Q)*FRES2
     &  +DTAN((PI-(PHI+PHI0))/Q)*FRES4)
      P=P1+P2
C
      P=P*CONST
C
60    Z1=PS11/PS12*PS13/PS14
      Z2=PS21/PS22*PS23/PS24
      PDR=SD(P,KR)
```

```
      WRITE(6,600) I,P,PDB,Z1,Z2
600   FORMAT(10X,I5,2(F10.5,5X),F10.5,2X,2F10.5)
      IF(XXX.EQ.0.0) GO TO 777
      PDB=PDB+50.0
      IF(PDB.LT.0.0) PDB=0.0
      SY=PDB*DSIN(PHI)
      SX=PDB*DCOS(PHI)
      WRITE(14,310) SX,SY
310   FORMAT(1X,2F15.5)
777   CONTINUE
10    CONTINUE
      STOP
      END
C
C
      FUNCTION SD(SS,KR)
      COMPLEX SS,SD
      REAL KR
      AA=SQRT(KR)
      ASS=CABS(AA*SS)
      SD=20.0*ALOG10(ASS)
      RETURN
      END
C
```

```
C         LINE SOURCE
          IMPLICIT REAL*8(A-H,O-Z)
          COMPLEX*16 C,CONST,THETAP,THETAM
          COMPLEX P,P1,P2,SD,PC,F1,F2,F3,F4,CE,FRES1,FRES2,FRES3,FRES4
          REAL KR,KR0,RR,RR2,PDH,SX,SY,A1,A2,A3,A4,C1,C2,C3,C4,S1,
         &  S2,S3,S4,AA1,AA2,AA3,AA4
          PI=3.141592
          DO 88 MJ=1,2
C%%%%%READ IN DATA%%%%%
C*    THETAP=COMPLEX IMPEDANCE OF THE TOP SURFACE
C*    THETAM=COMPLEX IMPEDANCE OF THE BOTTOM SURFACE
C*    PHI0=LOCATION OF THE SOURCE
C*    BETA=WEDGE ANGLE
          READ(3,500) THETAP,THETAM,PHI0,BETA
          KR=20.0
          P0=1.0
          KR0=KR
          N=BETA
500       FORMAT(6D10.5)
          WRITE(6,550) THETAP,THETAM,KR,PHI0,P0,BETA
550       FORMAT(10X,F10.5)
          RAD=PI/180.0
          THETAP=THETAP*RAD
          THETAM=THETAM*RAD
          PHI0=PHI0*RAD
          BETA=BETA*RAD
          C=CMPLX(0.0,1.0)
          AN=2.0*BETA/PI
          O=2.0*AN
          RR=KR+KR0
          RR2=KR*KR+KR0*KR0
          CE=C*(-KR+PI/4.0)
          CONST=-P0/(2.0*AN*C)
          NN=N+1
          MM=2.0*NN
```

```
      WRITE(14,300) MM
300   FORMAT(1X,I3)
C
      DO 10 M=1,MM
      I=M-1
      IF(M.GT.NN) I=M-MM
      PHI=I*RAD
C*   CALCULATE THE DIFFRACTION FUNCTIONS
C
      C1=DTAN((2.0*BETA-PHI-PHI0-PI)/4.0)*DTAN((PHI-PHI0+PI)/4.0)
      C2=DTAN((2.0*BETA+PHI+PHI0-PI)/4.0)*DTAN((-PHI+PHI0+PI)/4.0)
C
      IF(THETAM.EQ.0.0) GO TO 99
C
      PS11=CDSIN(THETAP)-DSIN(BETA-PHI)
C
      PS12=CDSIN(THETAP)+2.0*DSIN((BETA-PHI)/2.0)*DSIN((BETA-PHI0)/2.0
     *)
C
      PS13=CDSIN(THETAM)+4.0*C1*(DSIN((BETA-PHI)/2.0)*C1+
     *DSIN((BETA+PHI)/4.0)*DCOS((3.0*BETA-PHI)/4.0)*DCOS(BETA))
C
      PS14=CDSIN(THETAM)+4.0*C1*(DSIN((BETA-PHI)/2.0)*C1-
     *DSIN((BETA+PHI)/4.0)*DCOS((3.0*BETA-PHI)/4.0)*DSIN((BETA+PHI0)/2.0
     *))
      PS21=CDSIN(THETAM)-DSIN(BETA+PHI)
C
      PS22=CDSIN(THETAM)+2.0*DSIN((BETA+PHI)/2.0)*DSIN((BETA+PHI0)
     */2.0)
C
      PS23=CDSIN(THETAP)+4.0*C2*(DSIN((BETA+PHI)/2.0)*C2+
     *DSIN((BETA-PHI)/4.0)*DCOS((3.0*BETA+PHI)/4.0)*DCOS(BETA))
C
```

```
      PS24=CDSIN(THETAP)+4.0*C2*(DSIN((BETA+PHI)/2.0)*C2-
     *DSIN((BETA-PHI)/4.0)*DCOS((3.0*BETA+PHI)/4.0)*DSIN((BETA-PHI0)/2.0
     *))
C
      GO TO 199
99    PS11=CDSIN(THETAP)-DSIN(BETA-PHI)
C
      PS12=CDSIN(THETAP)+2.0*DSIN((BETA-PHI)/2.0)*DSIN((BETA-PHI0)/2.0
     *)
C
      PS13=DSIN((BETA-PHI)/2.0)+4.0*C1*DSIN((BETA+PHI)/4.0)
     &*DCOS((3.0*BETA-PHI)/4.0)*DCOS(BETA)
C
      PS14=DSIN((BETA-PHI)/2.0)-4.0*C1*DSIN((BETA+PHI)/4.0)
     &*DCOS((3.0*BETA-PHI)/4.0)*DSIN((BETA+PHI0)/2.0)
      PS21=-DCOS((BETA+PHI)/2.0)/DSIN((BETA+PHI0)/2.0)
C
      PS22=1.0
      PS23=1.0
      PS24=1.0
C
199   CONTINUE
      PS1=PS11/PS12*PS13/PS14
      PS2=PS21/PS22*PS23/PS24
C
      ARG1=-PHI+PHI0
      ARG2=PHI-PHI0
      ARG3=PHI+PHI0-2.0*BETA
      ARG4=PHI+PHI0+2.0*BETA
C
C     SET N+ AND N- TO NEAREST INTEGER
C
      ANNEG1=(-PI+ARG1)/(2.0*AN*PI)
      ANPOS1=(PI+ARG2)/(2.0*AN*PI)
      ANPOS2=(PI+ARG3)/(2.0*AN*PI)
      ANNEG2=(-PI+ARG4)/(2.0*AN*PI)
```

```
      IF(ANPOS1) 1,2,2
1     ANPOS1=ANPOS1-0.5
      GO TO 9
2     ANPOS1=ANPOS1+0.5
9     IF(ANPOS2) 3,4,4
3     ANPOS2=ANPOS2-0.5
      GO TO 13
4     ANPOS2=ANPOS2+0.5
13    IF(ANNEG1) 5,6,6
5     ANNEG1=ANNEG1-0.5
      GO TO 11
6     ANNEG1=ANNEG1+0.5
11    IF(ANNEG2) 7,8,8
7     ANNEG2=ANNEG2-0.5
      GO TO 12
8     ANNEG2=ANNEG2+0.5
12    NPOS1=ANPOS1
      NPOS2=ANPOS2
      NNEG1=ANNEG1
      NNEG2=ANNEG2
C     CALCULATE THE ARGUMENTS OF FRESNELS
C
      A1=DCOS(2.0*AN*NNEG1-ARG1)
      AA1=SQRT(2.0)*DCOS((2.0*AN*NNEG1-ARG1)/2.0)
      A2=DCOS(2.0*AN*NPOS1-ARG2)
      AA2=SQRT(2.0)*DCOS((2.0*AN*NPOS1-ARG2)/2.0)
      A3=DCOS(2.0*AN*NPOS2-ARG3)
      AA3=SQRT(2.0)*DCOS((2.0*AN*NPOS2-ARG3)/2.0)
      A4=DCOS(2.0*AN*NNEG2-ARG4)
      AA4=SQRT(2.0)*DCOS((2.0*AN*NNEG1-ARG4)/2.0)
      SS1=SQRT(RR2-2.0*KR*KR0*A1)
      SS2=SQRT(RR2-2.0*KR*KR0*A2)
      SS3=SQRT(RR2-2.0*KR*KR0*A3)
      SS4=SQRT(RR2-2.0*KR*KR0*A4)
```

```
      A1S=RR-SS1
      A2S=RR-SS2
      A3S=RR-SS3
      A4S=RR-SS4
      RPS1=DSQRT(RR+SS1)
      RPS2=DSQRT(RR+SS2)
      RPS3=DSQRT(RR+SS3)
      RPS4=DSQRT(RR+SS4)
C     CALCULATE FRESNEL INTEGRALS
C
      CALL CS(C1,S1,A1S)
      F1=CMPLX(C1,-S1)
      CALL CS(C2,S2,A2S)
      F2=CMPLX(C2,-S2)
      CALL CS(C3,S3,A3S)
      F3=CMPLX(C3,-S3)
      CALL CS(C4,S4,A4S)
      F4=CMPLX(C4,-S4)
C
      FRES1=1.0-SQRT(2.0)*CDEXP(C*PI/4.0)*F1
      FRES2=1.0-SQRT(2.0)*CDEXP(C*PI/4.0)*F2
      FRES3=1.0-SQRT(2.0)*CDEXP(C*PI/4.0)*F3
      FRES4=1.0-SQRT(2.0)*CDEXP(C*PI/4.0)*F4
C
      IF(I.EQ.-100) GO TO 777
C     CALCULATE THE FUNCTIONS
C
     P1=PS1*(1.0/DTAN((PI+(PHI-PHI0))/Q)*CDEXP(-C*SS1)*AA1/RPS1*FRES1
     $  +DTAN((PI+(PHI+PHI0))/Q)*CDEXP(-C*SS3)*AA3/RPS3*FRES3)
     P2=PS2*(1.0/DTAN((PI-(PHI-PHI0))/Q)*CDEXP(-C*SS2)*AA2/RPS2*FRES2
     $  +DTAN((PI-(PHI+PHI0))/Q)*CDEXP(-C*SS4)*AA4/RPS4*FRES4)
      P=P1+P2
C
      P=P*CONST
      Z1=PS11/PS12*PS13/PS14
      Z2=PS21/PS22*PS23/PS24
```

```
      PDB=SD(P,KR,KRO)
      WRITE(6,600) I,P,PDB,Z1,Z2
600   FORMAT(10X,I5,2(F10.5,5X),F10.5,2X,2F10.5)
      IF(XXX.EQ.0.0) GO TO 777
      PDB=PDB+100.0
      IF(PDB.LT.0.0) PDB=0.0
      SY=PDB*DSIN(PHI)
      SX=PDB*DCOS(PHI)
      WRITE(14,310) SX,SY
310   FORMAT(1X,2F15.5)
777   CONTINUE
10    CONTINUE
88    CONTINUE
      STOP
      END
C
      FUNCTION SD(SS,KR,KRO)
      COMPLEX SS,SD
      REAL KR,KRO
      AA=SQRT(KR*KR)
      ASS=CABS(AA*SS)
      SD=20.0*ALOG10(ASS)
      RETURN
      END
```

```
C         POINT SOURCE
          IMPLICIT REAL*8(A-H,O-Z)
          COMPLEX*16 C,CONST,THETAP,THETAM
          COMPLEX P,P1,P2,SD,PC,F1,F2,F3,F4,CE,FRES1,FRES2,FRES3,FRES4,
      $     RPS1,RPS2,RPS3,RPS4,PS11,PS12,PS13,PS14,PS21,PS22,PS23,PS24
          REAL KR,KR0,KR1,RR,RR2,PDB,SX,SY,A1,A2,A3,A4,C1,C2,C3,C4,S1,
      $    S2,S3,S4,AA1,AA2,AA3,AA4
          PI=3.141592
C%%%%%READ IN DATA%%%%%
C*    THETAP=COMPLEX IMPEDANCE OF THE TOP SURFACE
C*    THETAM=COMPLEX IMPEDANCE OF THE BOTTOM SURFACE
C*    PHI0=LOCATION OF THE SOURCE
C*    BETA=WEDGE ANGLE
          READ(3,500) THETAP,THETAM,PHI0,BETA,KR,KR0
          P0=1.0
          XXX=1.0
          N=BETA
500       FORMAT(8D10.5)
          WRITE(6,550) THETAP,THETAM,KR,KR0,PHI0,P0,BETA
550       FORMAT(10X,F10.5)
          RAD=PI/180.0
          THETAP=THETAP*RAD
          THETAM=THETAM*RAD
          PHI0=PHI0+0.0001
          PHI0=PHI0*RAD
          BETA=BETA*RAD
          C=CMPLX(0.0,1.0)
          AN=2.0*BETA/PI
          O=2.0*AN
          RR=KR+KR0
          RR2=KR*KR+KR0*KR0
          KR1=RR
          CE=C*(KR*KR0/KR1)
          CONST=-P0/SQRT(2.0)/AN/KR1*CDEXP(-C*KR1)/2.0
          NN=10*N+1
```

```
      MM=2.0*NN
      WRITE(14,300) MM
300   FORMAT(1X,I10)
C
      DO 10 M=1,MM
      I=M-1
      IF(M.GT.NN) I=M-MM
      PHI=I*RAD/10.0
C
C*    CALCULATE THE DIFFRACTION FUNCTIONS
      C1=DTAN((2.0*BETA-PHI-PHI0-PI)/4.0)*DTAN((PHI-PHI0+PI)/4.0)
      C2=DTAN((2.0*BETA+PHI+PHI0-PI)/4.0)*DTAN((-PHI+PHI0+PI)/4.0)
C
      PS11=CDSIN(THETAP)-DSIN(BETA-PHI)
C
      PS12=CDSIN(THETAP)+2.0*DSIN((BETA-PHI)/2.0)*DSIN((BETA-PHI0)/2.0
     *)
      PS23=CDSIN(THETAP)+4.0*C2*(DSIN((BETA+PHI)/2.0)*C2+
     *DSIN((BETA-PHI)/4.0)*DCOS((3.0*BETA+PHI)/4.0)*DCOS(BETA))
C
      PS24=CDSIN(THETAP)+4.0*C2*(DSIN((BETA+PHI)/2.0)*C2-
     *DSIN((BETA-PHI)/4.0)*DCOS((3.0*BETA+PHI)/4.0)*DSIN((BETA-PHI0)/2.0
     *))
C
      IF(THETAM.EQ.0.0) GO TO 99
       PS21=CDSIN(THETAM)-DSIN(BETA+PHI)
C
       PS22=CDSIN(THETAM)+2.0*DSIN((BETA+PHI)/2.0)*DSIN((BETA+PHI0)
     */2.0)
C
       PS13=CDSIN(THETAM)+4.0*C1*(DSIN((BETA-PHI)/2.0)*C1+
     *DSIN((BETA+PHI)/4.0)*DCOS((3.0*BETA-PHI)/4.0)*DCOS(BETA))
C
       PS14=CDSIN(THETAM)+4.0*C1*(DSIN((BETA-PHI)/2.0)*C1-
     *DSIN((BETA+PHI)/4.0)*DCOS((3.0*BETA-PHI)/4.0)*DSIN((BETA+PHI0)/2.0
     *))
```

```
      GO TO 199
99    PS21=-DCOS((BETA+PHI)/2.0)
      PS22=DSIN((BETA+PHI0)/2.0)
      PS13=DSIN((BETA-PHI)/2.0)+2.0*C1*
     $   DCOS(BETA)
C
      PS14=DSIN((BETA-PHI)/2.0)-4.0*C1*
     $   DSIN((2.0*BETA-PHI+PHI0)/4.0)*DCOS((PHI+PHI0)/4.0)
C
199   CONTINUE
      PS1=PS11/PS12*PS13/PS14
      PS2=PS21/PS22*PS23/PS24
C
      ARG1=-PHI+PHI0
      ARG2=-PHI+PHI0
      ARG3=PHI+PHI0-2.0*BETA
      ARG4=PHI+PHI0+2.0*BETA
C
C     SET N+ AND N- TO NEAREST INTEGER
C
      ANNEG1=(-PI+ARG1)/(2.0*AN*PI)
      ANPOS1=(PI+ARG2)/(2.0*AN*PI)
      ANPOS2=(PI+ARG3)/(2.0*AN*PI)
      ANNEG2=(-PI+ARG4)/(2.0*AN*PI)
C
      IF(ANPOS1) 1,2,2
1     ANPOS1=ANPOS1-0.5
      GO TO 9
2     ANPOS1=ANPOS1+0.5
9     IF(ANPOS2) 3,4,4
3     ANPOS2=ANPOS2-0.5
      GO TO 13
4     ANPOS2=ANPOS2+0.5
13    IF(ANNEG1) 5,6,6
5     ANNEG1=ANNEG1-0.5
      GO TO 11
```

```
6       ANNEG1=ANNEG1+0.5
11      IF(ANNEG2) 7,8,8
7       ANNEG2=ANNEG2-0.5
        GO TO 12
8       ANNEG2=ANNEG2+0.5
12      NPOS1=ANPOS1
        NPOS2=ANPOS2
        NNEG1=ANNEG1
        NNEG2=ANNEG2
C
C       CALCULATE THE ARGUMENTS OF FRESNELS
C
        A1=SQRT(2.0)*DCOS((2.0*AN*NNEG1-ARG1)/2.0)
        AA1=SQRT((KR*KR0)/KR1)*A1
        A2=SQRT(2.0)*DCOS((2.0*AN*NPOS1-ARG2)/2.0)
        AA2=SQRT((KR*KR0)/KP1)*A2
        A3=SQRT(2.0)*DCOS((2.0*AN*NPOS2-ARG3)/2.0)
        AA3=SQRT((KR*KR0)/KR1)*A3
        A4=SQRT(2.0)*DCOS((2.0*AN*NNEG2-ARG4)/2.0)
        AA4=SQRT((KR*KR0)/KR1)*A4
        A1S=AA1*AA1
        A2S=AA2*AA2
        A3S=AA3*AA3
        A4S=AA4*AA4
        RPS1=CDEXP(C*A1S)
        RPS2=CDEXP(C*A2S)
        RPS3=CDEXP(C*A3S)
        RPS4=CDEXP(C*A4S)
C       CALCULATE FRESNEL INTEGRALS
C
        CALL CS(C1,S1,A1S)
        F1=CMPLX(C1,-S1)
        CALL CS(C2,S2,A2S)
        F2=CMPLX(C2,-S2)
        CALL CS(C3,S3,A3S)
```

```
      F3=CMPLX(C3,-S3)
      CALL CS(C4,S4,A4S)
      F4=CMPLX(C4,-S4)
C
      FRFS1=1.0-SQRT(2.0)*CDEXP(C*PI/4.0)*F1
      FRES2=1.0-SQRT(2.0)*CDEXP(C*PI/4.0)*F2
      FRFS3=1.0-SQRT(2.0)*CDEXP(C*PI/4.0)*F3
      FRES4=1.0-SQRT(2.0)*CDEXP(C*PI/4.0)*F4
C
      IF(I.EQ.-100) GO TO 777
C     CALCULATE THE FUNCTIONS
C
      P1=PS1*(1.0/DTAN((PI+(PHI-PHI0))/Q)*ABS(A1)*RPS1*FRES1
     $ +DTAN((PI+(PHI+PHI0))/Q)*ABS(A3)*RPS3*FRES3)
      P2=PS2*(1.0/DTAN((PI-(PHI-PHI0))/Q)*ABS(A2)*RPS2*FRES2
     $ +DTAN((PI-(PHI+PHI0))/Q)*ABS(A4)*RPS4*FRES4)
      P=P1+P2
C
      P=P*CONST
      Z1=PS11/PS12*PS13/PS14
      Z2=PS21/PS22*PS23/PS24
      PDB=SD(P,KR,KR0,KR1)
      WRITE(6,600) I,P,PDB,Z1,Z2
600   FORMAT(10X,I5,2(F10.5,5X),F10.5,2X,2F10.5)
      IF(XXX.EQ.0.0) GO TO 777
      PDB=PDB+50.0
      IF(PDB.LT.0.0) PDB=0.0
      SY=PDB*DSIN(PHI)
      SX=PDB*DCOS(PHI)
      WRITE(14,310) SX,SY
310   FORMAT(1X,2F15.5)
777   CONTINUE
10    CONTINUE
      STOP
      END
```

```
      FUNCTION SD(SS,KR,KR0,KR1)
      COMPLEX SS,SD
      REAL KR,KR0,KR1
      AA=SQRT(KR)*KR0
      ASS=CABS(AA*SS)
      SD=20.0*ALOG10(ASS)
      RETURN
      END
C***************FRESNEL INTEGRAL SUBROUTINE************
C
      SUBROUTINE CS(C,S,X)
      Z=ABS(X)
    2 IF(Z-4.0) 3,3,4
    3 C=SQPT(Z)
      S=Z*C
      Z=Z*Z
      C=C*((((((.50998348E-10*Z-.10140729E-7)*Z+.11605284E-5)*Z
     $ -.85224622E-4)*Z+.36938586E-2)*Z-.079788405)*Z+.79788455)
      S=S*(((((-.66777447E-9*Z+.11225331E-6)*Z-.10525853E-4)*Z
     $ +.604353371E-3)*Z-.19997110E-1)*Z+.26596149)
      RETURN
    4 D=COS(Z)
      S=SIN(Z)
      Z=4.0/Z
      A=(((((((.87682583E-3*Z-.41692894E-2)*Z+.79709430E-2)*Z-
     $ .67928011E-2)*Z-.3095341E-3)*Z+.59721508E-2)*Z-.16064281E-4)*Z-
     $ .024933215)*Z-.44440909E-8
      B=(((((-.66339256E-3*Z+.34014090E-2)*Z-.72716901E-2)*Z+
     $ .74282459E-2)*Z-.40271450E-3)*Z-.93149105E-2)*Z-.12079984E-5)*Z
     $ +.1994711
      Z=SQPT(Z)
      C=.5+Z*(D*A+S*B)
      S=.5+Z*(S*A-D*B)
      RETURN
      END
```

DISTRIBUTION LIST FOR TM 83-95

Commander (NSEA 0342)
Naval Sea Systems Command
Department of the Navy
Washington, DC 20362 — Copies 1 and 2

Commander (NSEA 9961)
Naval Sea Systems Command
Department of the Navy
Washington, DC 20362 — Copies 3 and 4

Defense Technical Information Center
5010 Duke Street
Cameron Station
Alexandria, VA 22314 — Copies 5 through 10

END

FILMED

10-83

DTIC